Ph.D. Dissertation

International Doctoral School in Information and Communication Technology

DISI - University of Trento

Predicting the Tolerance Effects on the Radiation Pattern of Reflectarray Antennas through Interval Analysis

Nasim Ebrahimi

Advisor:
Andrea Massa, Professor
Università degli Studi di Trento

February 2018

Acknowledgements

I would like to express my thanks to Prof. Massa and the whole ELEDIA group for helping and supporting me during these three years.

I would like to express my sincere gratitude to Prof. Paolo Rocca, for his suggestions and indications for completing this thesis. I am truly thankful for his kindness and support. His patience and encouragement were key motivations throughout my Ph.D.

I want to thank my friends for listening, discussing, giving me advice and supporting me during these years. You were always beside me during happy and hard moments.

The greatest thank you is for my beloved family, my biggest supporter in my life. Thanks for their love, encouragement and valuable prayers. And Finally I wish to express my heartfelt love to my nephews Radmehr and Kohyar and my niece Kianaz. For their cute and lovely calling and supporting their Auntie Nasim.

Abstract

The thesis focuses on predicting tolerance effects on the radiation pattern of reflectarray antennas through Interval Analysis. In fact, the uncertainty on the actual size of all parameters under fabrication tolerances such as element dimensions and dielectric properties, are modeled with interval values. Afterwards, the rules of Interval Arithmetic are exploited to compute the bounds of deviation in the resonance frequency of each element, the phase response of the element and the radiated power pattern. Due to the redundancy problems of using Interval Cartesian ($IA-CS$) for complex structure, the interval bounds are overestimated and the reasons are the Dependency and Wrapping effects of using interval analysis for complex structures. Different techniques are proposed and assessed in order to eliminate the dependency effect such as reformulating the interval function and the Enumerative interval analysis. Moreover, the Minkowski sum approach is used to eliminate the wrapping effect. In numerical validation, a set of representative results, show the power bounds computations with Interval Cartesian method ($IA-CS$), a modified Interval Cartesian method ($IA-CS^*$), Interval Enumerative method ($IA-ENUM$) and Interval Enumerative Minkowski method ($IA-ENUM-MS$) and a comparative study is reported in order to assess the effectiveness of the proposed approach ($IA-ENUM-MS$) with respect to the other methods. Furthermore, different tolerances in patch width, length, substrate thickness and dielectric permittivity are considered which shows that the higher uncertainty produces the larger deviation of the pattern bounds and the larger deviation include the smaller deviation and the nominal one. To validate the inclusion properties of the interval bounds, the results are compared with Monte Carlo simulation results. Then, a numerical study is devoted to analyze the dependency of the degradation of the pattern features to steering angle and the bandwidth. Finally, the effect of feed displacement errors on the power pattern of reflectarray antennas is considered with Interval Enumerative Minkowski method. The maximal deviations from the nominal power pattern (error free) and its features are analyzed for several reflectarray structures with different focal-length-to-diameter ratios to prove the effectiveness of the proposed method.

Keywords
Reflectarray Antennas, Sensitivity Analysis, Antenna Uncertainties, Interval Analysis, Minkowski Sum, Feed Error, Phase Error.

Contents

List of Tables

List of Figures

Structure of the Thesis

The thesis is structured in chapters according to the organization detailed in the following.

The first chapter (chapter 1) deals with an introduction to the thesis and the state-of-the-art investigation, focusing on the introductory remarks on reflectarrays and the main motivations of using interval analysis for tolerance analysis of the reflectarray antenna.

Chapter 2 provides the different approaches used for the analysis of the radiation pattern of reflectarrays , focusing on the Aperture Field Method and Floquet model expansions. Techniques for computing the phase distribution on the reflectarray aperture surface are provided in this chapter. Approaches for designing the unit cell is also covered in this chapter. The analytical expression for the reflection coefficient is explained. The radiation pattern and its relation to the physical parameters of the unit cell is expressed.

Chapter 3 is devoted to the fundamental of the Interval Analysis method, focusing on the definition, properties and the key features of the interval arithmetic rules. Interval functions with inclusion theory are defined. Complex interval is explained. The two main problems of Dependency and Wrapping related to the use of Interval Analysis and Arithmetic of Intervals in complex structure are fully explained. These problems produce the redundancy in the interval bounds. Reformulating of the interval expression for solving the dependency effect is properly determined.

Mathematical formulation of the reflectarray analysis and its interval extension are described in chapter 4. A microstrip reflectarray antenna is considered as an illustration. Then Aperture Field method together with Floquet model expansions are considered for analysis the microstrip reflectarray antenna. To

consider the effect of the geometrical parameters error on the radiation performance of the antenna, interval analysis is applied. This chapter deals with the interval extension of the reflectarray radiation pattern expression. Geometrical parameters such patch length, width, substrate thickness and dielectric permittivity are modeled with interval values, then the interval function of the far field is computed. Different techniques for eliminating dependency effect in reflectarray antenna formulations are expressed. Minkowski Sum approach to remove the wrapping effect is explained.

Several representative results are presented in chapter 5. The inclusion properties are checked by comparing the resulting bounds with the Monte Carlo simulation results. A comparative study checks the improvement of Interval Enumerative Minkowski ($IA-ENUM-MS$) to Interval Cartesian ($IA-CS$). Pattern feature analysis versus steering angle, bandwidth are assessed and described. The effect of feed displacement errors on the radiation performance of the reflectarrays is also considered in this chapter. The bounds of the deviation as a result of the axial errors are computed by Interval Minkowski methods. The inclusion properties are checked by comparing the results with the Monte Carlo simulation results. Analysis versus different focal-length-to-diameter (F/D) ratios in different tolerance errors in the feed positions is evaluated. The results are explained and compared together.

Conclusions and further developments are presented in Chapter 6.

Chapter 1

Introduction and State-of-the-Art

In the introduction, the motivation of the thesis is pointed out starting from a brief overview on the reflectarrays and techniques presented in the state-of-the-art for tolerance analysis of the reflectarray antenna.

High gain antennas are needed in a variety of communication systems such as radar, long distance communication, wireless communication and remote sensing applications. Reflector and array antennas are traditionally two main antennas for high gain applications [1]. Curve surface of the reflector antennas makes the manufacturing process more difficult. Furthermore, high mass and volume of reflector antenna increase the launch cost specially in space communication. In recent years, phased array antennas have been used as an appropriate option for satellite communication due to the advantages of low profile, low cost, low mass and high gain radiation patterns [2]. Despite the previously mentioned advantages, the feeding system of the phased array antennas is quite complicated. The most ideal antennas for space communication are the ones which can combine the best features of the reflector and array antennas. Over the past few years, reflectarray antennas have proved to be an excellent alternative to reflector and array antennas. Reflectarray antennas first introduced in 1960s by Berry, Malech and Kennedy [3]. They were short-ended waveguide with variable-length waveguide. Then in mid-1970s "spiraphase" reflectarray was presented by Phelan [4]. In the 1980s, microstrip reflectarray antennas were developed [5].

Favorable features of low profile, low mass, low cost and high efficiency as well as the ability of being folded in space have made the reflectarrays the most applicable antennas for space communications [6], [7]. Reflectarray antenna structure include several radiating elements located in a reflective surface which are illuminated by a feed antenna. Microstrip patches, dipoles and rings are the radiating elements in the reflectarray antenna [8], [9] . These radiating elements produce the required phases to form a planar phase front in the far-field [10]. Different approaches can be used to produce the required phases[13]. These approaches are variable phase delay lines attached to element [11], variable-size patches [12], dipoles or rings and the element rotations . Among them variable-size approach has the disadvantages of the the limited realizable phase range. The achievable phase range by this approach is less that 360 [deg]. This unattainable phase range leads to phase error. To take a phase variation near to 360 [deg], patch size should change significantly about 40 percent which leads to an inefficiency [10]. By using element rotation better efficiency could be obtained due to the lack of specular reflection of the off-broadside incident rays [10]. Despite of all advantages of the reflectarray antenna, it has one main disadvantage which is its narrow bandwidth. It is usually beyond ten percent depending on its element design, aperture size and the focal length [14]. This bandwidth is mainly limited by the element geometry and differential spatial phase delay. For achieving wider bandwidth thick substrate, stacking multiple patches and sequentially rotated subarrays are proposed. More than 15 percent bandwidth is gained by these approaches [15], [16]. Reflectarray with larger focal-length-to-diameter (f/D) ratio have wider bandwidth. Curved reflectarray with piecewise flat surfaces has larger bandwidth than a flat reflectarray antenna. Despite of the bandwidth limitation of the reflectarray antenna, due to several capabilities, development and research

for reflectarray antenna are still an ongoing process. Several development and innovation techniques are used in reflectarray antenna design which is worth to mention. Using multi-layer stacked patch increase the bandwidth from a few percent to ten percent [15], [16]. This structure can improve the phase range far in excess of 360 [*deg*]. By varying the dimensions of three stacked patches, over 600 [*deg*] phase ranges can be achieved. In [17], the electrically largest reflectarray in the microwave and millimeter-wave spectra is introduced. It is a 3-m Ka-band circularly polarized inflatable reflectarray consisting of 200000 elements. In [3], an amplifying reflectarray antenna was developed in which each element receives the signal from feed, then goes to amplifier and retransmit the signal. It can give very high equivalent isotropic radiated power. Another improvement in reflectarray antenna design is applying optimization algorithm to synthesis the antenna pattern. There are different parameters in reflectarray antenna such as substrate thickness, patch size, incident angle, main beam and bandwidth. These parameters can be optimized in order to achieve the high gain, efficiency and the directivity. Genetic Algorithm (GA) and Particle Swarm Optimization (PSO) are properly used in [20] and [19] to synthesize the reflectarray antenna. A novel reflectarray antenna integrated with solar cells for satellite communication is developed in [21]. Over all of these innovations and developments, there is one main challenge which is not considered efficiently in reflectarray antenna design. Reflectarray antenna can be affected by surface deviations and the manufacturing tolerances due to its reflection mechanism, patch dimensions and the electrical phases [10]. The phase response of the patch element in microstrip reflectarray depends on its physical parameters [22]. Due to the inaccuracies in manufacturing process, the dimension of the single element and the position of the feed deviate from their actual values. This deviation causes a considerable change in phase response of the single element and eventually the degradation in the radiation pattern. To decrease the sensitivity toward manufacturing errors, two layer structure is suggested. As an example, a tolerance error of 0.1 mm in patch dimension will produce only 6.5 error in phase, which indicate the low sensitivity to manufacturing tolerances rather than a single layer reflectarray antenna [10]. The effect of manufacturing errors is more sensible when the frequency is increasing.

To improve the robustness of the system, any change in the phase response should be avoided. Different mechanisms have been applied to estimate the phase errors and the pattern degradation. Tolerance analysis has been applied to the reflectarray antenna in the work of Pozar et al. [24] where statistical approaches are implemented to estimate the deviation in phase response of microstrip patch element while the root-mean-square error of patch dimensions are known. In [23], numerical analysis is presented to compute radiation discrepancy of metallic reflectarray antenna experiencing manufacturing distortion at millimeter waves. Errors are modeled with normal distribution. Since reflectarray antennas are sensitive to manufacturing errors, the need for the tolerance analysis is unavoid-

able. Initial work on tolerance analysis of the antenna was based on statistical approaches. Tolerance analysis is used to consider the effect of tolerance in the position of the element due to mechanical errors [25]. A probabilistic analysis is exploited in [26] and [27] to calculate the maximum tolerance in array elements to satisfy the specific constrains. In [47], tolerance analysis based on Monte Carlo method is exploited to predict the effects of errors in the excitation and the position of each element. The above-mentioned methods are based on statistical approaches in which the a-priori knowledge of the error distribution is necessary. The main problem associated with Monte Carlo method is the lengthy computations of the infinite number of error combinations. Since it is not plausible to realize the infinite number of errors, the Monte Carlo results are not totally reliable [47].

To overcome the current limitations of statistical approaches in tolerance analysis, Arithmetic Interval is applied to perform operations between interval values [29]. Interval Analysis was first used to solve the linear and nonlinear functions [29] and optimization problems [30]. Its usage in electromagnetic field was initiated with the robust design of the magnetic devices [31] and reliable systems for target tracking radar [32]. Recently Interval Analysis was used to model the manufacturing tolerances in excitation and position of linear array antenna. Interval arithmetic was then exploited to compute the bounds of the radiation pattern degradation over the interval errors [33]. A closed form expression has been presented for the upper and lower bounds of the power pattern in the reflector antenna with bump-like surface by the features of Interval Analysis and the rules of arithmetic for intervals [49]. According to the state of the art, the significance of applying manufacturing tolerance analysis in antenna design is quite well-known. In order to apply interval analysis in reflectarray antenna, we need to apply proper analysis method. In the next chapter, different techniques for analysis of the reflectarray antenna radiation pattern will be explained.

Chapter 2

Radiation Analysis for Reflectarray Antenna

In this chapter different approaches for analysis of the radiation pattern of the reflectarray antenna are presented. Comparative studies among these approaches are provided. There are several approximations for feed antenna pattern and the element reflection coefficient. These approximations are explained in this section. The accurate method for analysis of the co- and cross-components of the radiation pattern is also provided.

2.1 Introduction

To compute the radiation characteristic of the reflectarray antenna, different approaches such as Array-Theory method and Aperture-Field method can be applied. Advantages and disadvantages of using these methods are described in this section. One of the most crucial part of the reflectarray analysis and design is the accurate evaluation of the unit cell element which provide a required phase-shift. The phase shift distribution of the reflectarray surface and unit cell design are clarified in this section.

2.2 Overview of Analysis Techniques

2.2.1 Array-Theory Method

Conventional array theory is applied to compute the far field radiation pattern of the reflectarray antenna. Considering the array antenna with $M * N$ elements. The total electric field of the array antenna is the multiplication of the element pattern and the element excitation as [35]:

$$\overline{E}(\hat{v}) = \sum_{m=1}^{M} \sum_{n=1}^{N} \overrightarrow{b}_{mn}(\hat{v}) \bullet \overrightarrow{a}_{mn}(\overrightarrow{r}_{mn}), \tag{2.1}$$

$$\hat{v} = \hat{x}sin\theta cos\phi + \hat{y}sin\theta sin\phi + \hat{z}cos\theta \tag{2.2}$$

Where $\overrightarrow{r}_{mn}$ is the position vector and b_{mn} , a_{mn} are the element factor and the excitation vector function, respectively. For the sake of simplicity element factors and the excitation vector are approximated by scalar functions. A cosine q model is considered for the element pattern as:

$$b_{mn}(\hat{v}) \approx cos^{qe}(\theta) e^{jk(\overrightarrow{r}_{mn} \bullet \hat{v})} \tag{2.3}$$

The excitation vector $\overrightarrow{a}_{mn}$ is approximated as:

$$a_{mn} \approx \frac{cos^{qf}\theta_f(m,n)}{|\overrightarrow{r}_{mn} - \overrightarrow{r}_f|} e^{-jk(|\overrightarrow{r}_{mn} - \overrightarrow{r}_f|)} |\Gamma_{mn}| e^{j\phi_{mn}} \tag{2.4}$$

The element excitation is the multiplication of the feed-horn pattern function and the receiving mode pattern of the element (Γ_{mn}). Feed horn pattern is approximated by cosine q model and taking into account the distance between the feed horn and the element. θ_f is the spherical angel and $\overrightarrow{r}_f$ is the position vector of feed. The receiving mode pattern of the element is as follows:

$$|\Gamma_{mn}| = cos^{qe}\theta_e(m,n) \tag{2.5}$$

With all of these approximations, the radiation pattern is presented as [35]:

$$E(\theta,\phi)=\sum_{m=1}^{M}\sum_{n=1}^{N} cos^{qe}\theta \frac{cos^{qf}\theta_f(m,n)}{|\overrightarrow{r}_{mn}-\overrightarrow{r}_f|} e^{-jk(|\overrightarrow{r}_{mn}-\overrightarrow{r}_f|-\overrightarrow{r}_{mn}\bullet\hat{v})} cos^{qe}\theta_e(m,n)e^{j\phi_{mn}} \tag{2.6}$$

where ϕ_{mn} is the required phase delay of mn-th element.

Advantages and disadvantages of this method are as follows [35]:

- Advantage: simplicity of the formulation and the program development
- Disadvantage: the cross-polarization is not modeled.

2.2.2 Aperture-Field Method

In this method, first the tangential electric field on the aperture surface is computed by considering the polarization of the field horn. A horn antenna is usually used as a feed in the reflectarray antenna. The radiation pattern of the horn antenna is given [10]:

For a x-polarized feed

$$E^{Fx}(\theta,\phi)=\frac{jke^{-jkr}}{2\pi r}(\hat{\theta}C_E(\theta)cos\phi-\hat{\phi}C_H(\theta)sin\phi) \tag{2.7}$$

For a y-polarized feed

$$E^{Fy}(\theta,\phi)=\frac{jke^{-jkr}}{2\pi r}(\hat{\theta}C_E(\theta)sin\phi+\hat{\phi}C_H(\theta)cos\phi) \tag{2.8}$$

C_H and C_E are the H-plane and E-plane radiation patterns of the horn antenna. They are modeled as $cos^q(\theta)$ functions. q is the value which is computed from the aperture efficiency and the feed horn data. In (2.7) and (2.8), the radiated field of the feed in the spherical coordinate is computed. The spherical components of the electric field is transformed to Cartesian components from the following matrix transformation.

$$\begin{bmatrix} E_x^F \\ E_y^F \\ E_z^F \end{bmatrix} = \begin{bmatrix} sin\theta cos\phi & cos\theta cos\phi & -sin\phi \\ sin\theta sin\phi & cos\theta sin\phi & cos\phi \\ cos\theta & -sin\theta & \end{bmatrix} \begin{bmatrix} \\ E_\theta^F \\ E_\phi^F \end{bmatrix}$$

Then this components should convert from feed coordinate system to the reflectarray coordinate system by a proper transformation matrix.

2.2.3 Radiation Patterns

After computing the tangential electric field, the radiated far field is obtained by an asymptotic evaluation of the integrals. The radiated far field are as follow [10]:

$$E(\theta,\phi) = jk[(\hat{\theta}cos\phi - \hat{\phi}sin\phi cos\theta)\tilde{E}_{Rx}(u,v) + (\hat{\theta}sin\phi + \hat{\phi}cos\phi cos\theta)\tilde{E}_{Ry}(u,v)]\frac{e^{-jkr}}{2\pi r} \tag{2.9}$$

Where $\tilde{E}_{Rx}(u,v)$ and $\tilde{E}_{Ry}(u,v)$ are the Fourier transform of the Cartesian components of the tangential electric field $E_{Rx}(u,v)$ and $E_{Ry}(u,v)$, expressed as follows:

$$\tilde{E}_{Rx/y}(u,v) = \int\int_{RA} E_{Rx/y}(x,y)e^{jk_0(ux+vy)}dxdy \tag{2.10}$$

Where u and v are the angular coordinates as:

$$u = sin\theta cos\phi \tag{2.11}$$

$$v = sin\theta sin\phi \tag{2.12}$$

To compute the (2.10) element by element, variable change in the coordinate is used for the coordinate (x,y):

$$x = x^{'} + mp_x - \frac{(N_x-1)p_x}{2}; m = 0,1,2,...,N_x-1 \tag{2.13}$$

$$y = y^{'} + np_y - \frac{(N_y-1)p_y}{2}; n = 0,1,2,...,N_y-1 \tag{2.14}$$

Central point of the element (m,n) are $(mp_x - \frac{(N_x-1)p_x}{2}, np_y - \frac{(N_y-1)p_y}{2})$. $x^{'}$ and $y^{'}$ are withing the following bounds [10]:

$$-\frac{p_x}{2} \leq x^{'} \leq \frac{p_x}{2} \tag{2.15}$$

$$-\frac{p_y}{2} \leq y^{'} \leq \frac{p_y}{2} \tag{2.16}$$

where p_x and p_y are the periodicity along x and y, directions. Maximum number of element in x and y direction are N_x and N_y, respectively. By substituting (2.13), (2.14) in (2.10), the spectral function is as:

$$\tilde{E}_{Rx/y}(u,v) = K_1 \sum_{m=0}^{M-1}\sum_{n=0}^{N-1}[e^{jk_0(ump_x+vnp_y)}\int_{\frac{-p_x}{2}}^{\frac{-p_x}{2}}\int_{-\frac{p_y}{2}}^{\frac{p_y}{2}} E_{Rx/y}^{m,n}(x^{'},y^{'})e^{jk_0(ux^{'}+vy^{'})}dx^{'}dy^{'}] \tag{2.17}$$

where

$$K_1 = e^{-j\frac{k_0}{2}[u(M-1)d_x + v(N-1)d_y]} \tag{2.18}$$

Tangential field components in each cell of the reflectarray is shown with the complex coefficient of the reflected field.

$$E^{m,n}_{Rx/y}(x^{'}, y^{'}) = a_{x/Y}(m,n) = Ax/y(m,n)e^{j\phi_{x/y}(m,n)} \tag{2.19}$$

By substituting (2.19) in (2.17), the integration can be written by the summation as:

$$\tilde{E}_{Rx/y}(u,v) = K_1 p_x p_y sinc(\frac{k_0 u p_x}{2}) sinc(\frac{k_0 v p_y}{2}) \sum_{m=0}^{M}\sum_{n=0}^{N} A_{x/y}(m,n)e^{j\phi_{x/y}(m,n)}e^{jk_0(umd_x + vnd_y)} \tag{2.20}$$

In every reflectarray element, Cartesian components of the reflected and the incident field are related to each other by scattering matrix as:

$$\begin{bmatrix} a_x(m,n) \\ a_y(m,n) \end{bmatrix} = \begin{bmatrix} S_{11} & S_{12} \\ S_{21} & S_{22} \end{bmatrix} \begin{bmatrix} E^F_x \\ E^F_y \end{bmatrix} \tag{2.21}$$

This scattering matrix can be computed by the Method of Moment in the spectral domain. The element of the scattering matrix can also be replaced by the reflection coefficient.

$$\begin{bmatrix} a_x(m,n) \\ a_y(m,n) \end{bmatrix} = \begin{bmatrix} \Gamma_{xx} & \Gamma_{xy} \\ \Gamma_{yx} & \Gamma_{yy} \end{bmatrix} \begin{bmatrix} E^F_x \\ E^F_y \end{bmatrix} \tag{2.22}$$

As it is obvious in (2.21) and (2.22), scattering matrix and the reflection coefficient are the main parts for computing the radiation pattern. These coefficients relate to element performance of the unit cell. In the following part, different techniques for analysis of the unit cell element are proposed.

2.2.4 Unit Cell Design

Each element in reflectarray antenna should produce the required phases in order to compensate different spatial distances from feed to element. This phase shift distribution is computed from the following expressions.

2.2.4.1 Phase-Shift Distribution Technique

Each element must produce a phase-shift to provide a collimated beam in a given direction. From the array theory, the phase distribution to produce a beam in the main beam direction (θ_b, ϕ_b) is as [10]:

$$\phi(x_{mn}, y_{mn}) = -k_0 sin\theta_b cos\phi_b x_{mn} - k_0 sin\theta_b sin\phi_b y_{mn} \tag{2.23}$$

(x_{mn}, y_{mn}) is the location of the mn-th element in the reflectarray surface. k_0 is the propagation constant. Phase of the reflected electric field can also be computed from the following way. Phase of the reflected field is equal to the phase of the incident field plus phase-shift produced by each element as:

$$\phi(x_{mn}, y_{mn}) = -k_0 R_{mn} + \phi_R(x_{mn}, y_{mn}) \tag{2.24}$$

R_{mn} is the distance from phase center of the feed to element. $\phi_R(x_{mn}, y_{mn})$ is a phase-shift for mn-th element. From (2.23) and (2.24), the required phase shift for each element is:

$$\phi_R(x_{mn}, y_{mn}) = k_0(R_{mn} - (x_{mn}cos\phi_b + y_{mn}sin\phi_b)sin\theta_b) \tag{2.25}$$

In reflectarray antenna phase of the reflection coefficient should change in order to match these phases. Different techniques can be used to provide these phases. These techniques are as follows:

- Connecting variable-length stubes to element
- Patch with variable sizes
- Element loaded with MEMS, varactors and liquid cristal polymers

Performance of the antenna element in reflectarray antenna related to its physical parameters such as

- patch dimensions length (l) and width (w)
- substrate thickness (d)
- dielectric constant (ε_r)
- dielectric and conductor losses ($tan\delta$, σ)
- spacing between elements (p_x, p_y)

In the following section, recent techniques for analysis and design of the single element are provided.

2.2.4.2 Techniques for Analysis of the Unit Cell

In this section, different methods for analysis of the unit cell elements are mentioned. And the most recent theoretical method for analysis of the single element is explained with more details. Techniques of the analysis of the single element are as follows:

- Numerical methods such as spectral domain method of moments (MoM), finite element method (FEM), finite difference time domain (FDTD)

- Commercial packages such as HFSS, CST, FEKO
- Theoretical model based on full-wave simulations
- Analytical approach based on Q factor analysis

Since in this thesis we want to compute the radiation pattern analyticaly, analytical approach based on Q factor is explained with more details in the following part.

2.2.4.3 Analytical Approach Based on Q Factor Analysis

A complete analytical approach based on Q factor is introduced to extract the reflection properties of the unit cell. In order to extract the closed-form formulas, we need to express the incident and the reflected field in terms of orthogonal Floquet modes. Let us provide a short explanation about Floquet harmonics and its expression.

2.2.4.4 Floquet Harmonics

An arbitrary incident field can be defined as a summation of the TE and TM Floquet space harmonics with complex amplitude. The incident electric field propagating toward -z with Floquet harmonic expansion is written as [10]:

$$E_1^i = \sum_{l=1}^{2L} d_1 e_1 exp(j(k_{xm}x + k_{yn}y + k_{zl}z)) \tag{2.26}$$

The transverse reflected electric field propagate toward z with the Floquet harmonic expansion is:

$$E_1^r = \sum_{l=1}^{2L} a_1 e_1 exp(j(k_{xm}x + k_{yn}y - k_{zl}z)) \tag{2.27}$$

The normalized modal fields for TE and TM Floquet harmonics e_l are as:

for $(TE)\ 1 \leq l \leq L$

$$e_l = \frac{1}{k_{cl}}(-k_{yn}\hat{x} + k_{xm}\hat{y}) \tag{2.28}$$

for $(TM)L + 1 \leq l \leq 2L$

$$e_l = \frac{1}{k_{cl}}(k_{xm}\hat{x} + k_{yn}\hat{y}) \tag{2.29}$$

with

$$k_{cl} = \sqrt{k_{xm}^2 + k_{yn}^2} \tag{2.30}$$

$$k_{xm} = k_0 sin\theta cos\phi + \frac{2m\pi}{p_x} = k_{x0} + \frac{2m\pi}{p_x} \tag{2.31}$$

$$k_{yn} = k_0 sin\theta cos\phi + \frac{2n\pi}{p_y} = k_{y0} + \frac{2n\pi}{p_y} \tag{2.32}$$

Complex amplitude of the incident field are (d_x) and (d_y). They can be converted to $d_l(TE)$ and $d_{L+1}(TM)$ components by a matrix transformation. This transformation is as follows:

$$\begin{bmatrix} d_l \\ d_{L+1} \end{bmatrix} = \frac{1}{k_{cl}} \begin{bmatrix} -k_{y0} & k_{x0} \\ k_{x0} & k_{y0} \end{bmatrix} \begin{bmatrix} d_x \\ d_y \end{bmatrix} \tag{2.33}$$

Similarly, the TE/TM components of the reflected field $a_l(TE)$ and $a_{L+1}(TM)$ can convert to x/y components as:

$$\begin{bmatrix} a_x \\ a_y \end{bmatrix} = \frac{1}{k_{cl}} \begin{bmatrix} -k_{y0} & k_{x0} \\ k_{x0} & k_{y0} \end{bmatrix} \begin{bmatrix} a_l \\ a_{L+1} \end{bmatrix} \tag{2.34}$$

The incident and reflected fields of the reflectarray are represented by Floquet modes. They are connected to each other by the reflection coefficient. The expression for the reflection coefficient is explained using coupled-mode theory. Theoretical expression for the reflection coefficient are described in the next part.

2.2.4.5 Theoretical Expression for The Reflection Coefficient

In order to extract the reflection coefficient expression for a single element, the antenna element is considered inside a waveguide supporting Floquet modes. By considering the waveguide with two orthogonal polarized fundamental Floquet modes (TE_{00}, TM_{00}), the co-coupling and cross-coupling reflection coefficient are as follows [22]:

When the incident field is TE , the fraction of the reflected power into TE mode is called TE co-coupled reflection coefficient with the following expression [22]:

$$\Gamma_{TEco}(f) = \frac{\frac{1}{QradTE} - (\frac{1}{QradTM} + \frac{1}{Q_0}) - \frac{2j(f-f_0)}{f_0}}{\frac{1}{QradTE} + \frac{1}{Q_{radTM}} + \frac{1}{Q_0} + \frac{2j(f-f_0)}{f_0}} \tag{2.35}$$

when the incident field is TM , the fraction of the reflected power into TM mode is called TM co-coupled reflection coefficient with the following expression [22]:

$$\Gamma_{TMco}(f) = \frac{\frac{1}{QradTM} - (\frac{1}{QradTE} + \frac{1}{Q_0}) - \frac{2j(f-f_0)}{f_0}}{\frac{1}{QradTE} + \frac{1}{Q_{radTM}} + \frac{1}{Q_0} + \frac{2j(f-f_0)}{f_0}} \tag{2.36}$$

Cross-coupling is a fraction of the reflected power into (TE/TM) when the incident field is (TM/TE). The cross-coupling expression is as [22]:

$$\Gamma_{cross}(f) = \frac{\frac{2}{\sqrt{Q_{radTE}Q_{radTM}}}}{\frac{1}{QradTE} + \frac{1}{Q_{radTM}} + \frac{1}{Q_0} + \frac{2j(f-f_0)}{f_0}} \tag{2.37}$$

where, Q_{radTE} and Q_{radTM} are the radiation Q factors for the TE and TM modes, respectively. f is the working frequency. f_0 is the resonant frequency. Q_0 is a combined Q factors of conductor and dielectric losses as:

$$Q_c = d\sqrt{\pi f \mu \sigma} \tag{2.38}$$

$$Q_d = \frac{1}{tan\delta} \tag{2.39}$$

$$Q_0 = \frac{Q_c Q_d}{Q_c + Q_d} \tag{2.40}$$

where substrate thickness is (d) and the loss tangent is $tan\delta$. The effect of the incident angle and the physical parameters are obvious in the Q factor expression. As an example, the closed form expression for a rectangular microstrip patch in term of unit cell's physical parameters and the incident angle as [22]:

$$QradTE = \frac{f_0 \pi \varepsilon}{4d} \frac{l}{w} p_x p_y \frac{\eta_0}{cos\theta cos^2\phi} \tag{2.41}$$

$$QradTM = \frac{f_0 \pi \varepsilon}{4d} \frac{l}{w} p_x p_y \frac{\eta_0 cos\theta}{sin^2\phi} \tag{2.42}$$

These expressions help us to properly investigate the effect of physical parameters errors on the reflection coefficient and the radiation pattern. By substituting (5.24) ,(2.42), (2.38), (2.39) and (2.40) in (5.22),(2.36) and (2.37), the reflection coefficient of the unit cell are obtained.

If we consider incident field of the reflectarray in terms of the TE and TM Floquet harmonics (2.22), the reflected TE and TM components related to the incident Floquet harmonics by the reflection coefficients as:

$$\begin{bmatrix} E_{ref}^{TE} \\ E_{ref}^{TM} \end{bmatrix} = \begin{bmatrix} \Gamma_{TEco} & \Gamma_{cross} \\ \Gamma_{cross} & \Gamma_{TMco} \end{bmatrix} \begin{bmatrix} E_{inc}^{TE} \\ E_{inc}^{TM} \end{bmatrix} \tag{2.43}$$

By substituting (2.43) in (2.22) and consequently in the (2.17) and (2.9), the total power pattern expression can be achieved. By using analytical expression for the reflection coefficient, the analytically expression for the total power pattern is obtained. In this total power pattern, the direct relation between the radiation pattern and the physical parameters are described. The physical parameters deviate from their nominal values due to manufacturing uncertainties. This random manufacturing uncertainties produce different radiation patterns. Our goal is to define an efficient strategy to compute inclusive pattern bounds for a given maximum tolerances on the reflectarray geometrical parameters. After providing the analytical expression for the radiation pattern, the tolerance analysis should be applied in order to compute the power pattern deviation bounds. As it is mentioned in the chapter 1, Interval Analysis proved to be an efficient

tools for the tolerance analysis of the antenna. In the next chapter, Interval Analysis method with their properties and features are explained.

Chapter 3

Fundamentals of Interval Analysis

In this chapter, an overview for learning Interval Analysis is introduced. First the interval values and their need in our real life are described by examples. Then Interval Analysis approaches are defined. The rules for the arithmetic Interval operations such as addition, subtraction, multiplication and division are provided. Then the properties of Interval Arithmetic are presented. Interval function and their features are fully described in this chapter. Dependency and wrapping effect in interval arithmetic are completely explained.

3.1 Introduction

Uncertainty is part of our "every-day" life. The need to enclose the number is obvious in many different applications.In the following example, we want to show the appearance of the uncertainty in our daily life.

Suppose we want to measure the dimension of the table. The table with the dimensions is shown in the Fig (3.1).

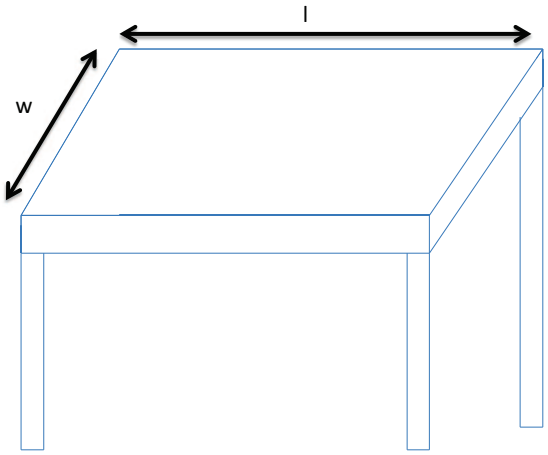

Figure 3.1: Sketch of the table and its dimension

Different measurement instruments such as tailor or caliper can be used to measure the dimensions. First we use a a tailor to measure the dimensions. The dimension are shown as follows:

$$l = 1.2 + / - 0.1m \tag{3.1}$$

$$w = 0.8 + / - 0.1m \tag{3.2}$$

Then with a caliper or more precise devices, the dimension values are as follows:

$$l = 1.20m + / - 0.01m \tag{3.3}$$

$$w = 0.80m + / - 0.01m \tag{3.4}$$

As it is clear from the measurement, uncertainty is always available regardless of the accuracy of the instrument. By using caliper, the correct length/width lies within certain ranges.

$$0.19 < l < 1.21 \rightarrow l \in [1.19, 1.21] \tag{3.5}$$

$$0.79 < w < 0.81 \rightarrow w \in [0.79, 0.81] \tag{3.6}$$

Clearly, the length and width belongs to the intervals. As it is mentioned before, uncertainty is unavoidable part of our life. We need to apply the proper mathematical tools to deal with uncertain values. I would like to explain the need for Interval Analysis by the other example from physical science. By considering Newtons law as [36]:

$$F = ma \tag{3.7}$$

If the quantity of the force F and the mass m lie in the certain ranges as:

$$F_0 - \Delta F \leq F \leq F_0 + \Delta F \tag{3.8}$$

Then the acceleration a is defined with the bounds as follows:

$$a_l \leq a \leq a_u \tag{3.9}$$

lower and upper range of the the acceleration (a_l , a_u) depends on F_0, m_0, ΔF , Δm . Since the quantity of force is not an exact value and can be defined in a certain range then the accelerations is also describe within the range whose upper and lower bounds depends on the upper and lower bounds of the force. One of the strong mathematical tool to cope with uncertain world is the Interval Analysis method. In the following section, the definition of interval numbers and the interval arithmetic rules will be described.

3.2 Interval Analysis

A real interval $[X]$ is a non-empty compact set of real numbers between and including the endpoints x_{inf} and x_{sup} [36].

$$[X] = \{x \in R : x_{inf} \leq x \leq x_{sup}\} \tag{3.10}$$

As it is shown in Fig (3.2), left end point infimum of $[X]$ and the right end point supremum of $[X]$ are the maximum and minimum of all points in the interval:

$$x_{inf} = min\{x \in [X]\} \tag{3.11}$$

$$x_{sup} = max\{x \in [X]\} \tag{3.12}$$

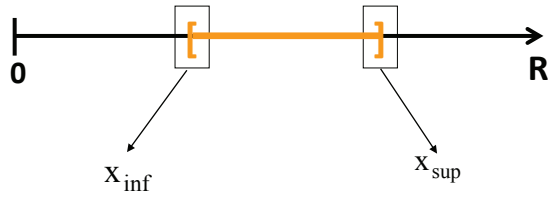

Figure 3.2: Interval end points

Two intervals $[X]$ and $[Y]$ are equal if their endpoints are equal. The absolute value of the interval $|[X]|$ is the maximum of the absolute values of its endpoints.

$$|[X]| = max\{|x_{inf}|, |x_{sup}|\} \tag{3.13}$$

Width and the midpoint of the interval $[X]$ are shown in figure (3.3). The definition of the width of the interval $[X]$ based on the endpoints is as:

$$w([X]) = x_{sup} - x_{inf} \tag{3.14}$$

Midpoint of $[x]$ is related to the endpoints given as:

$$m([X]) = \frac{x_{inf} + x_{sup}}{2}$$

Width of the interval with the interval mid-point are shown in Fig. 3.3

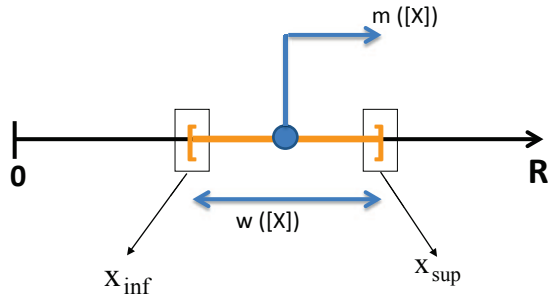

Figure 3.3: Interval midpoint and width

3.2.1 Interval Elementary Operations

Elementary operations can also be applied for the interval numbers. This elementary operations include sum, difference, product , inverse and the division. In interval domain, operations are dealing with sets than a value. By performing an operation between two intervals, the resulting is a set containing all pairs from two initial sets as given below [36]:

$$\begin{array}{c} [X]+[Y]=\{x+y : x\in[X], y\in[Y]\} \\ [X]-[Y]=\{x-y : x\in[X], y\in[Y]\} \\ [X].[Y]=\{xy : x\in[X], y\in[Y]\} \\ \frac{[X]}{[Y]}=\{\frac{x}{y}; x\in[X], y\in[Y]\} \end{array} \tag{3.15}$$

Whatever the operation is, the resulting interval enclose all the possible results.

3.2.2 Interval Arithmetic

Interval arithmetic is a set of rules for performing elementary arithmetic operations on intervals.

Endpoint Formulas for Arithmetic of Intervals

Let us show the operational formulas for the elementary operation related to boundary of intervals. For the sum of two intervals $[X]$ and $[Y]$, the operation is as [36]:

$$[X]+[Y]=[x_{inf}+y_{inf}, x_{sup}+y_{sup}] \tag{3.16}$$

The operational formula for interval subtraction in term of endpoints is as:

$$[X]-[Y]=[x_{inf}-y_{sup}, x_{sup}-y_{inf}] \tag{3.17}$$

The relation of the product of two intervals $[X]$ and $[Y]$ to their endpoints is:

$$[X][Y]=\begin{array}{c}[min(x_{inf}y_{inf}, x_{inf}y_{sup}, x_{sup}y_{inf}, x_{sup}y_{sup}), \\ max(x_{inf}y_{inf}, x_{inf}y_{sup}, x_{sup}y_{inf}, x_{sup}y_{sup})]\end{array} \tag{3.18}$$

The inverse of the interval is :

$$\frac{1}{[X]}=[\frac{1}{x_{sup}}, \frac{1}{x_{inf}}]; 0\notin[X] \tag{3.19}$$

Division of two intervals can be accomplished by using the multiplication of the interval and the inverse of the interval as:

$$[X][Y]=\begin{array}{c}[min(x_{inf}/y_{inf}, x_{inf}/y_{sup}, x_{sup}/y_{inf}, x_{sup}/y_{sup}), \\ max(x_{inf}/y_{inf}, x_{inf}/y_{sup}, x_{sup}/y_{inf}, x_{sup}/y_{sup})]\end{array} \tag{3.20}$$

$$0\notin[Y]$$

The key feature of the operation is that the operations involve the boundaries of the intervals such as x_{inf}, x_{sup}, y_{inf} and y_{sup}. The resulting interval include all the possible results.

3.2.3 Properties of the Interval Arithmetic

3.2.4 Algebraic Properties

Interval addition and multiplication are commutative and associative. Let us consider three intervals $[X]$ and $[Y]$ and $[Z]$, the commutative and associative features are shown as [36]:

$$\begin{array}{c} [X]+[Y]=[Y]+[X] \\ [X]+([Y]+[Z])=([X]+[Y])+[Z] \\ [X].[Y]=[Y].[X] \\ [X].([Y].[Z])=([X].[Y]).[Z] \end{array} \tag{3.21}$$

0 and 1 are additive and multiplicative identity element in the interval domain.

$$0+[X]=[X]+0 \tag{3.22}$$

$$1.[X]=[X].1=[X] \tag{3.23}$$

$$0.[X]=[X].0=0 \tag{3.24}$$

In a real numbers, $-x$ is an additive inverse for x. But this is not true in interval domain. In interval systems for any interval $[X]$, we have:

$$[X]+(-[X])=[x_{inf},x_{sup}]+[-x_{sup},-x_{inf}]=[x_{inf}-x_{sup},x_{sup}-x_{inf}] \tag{3.25}$$

If $x_{xup}=x_{inf}$ then this equals $[0,0]$. Otherwise

$$[X]-[X]=w[X][-1,1] \tag{3.26}$$

There is no multiplicative inverses except $w[X]=0$, in general we have

$$\frac{[X]}{[X]}=\begin{cases} [\frac{x_{inf}}{x_{sup}},\frac{x_{sup}}{x_{inf}}]\ if\ 0<x_{inf} \\ [\frac{x_{sup}}{x_{inf}},\frac{x_{inf}}{x_{sup}}]\ if\ x_{sup}<0 \end{cases} \tag{3.27}$$

For the interval systems we have the following inequality:

$$[X]([Y]+[Z])\neq[X][Y]+[X][Z] \tag{3.28}$$

This rule can be shown by considering three following intervals as

$$[X]=[1,2],[Y]=[1,1],[Z]=-[1,1] \tag{3.29}$$

Left side of the (3.28) by considering the values of 3.29 is as:

$$[X]([Y]+[Z])=[1,2].([1,1]-[1,1])=[1,2].[0,0]=[0,0] \tag{3.30}$$

Whereas, the right side by using interval arithmetic rules is as:

$$[X][Y] + [X][Z] = [1,2].[1,1] - [1,2].[1,1] = \\ [min(1,2), max(1,2)] - [min(1,2), max(1,2)] = [1,2] - [1,1] = [-1,1] \tag{3.31}$$

As it is shown in (3.30) and (3.31), the right and left side are not equal. If $[Y][Z] > 0$ then $[X]([Y]+[Z]) = [X][Y]+[X][Z]$ hold true. In general, following rule hold true for the interval.

$$[X]([Y] + [Z]) \subseteq [X][Y] + [X][Z] \tag{3.32}$$

A real number can multiply to the summation of two intervals as:

$$x([Y] + [Z]) = x[Y] + x[Z] \tag{3.33}$$

Cancellation law is also valid in interval systems:

$$[X] + [Z] = [Y] + [Z] \Rightarrow [X] = [Y] \tag{3.34}$$

3.2.5 Inclusion Property of Interval Arithmetic

If we consider two intervals $[x] = [x_{inf}, x_{sup}]$,$[y] = [y_{inf}, y_{sup}]$ and perform the operation between two intervals, the resulting interval $[Z] = [X]op[Y]$ from whatever operation between two intervals includes all values $z = \{xopy\}$(belongs to $[Z]$ (i.e.,$z \in [Z]$)) which is the resulting $z = \{xopy\}$ value from the same operation on the real numbers of the $x \in [X]$ and $y \in [Y]$.

3.2.6 Interval Function

Interval function is an interval valued function of one or more intervals arguments. Let us consider f as a real-valued function of a variable x. The range of $f(x)$ as x represent by interval $[X]$ is the interval function. In more general case for a given function $f = f(x_1, ..., x_n)$ of several variables, the interval of f is as:

$$f([X_1], ..., [X_n]) = \{f(x_1, ..., x_n) : x_1 \in [X_1], ..., x_n \in [X_n]\} \tag{3.35}$$

where $[X_1], ..., [X_n]$ are specific intervals. An example of the interval function is shown in Fig. (3.5)

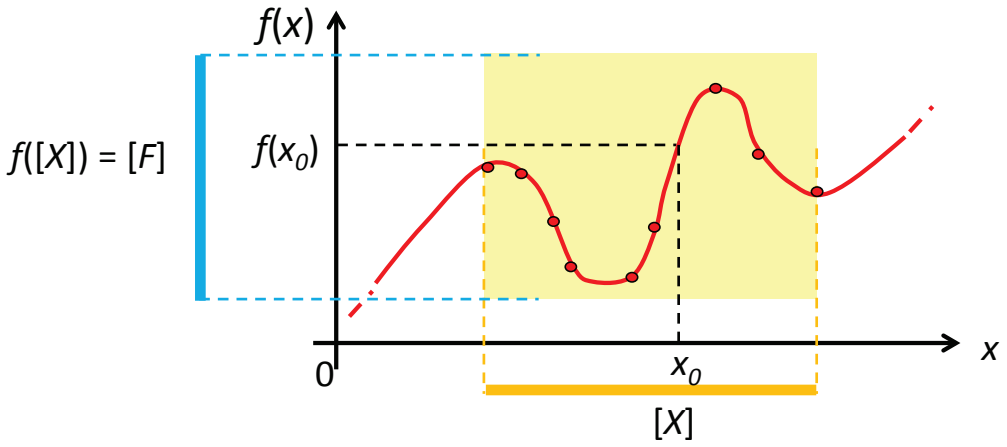

Figure 3.4: Interval function

Let us consider elementary function of intervals by providing following function $f(x) = x^2$, if $[X] = [x_{inf}, x_{sup}]$then the interval of $f[X]$can be expressed as follows:

$$f([X]) = \begin{cases} [x_{inf}^2, s_{sup}^2], 0 \leq x_{inf} \leq x_{sup} \\ [x_{inf}^2, s_{sup}^2], x_{inf} \leq x_{sup} \leq 0 \\ [0, max\{x_{inf}^2, x_{sup}^2\}], x_{inf} \leq 0 \leq x_{sup} \end{cases} \tag{3.36}$$

Monotonic Functions

If $f(x)$ is a monotonic, it maps the interval $[X] = [x_{inf}, x_{sup}]$ into interval $f([X]) = [f(x_{inf}), f(x_{sup})]$. As an example, $f(x) = exp(x) = e^x (x \in R)$ then $exp[X] = [exp(x_{inf}), exp(x_{sup})]$. Similarly for logarithmic is a monotonic function and its interval is,

$$\begin{gathered} f(x) = logx(x > 0) \\ log[X] = [logx_{inf}, logx_{sup}] \end{gathered} \tag{3.37}$$

The expression for the square root of interval is as:

$$\sqrt{[X]} = [\sqrt{x_{inf}}, \sqrt{x_{sup}}] \tag{3.38}$$

3.2.7 Interval Function Property

If $[F] = f([X])$ is an interval extension of the function f then the interval function $f([X]) = [F]$ must include all the values $f(X)$ for $x \in [X]$.

3.2.8 Inclusion Monotonicity

An interval function $f([X_1], [X_2], ..., [X_N])$ is inclusion monotonic with respect to function $f(x_1, x_2, ..., x_N)$ when $[F] = f([X_1], [X_2], ..., [X_N])$ contains the range

of values of $f(x_1, x_2, ..., x_N)$ for all $x_n \in [x_n] n = 1, ..., N$. If we consider $f([X]) = [F]$ and $[X'] \subseteq [X]$ then $[F'] = f([X']) \subseteq [F] = f([x])$ [37]. Inclusion monotonicity property is shown in Fig (3.5) .

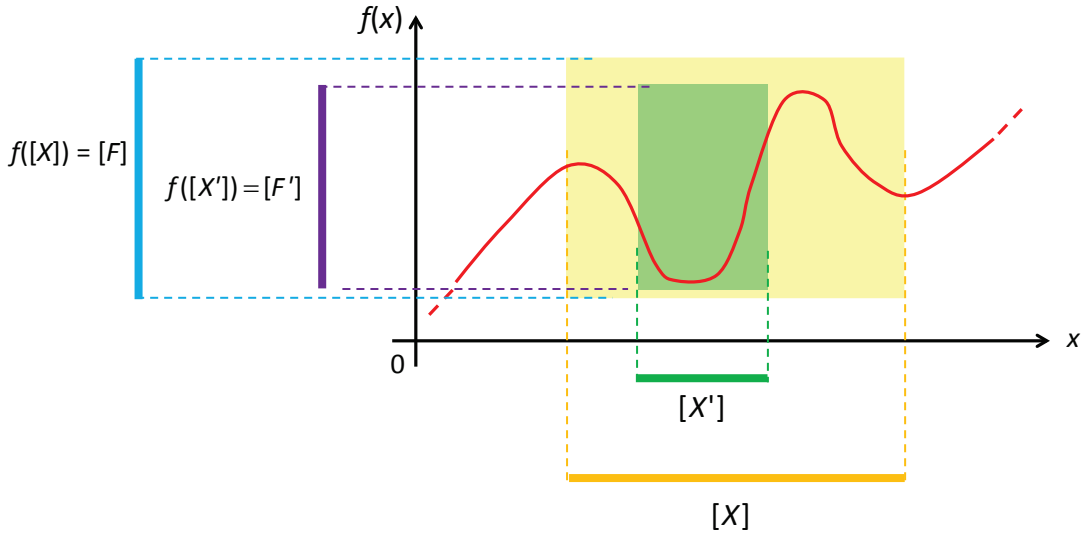

Figure 3.5: Inclusion Monotonicity

As it is obvious, if $[X'] \subseteq [X]$ then $[F'] = f([X']) \subseteq [F] = f([x])$.

3.2.9 Dependency Problem

In general, each occurrence of a given variable in an interval computation is treated as a different variable. This cause widening of computed sharp numerical bounds. This unwanted extra interval width is called the dependency problem.

Let us suppose we want to evaluate the interval perimeter $[P]$ of a rectangular table which has a interval length $[L] = [1.19, 1.21]$ and width $[W] = [0.79, 0.81]$. We apply two different ways to compute:

- First adding intervals of the $[L]$ and $[W]$: $[P] = [L] + [W] = [1.98, 2.02]m$
- Subtracting $[W]$ and $[L]$ from $[2P]$: $[P] = [2P] - [W] - [L] = [1.94, 2.06]m$

As it is shown, two different results are achieved from the same quantity. The appearance of the dependency effect in subtracting $[W]$ and $[L]$ from $[2P]$ is explained with details:

$$\begin{gathered}[P] = [2P] - [W] - [L] = [W] + [W] + [L] + [L] - [W] - [L] = \\ +[L] + ([W] - [W]) + ([L] - [L]) = \\ +[1.19, 1.21] + ([0.79, 0.81] - [0.79, 0.81]) + ([1.19, 1.21] - [1.19, 1.21]) = \\ [1.98, 2.02] + ([-0.02, 0.02] + [-0.02, 0.02]) = \\ [1.98, 2.02] + [-0.04, 0.04] = [1.94, 2.06]m\end{gathered} \tag{3.39}$$

As we can see in (3.39) , $[W] - [W] \neq 0$ and $[L] - [L] \neq 0$, this is because of the dependency effect in the interval analysis. Every occurrence of an interval variable is considered as an independent variable $[W] - [W] = [W_1] - [W_2]$ even if $[W] = [W_1] = [W_2]$ are the same interval. The dependency problem increase the width of the resulting interval. Following rules can be applied to avoid dependency problem:

- Reduce the number of occurrence of each variable: as an example of interval perimeter of the table

$$[P] = [W] + [W] + [L] + [L] - [W] - [L] \rightarrow [P] = [W] + [L]$$

- Redefine interval operations/functions $[W] - [W] = 0$ instead of $[w_{inf} - w_{sup}, w_{sup} - w_{inf}] \neq 0$

By using proper interval function definition, the optimal interval solution will be obtained.

3.2.9.1 Dependency Problem in Interval Function

Assume that we have the functions $f(x) = f_1(x) = f_2(x)$ then we want to evaluate interval extension of f . Interval extension of $f_1([X])$ and $f_2([X])$ has the bounds of $[F_1]$ and $[F_2]$. These two bounds are not the same. $[F_1]$ and $[F_2]$ include all values of $f(x)$ for $x \in [X]$ but $w([F_1])$ is larger than $w([F_2])$. As it is clear, $f_1(x) = f_2(x)$ for same $[X]$, but $f_1([X]) \subset f_2([X])$. The reason is the dependency in the interval function. To solve this problem, we need to define a function in a suitable way. In the following example, the dependency effect in the interval function will be shown. Let us evaluate $f(x) = x^2 + 1$ over interval $[X] = [-1, 2]$. The interval bounds by interval arithmetic rules are as follows:

$f([-1, 2]) = [-1, 2].[-1, 2] + [1, 1] = [min(1, -2, -2, 4), max(1, -2, -2, 4)] + [2, 2] = [-2, 4] + [1, 1] = [-1, 5]$

Since the value of $[X]^2 + 1$ can not be a negative value therefore the bounds are not the proper bounds. There is the dependency problem. In order to remove the dependency problem, we need to apply proper definition of non-elementary functions. Suitable definition for removing dependency from $[X]^2$ is as:

$$[X]^2 = \begin{cases} [x_{inf}^2, x_{sup}^2] \; if \; x_{inf} \geq 0 \\ [x_{sup}^2, x_{inf}^2] \; if \; x_{sup} \leq 0 \\ [0, max(x_{inf}^2, x_{sup}^2)] \; if \; x_{inf} \leq 0 \leq x_{sup} \end{cases} \tag{3.40}$$

We will evaluate the function$f(x) = x^2 + 1$ over the interval $[-1, 2]$ after using the proper definition for $[X]^2$. The bounds are as follows:

$$f([-1, 2]) = [-1, 2]^2 + [2, 2] = [0, 4] + [1, 1] = [1, 5] \tag{3.41}$$

As compared to previous bounds, with this method, better bounds are achieved and the inclusion property is satisfied. Another way to remove the dependency is redefining the interval function. It will be defined by the following examples. Interval of $f(x) = x^2 + x$ over $[-1, 1]$ by using natural interval extension is:

$$[-1, 1]^2 + [-1, 1] = [0, 1] + [-1, 1] = [-1, 2] \tag{3.42}$$

The better expression for $f(x) = x^2 + x$ to remove dependency is when x only appear once. We can rewrite the expression $f(x) = x^2 + x$ as follows:

$$f(x) = (x + \frac{1}{2})^2 - \frac{1}{4} \tag{3.43}$$

Therefore the bounds are :

$$([-1, 1] + \frac{1}{2})^2 - \frac{1}{4} = [-\frac{1}{2}, \frac{3}{2}]^2 - \frac{1}{4} = [0, \frac{9}{4}] - \frac{1}{4} = [-\frac{1}{4}, 2] \tag{3.44}$$

By rewriting the expression, more meaningful bounds are achieved.

3.3 Complex Intervals

A complex interval $[Z]$ is an ordered pair of intervals $[Z] = [[X], [Y]]$ with $[X] = [x_{inf}, x_{sup}]$ and $[Y] = [Y_{inf}, Y_{sup}]$ real intervals. Complex interval with the bounds for the real and imaginary parts are shown in Fig. 3.6 [38].

$$[Z] = \{z = (x + iy) \in C; x_{inf} \leq x \leq x_{sup}; y_{inf} \leq y \leq y_{sup}\} \tag{3.45}$$

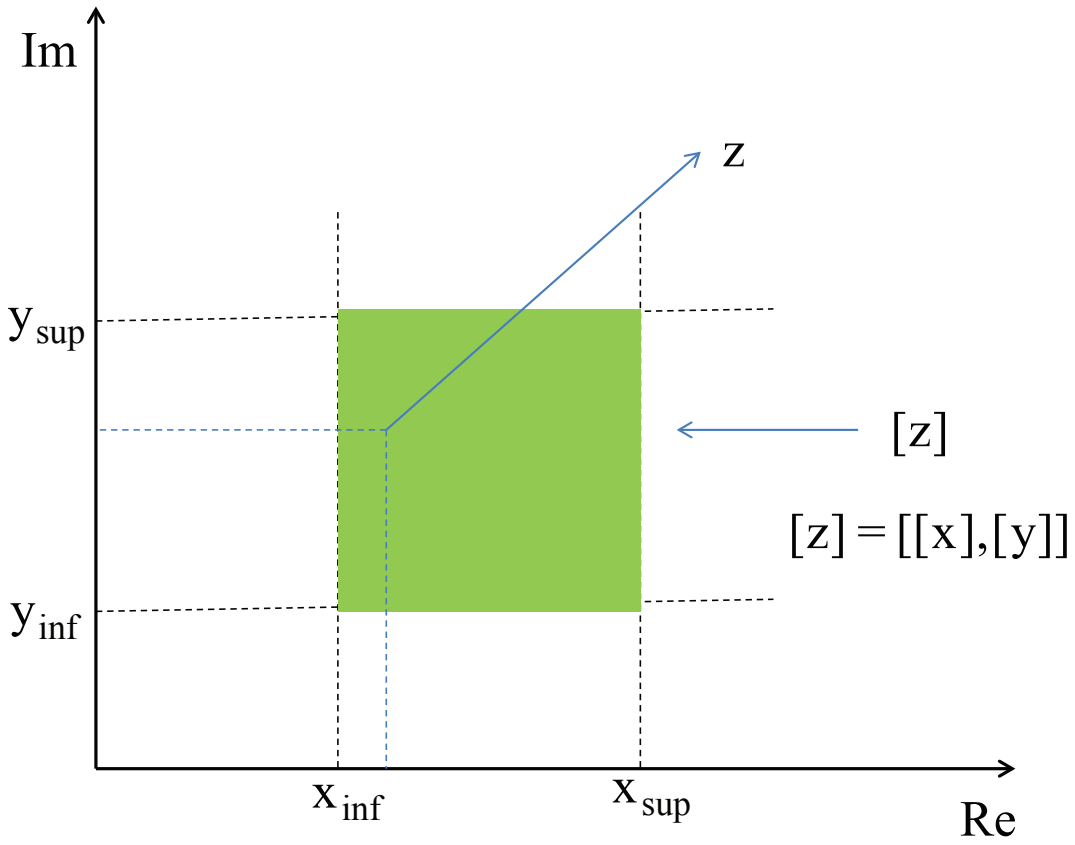

Figure 3.6: Complex Interval Value

Let us consider complex elementary operations by two complex intervals $[Z] = [X, Y]$ and $[Z^{'}] = [X^{'}, Y^{'}]$ whose real and imaginary parts have the following intervals [38]:

$$\begin{array}{c} [X] = [X_{inf}, X_{sup}]\ [Y] = [Y_{inf}, Y_{sup}] \\ [X^{'}] = [X^{'}_{inf}, X^{'}_{sup}]\ [Y^{'}] = [Y^{'}_{inf}, Y^{'}_{sup}] \end{array} \tag{3.46}$$

Elementary operations on the complex intervals are as follows:

- Sum:

$$[Z] + [Z^{'}] = [X + X^{'}, Y + Y^{'}] \tag{3.47}$$

- Sum of Negative:

$$[Z] - [Z] = [0, 0] \tag{3.48}$$

- Sum of complex conjugate:

$$[Z] + [Z]^{*} = [2X, 0] \tag{3.49}$$

- Subtraction:

$$[Z] - [Z^{'}] = [X - X^{'}, Y - Y^{'}] \tag{3.50}$$

- Product:

$$[Z][Z^{'}] = [XX^{'} - YY^{'}, XY^{'} + YX^{'}]$$

- Product of Complex Conjugate:

$$[Z][Z^{*}] = [X^2 + Y^2, 0]$$

- Inverse:

$$\frac{1}{[Z]} = \frac{[X, -Y]}{[X^2 + Y^2, 0]}$$

- Division:

$$\frac{[Z]}{[Z^{'}]} = [\frac{(xx^{'} + yy^{'})}{(x^{'2} + y^{'2})}, \frac{(yx^{'} - xy^{'})}{(x^{'2} + y^{'2})}]$$

The main feature of the previous operations is that they involve real intervals $[X], [Y], [X^{'}], [Y^{'}]$.

3.3.1 Complex Interval Function

Evaluation of complex interval function react as evaluation of real interval functions. Following features hold true for complex intervals:

- Results for real hold true also for complex interval functions
- Dependency problem still remains
- Inclusion theorem holds true for complex interval functions

3.3.1.1 Wrapping Problem

Wrapping problem is related to the representation of complex intervals. Complex interval can be presented by Cartesian interval representation and Polar interval representation. Curved in red is the Cartesian representation and the curve in blue is the polar representation. In Cartesian interval representation, there is an overestimation in the interval bounds which called wrapping effect as it is shown in Fig(3.7).

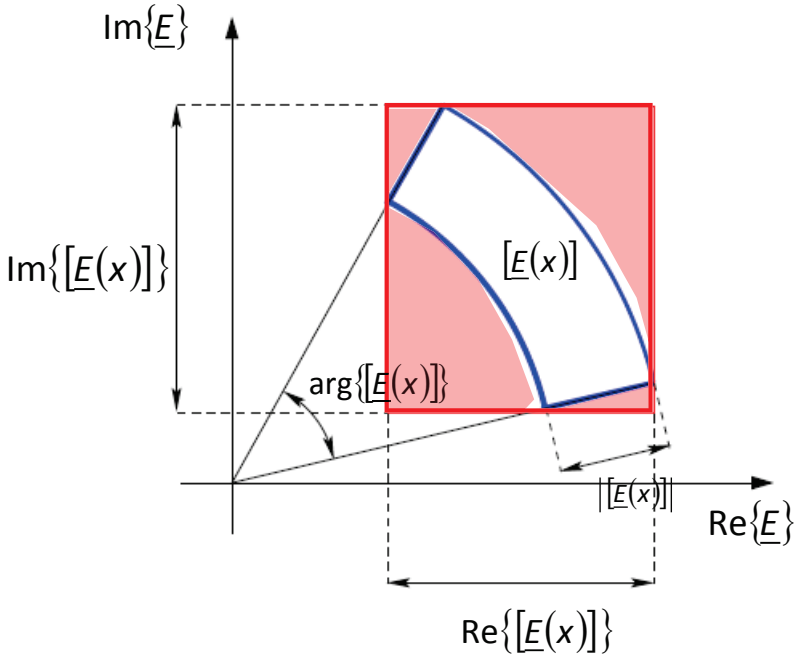

Figure 3.7: Wrapping Effect of The Complex Interval

As it is clear in the Fig (3.7), by polar representation the overestimation of the power bounds will be eliminated.

- **Cartesian Interval Representation**

In Cartesian Interval, complex interval represented in terms of the interval of real and imaginary parts. Classical IA methods are used in complex interval computation. Interval arithmetic for Cartesian Interval is simple and available. In Fig 3.8 , we can see the example for the summation of two complex interval with Cartesian representation. Overestimation will be happened in using complex interval with Cartesian representation.

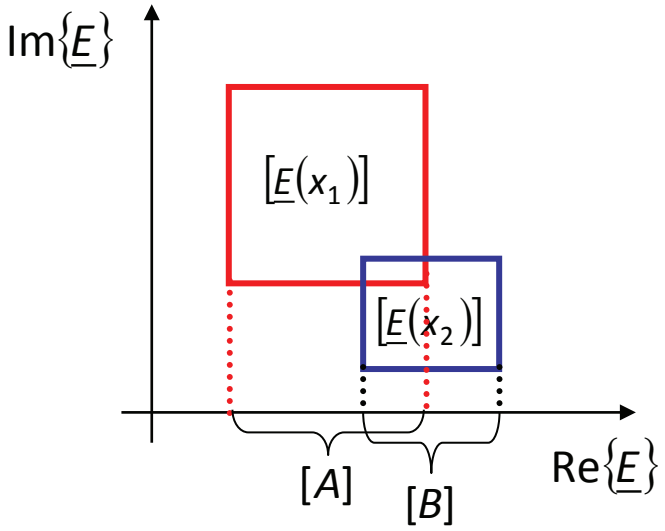

Figure 3.8: Cartesian Interval Representation

- **Polar Interval Representation**

Complex interval can be presented by polar representation as shown in Fig. 3.9. Polar representation is the best representation for the complex interval (4.3). However interval arithmetic are not available for this representation.

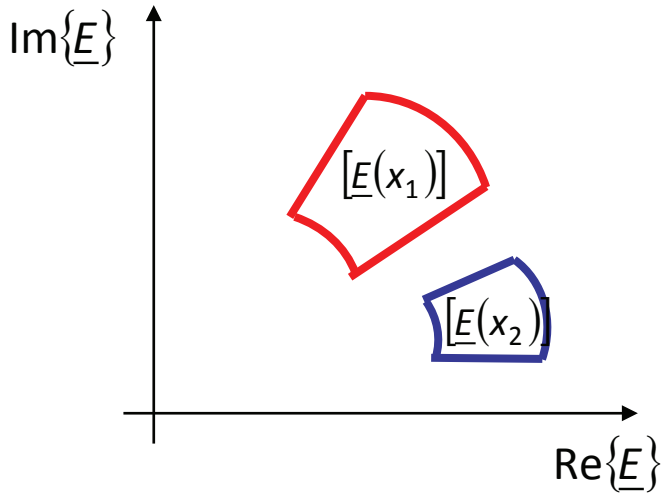

Figure 3.9: Polar Interval Representation

Chapter 4

Interval Analysis Method for Reflectarray Antennas

In this chapter, the interval extension of the reflectarray antenna is described and assessed. Uncertainty on etching patch dimensions and constructing substrate thickness are modeled with interval values. By exploiting interval arithmetic rules, bounds of the deviation in the radiation field are obtained. By reformulating the interval extension function and using Enumerative strategy, Dependency effect is removed. Some comparative results are shown the process. Wrapping effect is also eliminated by using Minkowski sum approach. Some results are reported for the assessment as well as for comparison purposes.

4.1 Introduction

In this chapter, inaccuracies in etching the microstrip patches and constructing the substrate thickness are modeled via interval values. Then the bounds of the deviation in the power pattern as a result of the bounded random errors in the patch length, width, substrate thickness and the dielectric permittivity are computed. This approach is proved to be a useful tool in reflectarray antenna to compute the worst-case bound. Cartesian interval analysis ($IA-CS$) can be used to compute the power pattern deviations of the reflectarray antenna. Nominal power pattern of the reflectarray antenna is analytically computed by the Aperture Field method together with the analytical expression of the reflection coefficient [22]. As it is mentioned in the previous chapter, $IA-CS$ has the dependency and wrapping problem in dealing with complex structure which can make an overestimation in the power pattern [39]. Dependency problem appears due to the use of an interval variable more than once in the interval function. However, Wrapping problem arises from the representation of the $IA-CS$ in the complex domain. Using $IA-CS$ for reflectarray interval analysis cause the overestimation in the power bounds [40]. In this chapter, a solution for removing redundancy problems are properly explained. This redundancy will appear in the interval extension of the reflectarray power pattern. To tackle the Dependency problem, the complex reflection coefficient of each cell is rewritten in the proper way and it is extended to the interval function ($IA-CS^*$). Since in the reflection coefficient function, parameters are recursively connected to each other, we could not eliminate all dependency problem by rewriting the function. In order to fully eliminate this problem, an enumerative strategy is used by sampling among the interval of the geometrical parameters. The maximum and minimum of the phase and amplitude of the complex reflection coefficient for these samples are computed ($IA-ENUM$) [52]. The wrapping problem can be solved by means of the Minkowski sum ($IA-ENUM-MS$) . In Minkowski sum approach, instead of using rectangular and circular representation of intervals, interval phasors are considered [42]. The smallest convex polygon encircling these interval phasors is used to compute the interval Minkowski convex polygon. The upper and lower bounds are computed among the vertices of the resulting polygons. The final bounds are narrower, reliable and still inclusive. The validity of the $IA-ENUM-MS$ bounds are checked with the number of the Monte Carlo patterns. A number of comparative results shows the improvement in the $IA-CS$ bounds with respect to the $IA-ENUM-MS$. These comparative bounds are considered for the error on all geometrical parameters such as width, length, substrate thickness and dielectric permittivity.

4.2 Mathematical Formulation

Let us consider a reflectarray antenna as it is shown in Fig (4.1), lying on the xy-plane whose rectangular microstrip patches are located on a square grid with inter-element spacing p_x and p_y along the x and y direction, respectively. To compute radiation pattern analytically, we consider Aperture Field Method [35]. The radiated far field is obtained from the following expression [10].

$$\underline{E}(\theta,\phi) = \frac{e^{-jkr}}{r}\left[(\underline{\hat{\theta}}cos\phi - \underline{\hat{\phi}}sin\phi cos\theta)\widetilde{E}_{Rx}(u,v) + (\underline{\hat{\theta}}sin\phi + \underline{\hat{\phi}}cos\phi cos\theta)\widetilde{E}_{Ry}(u,v)\right] \tag{4.1}$$

where $j=\sqrt{-1}$, $k=\frac{2\pi}{\lambda}$ is the wavenumber, λ being the wavelength, and $u=\sin\theta\cos\phi$ and $v=\sin\theta\sin\phi$ are the direction cosine coordinates with $\theta\in\left[0;\,\frac{\pi}{2}\right]$ and $\phi\in[0;\,\pi]$. $\widetilde{E}_{Rx/y}(u,v)$ (slash means x or y components) is the Fourier transformation of the Cartesian components of the tangential electric field. It can be expressed as [10]:

$$\widetilde{E}_{Rx/y}(u,v) = K\sum_{m=0}^{M-1}\sum_{n=0}^{N-1}(\Gamma_{mn}^{xx/yy}(f)A_{mn}^{x/y} + \Gamma_{mn}^{xy/yx}(f)A_{mn}^{y/x})e^{jk(ump_x+vnp_y)} \tag{4.2}$$

where

$$K = p_x p_y sinc(\frac{k_0 u p_x}{2})sinc(\frac{k_0 v p_y}{2})e^{j\frac{k}{2}[u(N-1)p_x+v(M-1)p_y]}. \tag{4.3}$$

As it is shown in Fig. 4.1, M and N are the maximum number of elements in x and y directions, respectively. As it can be seen in (4.2), tangential electric field in each cell is approximated by a complex coefficient defined as the multiplication of the complex reflection coefficient of each cell $\Gamma_{mn}^{xx/yy}(f)$,$\Gamma_{mn}^{xy/yx}(f)$, and the complex amplitude of the incident field Floquet harmonic $A_{mn}^{x/y}$, $A_{mn}^{y/x}$ illuminating the mn-th cell.

More specifically, $\Gamma_{mn}^{xx/yy}(f)$ is the co reflection coefficient of x/y-polarization when unit cell is illuminated by x/y-polarization wave. $\Gamma_{mn}^{xy/yx}(f)$ is the cross reflection coefficient of x/y-polarization when the unit cell is illuminated by y/x-polarization. We choose the reflection coefficient expression from [22], in which we can see the relationship between the complex reflection coefficient and the length l, width w, substrate thickness d and the dielectric permittivity ε_r of the element. The expression can be as the follows [22].

$$\Gamma_{mn}^{xx/yy}(f) = \frac{\frac{1}{Q_{mn}^{rad}} - \frac{1}{Q^0} - 2j\frac{f-f_{mm}^0}{f_{mn}^0}}{\frac{1}{Q_{mn}^{rad}} + \frac{1}{Q^0} + 2j\frac{f-f_{mm}^0}{f_{mn}^0}} \tag{4.4}$$

where working frequency is f, the resonance frequency of the mn-th element f_{mn}^0 , combined quality factor Q^0 and radiation quality factor of the mn-th

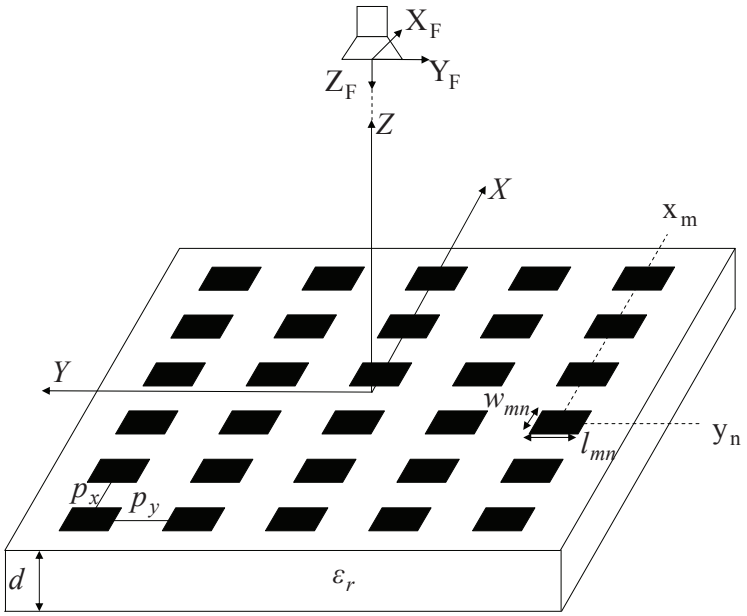

Figure 4.1: Sketch of the reflectarray antenna with its parameters .

element Q_{mn}^{rad} . Radiation quality factor in the case of rectangular microstrip patch illuminated under the normal incident plane wave is as [22]:

$$Q_{mn}^{rad} = \frac{f_{mn}^{0}\pi\varepsilon_0\varepsilon_r}{4d}\frac{l_{mn}}{w_{mn}}p_x p_y \eta_0 \tag{4.5}$$

where d and ε_r are the substrate thickness and the relative dielectric permittivity, l_{mn} and w_{mn} are the length and width of the mn-th element in the aperture of the reflectarray antenna. and η_0 is the free space wave impedance. The combined quality factor Q^0 depends on the conductor and dielectric loss quality factors Q^c and Q^d by the following expressions [22]:

$$Q^0 = \frac{Q^c Q^d}{Q^c + Q^d} \tag{4.6}$$

The expression of the conductor and dielectric loss is given by [22]:

$$Q^d = \frac{1}{tan\delta}; Q^c = d\sqrt{\pi f \mu\sigma} \tag{4.7}$$

here, $tan\delta$ is the loss tangent, μ,σ are the permeability of the free space and the metal conductivity, respectively. The relationship between the resonance frequency and the antenna geometries of the rectangular microstrip patch can be determined as follows:

$$f_{mn}^{0} = \frac{C}{2l_{eff}\sqrt{\varepsilon_{reff}}} \tag{4.8}$$

where $l_{eff} = l_{mn} + 2\delta l$ and ε_{reff} are the effective permittivity and the effective electrical length of the patch antenna. The expression for δl and ε_{reff} are defined by:

$$\delta l = 0.412d\frac{(\varepsilon_{reff} + 0.3)}{(\varepsilon_{reff} - 0.258)}\frac{(\frac{w_{mn}}{d} + 0.264)}{(\frac{w_{mn}}{d} + 0.8)} \tag{4.9}$$

$$\varepsilon_{reff} = \frac{\varepsilon_r + 1}{2} + \frac{\varepsilon_r - 1}{2}\sqrt{\frac{1}{1 + 12\frac{d}{w_{mn}}}} \tag{4.10}$$

If we substitute (4.10,4.9,4.8, 4.7,4.6,4.5) in(4.4), then by substituting (4.4) in (4.2) and (4.2,4.1), we can extract the expression which shows the relationship between the electric field and the antenna geometrical parameters. In order to realize the uncertainty in fabrication process of the antenna structure, we will apply Interval Arithmetic rules. In the following, we will define the interval extension of the previous expressions.

4.2.1 Cartesian $(IA - CS)$

Within the interval analysis approach, the actual values of the mn-th patch width (w_{mn}), length (l_{mn}), substrate thickness (d) and dielectric permittivity (ε_r) are between infimum and supermum values as follows [52]

$$[w_{mn}] = [w_{mn} - \triangle_w; w_{mn} + \triangle_w] \qquad [l_{mn}] = [l_{mn} - \triangle_l; l_{mn} + \triangle_l] \tag{4.11}$$

$$[d = [d - \triangle_d; d + \triangle_d] \qquad [\varepsilon] = [\varepsilon - \Delta_\varepsilon; \varepsilon + \Delta_\varepsilon] \tag{4.12}$$

These infimum and supremum values are calculated from the maximum tolerance error on etching patch width ($\triangle_w$) and length ($\triangle_l$). $\triangle_d$ and $\triangle_\varepsilon$ are the maximum tolerance errors on the material properties. These deviation from the actual values can affect the effective electrical length of the patch antenna, the effective dielectric permittivity, resonance frequency and the reflection coefficient. We can extract the analytical expression for the upper and lower bounds of the previous functions. In the first example, error on the patch width of the antenna is considered while other geometrical parameters are fixed in their nominal values. So the patch width is presented by interval value $[w_{mn}]$ to encompass all these random errors. Since nominal effective permittivity depends on the width of the patch. By substituting interval of the width, interval function of the effective

dielectric permittivity can be computed. Analytical expression of the lower and upper bounds of the effective dielectric permittivity is as:

$$[\varepsilon_{reff}] = [\varepsilon_{reff}^{INF}; \varepsilon_{ref}^{SUP}] \tag{4.13}$$

$$\varepsilon_{reff}^{INF} = \frac{\varepsilon_r + 1}{2} + \frac{\varepsilon_r - 1}{2}\sqrt{\frac{1}{1 + 12(\frac{d}{w_{mn} - \Delta_w})}} \tag{4.14}$$

$$\varepsilon_{reff}^{SUP} = \frac{\varepsilon_r + 1}{2} + \frac{\varepsilon_r - 1}{2}\sqrt{\frac{1}{1 + 12(\frac{d}{w_{mn} + \Delta_w})}} \tag{4.15}$$

Interval function for additional length value in effective electrical length can be extracted from its crisp function as

$$[\delta l] = 0.412d\frac{([\varepsilon_{reff}] + 0.3)}{([\varepsilon_{reff}] - 0.258)}\frac{(\frac{[w_{mn}]}{d} + 0.264)}{(\frac{[w_{mn}]}{d} + 0.8)} \tag{4.16}$$

By applying the interval arithmetic rules for the multiplication and division of two interval values, we can extract the analytical expression for the upper and lower bounds of the interval function of additional length in effective electrical length expression. If we rewrite the (4.16) as follows:

$$[\delta l] = 0.412d\frac{[G_1^{INF}; G_1^{SUP}]}{[G_2^{INF}; G_2^{SUP}]}\frac{[G_3^{INF}; G_3^{SUP}]}{[G_4^{INF}; G_4^{SUP}]} \tag{4.17}$$

Where

$$\begin{aligned} G_1^{INF} &= \varepsilon_{reff}^{INF} + 0.3; G_1^{SUP} = \varepsilon_{reff}^{SUP} + 0.3 \\ G_2^{INF} &= \varepsilon_{reff}^{INF} - 0.258; G_2^{SUP} = \varepsilon_{reff}^{SUP} - 0.258 \end{aligned} \tag{4.18}$$

$$\begin{aligned} G_3^{INF} &= \frac{w_{mn}^{INF}}{d} + 0.264; G_3^{SUP} = \frac{w_{mn}^{SUP}}{d} + 0.264 \\ G_4^{INF} &= \frac{w_{mn}^{INF}}{d} + 0.8; G_4^{SUP} = \frac{w_{mn}^{SUP}}{d} + 0.8 \end{aligned} \tag{4.19}$$

$$[\delta l] = [\delta l^{INF}; \delta l^{SUP}] \tag{4.20}$$

$$\delta l^{INF} = 0.412d\frac{min[G_1^{INF}G_3^{INF}, G_1^{INF}G_3^{SUP}, G_1^{SUP}G_3^{INF}, G_1^{SUP}G_3^{SUP}]}{max[G_2^{INF}G_4^{INF}, G_2^{INF}G_4^{SUP}, G_2^{SUP}G_4^{INF}, G_2^{SUP}G_4^{SUP}]} \tag{4.21}$$

$$\delta l^{SUP} = 0.412d\frac{max[G_1^{INF}G_3^{INF}, G_1^{INF}G_3^{SUP}, G_1^{SUP}G_3^{INF}, G_1^{SUP}G_3^{SUP}]}{min[G_2^{INF}G_4^{INF}, G_2^{INF}G_4^{SUP}, G_2^{SUP}G_4^{INF}, G_2^{SUP}G_4^{SUP}]} \tag{4.22}$$

Interval Arithmetic rules are implemented to compute the bounds of the interval functions of resonance frequency of each patch $[f_{mn}^0]$. Then with the same rules, upper and lower bounds of $[Q_{mn}^{rad}]$ are computed. Eventually according to complex interval analysis [36], bounds of the interval function are obtained. As it is clear from the crisp expression of the Fourier transform of the reflected field (4.2), Interval of the Fourier transform of the tangential electric field $[\widetilde{E}_{Rx/y}(u,v;[w_{mn}])]$ is the summation of the interval of the reflection coefficient of each cell. Here the incident feed is a y-polarized feed horn illuminating the reflectarray antenna under normal incident angle. In normal incident angle cross coupling reflection coefficient $[\Gamma_{mn}^{xy/yx}(f)]$ is zero. Therefore the interval of the Fourier transform can be presented as

$$\widetilde{[E}_{Rx/y}(u,v;[w_{mn}])] = K\sum_{m=0}^{N_x-1}\sum_{n=0}^{N_y-1}([\Gamma_{mn}^{yy}(f;[w_{mn}])]A_{mn}^{x/y})e^{jk(ump_x+vnp_y)} \tag{4.23}$$

Then the interval of the radiated far field is computed from the previous interval (4.23) as

$$[\underline{E}(\theta,\phi;[w_{mn}])] = [E_\theta(\theta,\phi;[w_{mn}])]\hat{\theta} + [E_\phi(\theta,\phi;[w_{mn}]]\hat{\phi} \tag{4.24}$$

$$\begin{gathered}[E_\theta(\theta,\phi;[w_{mn}])] = \\ \tfrac{e^{-jkr}}{r}((cos\phi)[\widetilde{E}_{Rx}(u,v;[w_{mn}])] + (sin\phi)[\widetilde{E}_{Ry}(u,v;[w_{mn}])])\end{gathered} \tag{4.25}$$

$$\begin{gathered}[E_\phi(\theta,\phi;[w_{mn}])] = \\ \tfrac{e^{-jkr}}{r}((sin\phi cos\theta)[\widetilde{E}_{Rx}(u,v;[w_{mn}])] + ((cos\phi)cos\theta)[\widetilde{E}_{Ry}(u,v;[w_{mn}]))\end{gathered} \tag{4.26}$$

Interval of the *co-* and *cross-* components of the far electric field for the y polarized feed are[10]

$$[E_{co}(\theta,\phi;[w_{mn}])] = sin(\phi)[E_\theta(\theta,\phi;[w_{mn}])] + cos(\phi)[E_\phi(\theta,\phi;[w_{mn}])] \tag{4.27}$$

$$[E_{cross}(\theta,\phi;[w_{mn}])] = cos(\phi)[E_\theta(\theta,\phi;[w_{mn}])] - sin(\phi)[E_\phi(\theta,\phi;[w_{mn}])] \tag{4.28}$$

According to the complex interval rules [33], interval of the power pattern of the *co−* and *cross−* components is

$$[P_{co}(\theta,\phi;[w_{mn}])] = [E^{\Re}_{co}(\theta,\phi;[w_{mn}])]^2 + [E^{\Im}_{co}(\theta,\phi;[w_{mn}])]^2 \tag{4.29}$$

$$[P_{cross}(\theta,\phi;[w_{mn}])] = [E^{\Re}_{cross}(\theta,\phi;[w_{mn}])]^2 + [E^{\Im}_{cross}(\theta,\phi;[w_{mn}])]^2 \tag{4.30}$$

where $[E^{\Re}_{co}(\theta,\phi;[w_{mn}])], [E^{\Im}_{co}(\theta,\phi;[w_{mn}])]$ is the real and imaginary part of *co*-polar electric field. And $[E^{\Re}_{cross}(\theta,\phi;[w_{mn}])], [E^{\Im}_{cross}(\theta,\phi;[w_{mn}])]$ are the real and imaginary parts of the *cross*-polar electric field. As it is clear in (4.16), interval of the effective dielectric permittivity and the width of the patch repeat more than once in the nominator and denominator. This repetition makes the so-called Dependency problem which overestimate the bounds. Such redundancy can be removed by the following strategies.

4.2.2 Cartesian $(IA - CS^*)$

In this part, we will show how to tackle with the Dependency effect in the Interval analysis application. If an interval parameter accrues several time in the calculation of the interval functions and each occurrence is considered separately, the unwanted resulting interval is appeared [52]. This effect can make extra bounds in the output interval. This problem can be solved by rewriting the functions in a proper way before expanding them to interval to decrease the occurrence of the interval variable. If the expression has the simple relation to the interval variable, by reformulating the expression, dependency can be fully removed. Otherwise, in the complicated interval function, reformulating can partially remove the dependency problem. In (4.31), repeating the interval values of $[\varepsilon_{reff}]$ and $[w_{mn}]$ causes dependency effect and overestimate the interval bounds in $[\delta l]$.

$$[\delta l] = 0.412d\frac{([\varepsilon_{reff}]+0.3)}{([\varepsilon_{reff}]-0.258)}\frac{(\frac{[w_{mn}]}{d}+0.264)}{(\frac{[w_{mn}]}{d}+0.8)} \tag{4.31}$$

By reformulating the interval function (4.16) in the following way, the interval variable appears only once. The dependency removed function of (4.16)(width is realized with interval values and the substrate thickness is fixed in its actual value) given by:

$$[\delta l] = 0.412(\frac{1}{1-(\frac{0.258}{[\varepsilon_{reff}]})}+\frac{0.3}{[\varepsilon_{reff}]-0.258})(\frac{d}{1+0.8(\frac{d}{[w_{mn}]})}+\frac{0.264d^2}{[w_{mn}]+0.8d}) \tag{4.32}$$

The comparison of the the upper and lower bound of the $[\delta l]$ in (4.20) and (4.32) is shown in Fig. 4.2. It is obvious that the upper and lower bounds of the interval effective electrical length with dependency effect are much larger

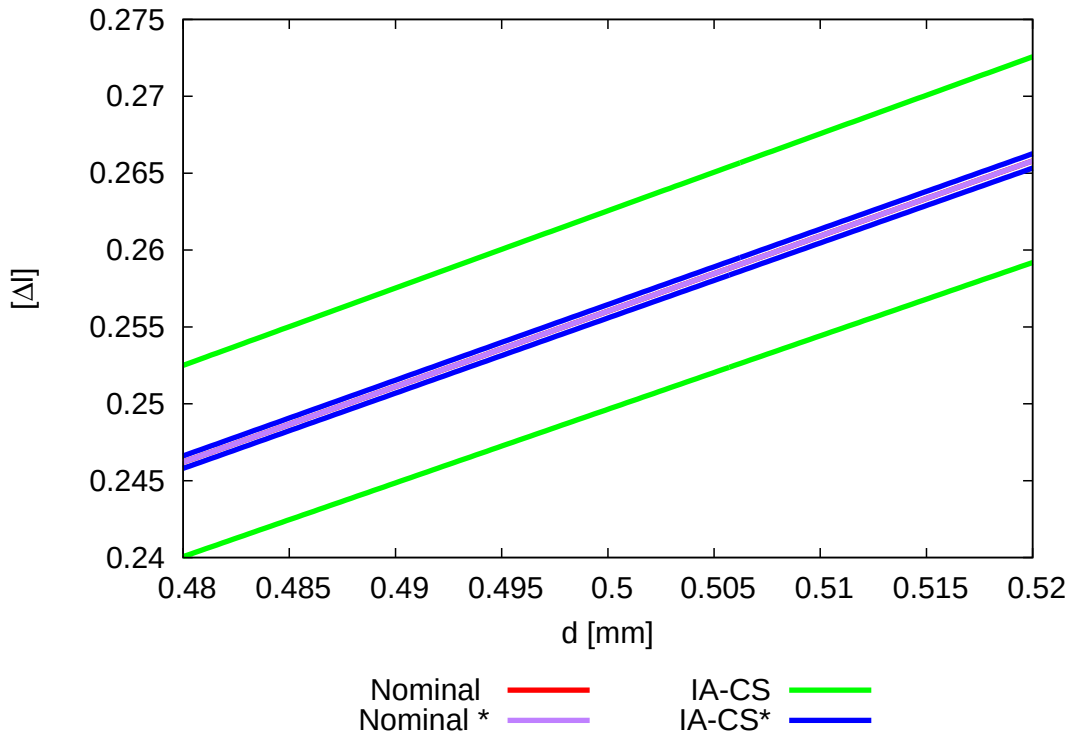

Figure 4.2: Dependency assessment - inf and sup of the effective electrical length with dependency and dependency free interval function.

than its dependency free bounds. If we consider the substrate thickness $[d]$ as an interval value and fix the patch width on its actual value, the dependency removed interval function is as follows

$$[\Delta l] = 0.412\left(\frac{1}{1-\left(\frac{0.258}{[\varepsilon_{reff}]}\right)} + \frac{0.3}{[\varepsilon_{reff}]-0.258}\right)\left(\frac{1}{\frac{1}{[d]}+\left(\frac{0.8}{w_{mn}}\right)} + \frac{0.264}{w\left(\frac{1}{[d]}+\frac{0.4}{w_{mn}}\right)^2 - \frac{0.16}{w_{mn}^2}}\right) \tag{4.33}$$

Since the power pattern expression is complicated and parameters are recursively connected to each other, by this way, dependency is partially removed. In order to remove all dependency effect, we need to implement an alternative method.

4.2.3 Enumerative Strategy $(IA-ENUM)$

By pursuing the following steps, we can find a surrogate method to suppress the dependency problem, the steps of Enumerative method are defined as:

- Step 1: Get the efficient number of sample points between the infimum and supremum of the interval values. These interval values can be a patch length, width, substrate thickness and the dielectric permittivity. By considering χ_i as a sampling parameters such as patch length and width (l_{mn}) , (w_{mn}), substrate thickness (d) and dielectric permittivity (ε_r) then the sampling procedure is as

$$\chi_i = inf\{\chi_i\} + \frac{i}{I_i}(SUP\{\chi_i\} - INF\{\chi_i\}) \tag{4.34}$$

where $i = 0, ..., I_i$, I_i is the maximum number of the sampling. For each i, there is a new value for each geometrical parameter of the patch.

- Step 2: Let us consider the behaviour of the reflection amplitude ($|\Gamma_{mn}(f, \chi_i)|$) (Fig. 4.3a) and phase ($\arg\Gamma_{mn}(f, \chi_i)$) (Fig. 4.3$b$) versus nominal parameter χ_i. Then calculate the amplitude and phase of the crisp reflection coefficient $\Gamma_{mn}(f, \chi_i)$ for each value of the sampling parameter.

- Step 3: Specify the interval amplitude and phase of the reflection coefficient of each cell by the following ways:

$$INF\{|\Gamma_{mn}(f, \chi_i)|\} = min_{i=0,...,I_i}\{|\Gamma_{mn}(f, \chi_i)|\} \tag{4.35}$$

$$SUP\{|\Gamma_{mn}(f, \chi_i)|\} = max_{i=0,...,I_i}\{|\Gamma_{mn}(f, \chi_i)|\} \tag{4.36}$$

$$INF\{[arg(\Gamma_{mn}(f, \chi_i))]\} = min_{i=0,...,I_x}\{arg(\Gamma_{mn}(f, \chi_i))\} \tag{4.37}$$

$$SUP\{[arg(\Gamma^{yy}_{mn}(f, \chi_i))]\} = max_{i=0,...,I_i}\{arg(\Gamma_{mn}(f, \chi_i))\} \tag{4.38}$$

- Step 4: Compute the Fourier transform of the reflected electric field from the interval of the reflection coefficient of step 3.

$$[\widetilde{E}^{ENUM}_{Rx/y}(u, v; [\chi_i])] = K \sum_{m=0}^{M} \sum_{n=0}^{N} [|\Gamma_{mn}(f, \chi_i)|](cos([arg(\Gamma_{mn}(f, \chi_i))]) + jsin([arg(\Gamma_{mn}(f, \chi_i))]))A^{x/y}_{mn})e^{jk(ump_x + vnp_y)}) \tag{4.39}$$

- Step 5: Compute the power pattern bounds from the same procedure in (4.29).

By this procedure, we can remove the dependency problem. The overestimation in the power pattern bounds can be decreased by the $IA - ENUM$ procedure. There is still the Wrapping effect which can enlarge the output bounds. This

effect can be prevented by using Minkowski Sum which is explained in the following.

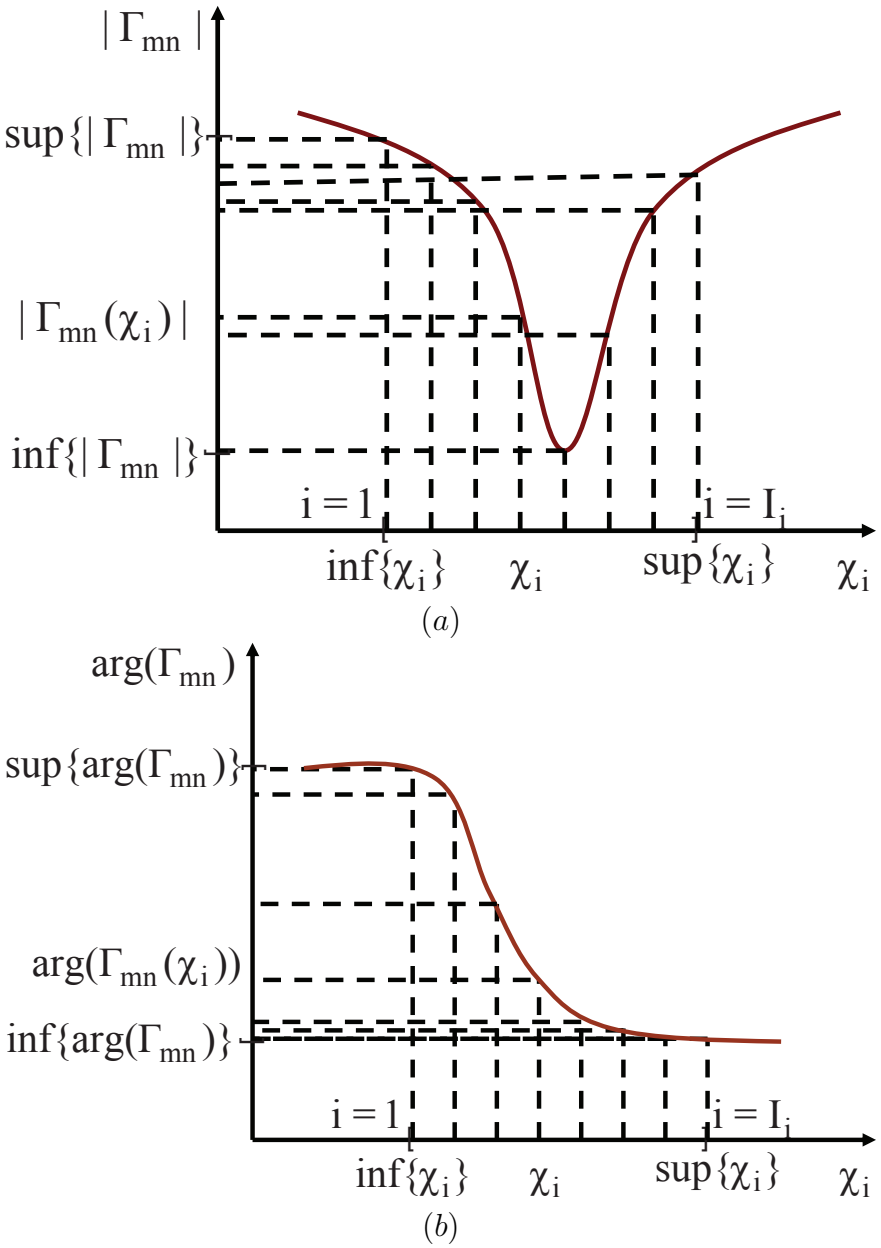

Figure 4.3: Enumerative strategy (*a*) Sampling of the amplitude of the reflection coefficient (*b*) Sampling of the reflection phase.

4.2.4 Minkowski $(IA - MS)$

The $IA - CS$, $IA - CS^*$ and $IA - ENUM$ still produce overestimated power bounds due to wrapping effect produced by rectangular representation of the complex interval in the complex domain. This redundancy is proportional to the number of elements. Since reflectarray antenna consist of several elements, we need to properly remove this obstacle from analysis. Using Minkowski sum to calculate the interval phasors can remove the relevant redundancy effect. In following, detail of the Minkowski sum computation will be defined.
Interval power pattern $[P_{co}(\theta, \phi)]$ is the function of the interval Fourier transform of the electric field $[\widetilde{E}_{Rx/y}(u, v)]$. This interval is the summation of the interval phasor of $[|\Gamma^{yy}_{mn}(f)|]e^{j[arg(\Gamma^{yy}_{mn}(f))]}$. Let us provide some details about how to perform Minkowski sum of two phasors of the first and second cells ($[A_q]q = 1, ..., Q$ and $[B_q]q = 1, ..., Q$).

- Step I, by referring to Fig. 4.4, a small convex polygons encircling the following four main vertices from the combination of the minimum and maximum of the amplitudes and phases as:

$$A_1 = INF[|\Gamma^{yy}_{11}(f)|]e^{jINF[arg(\Gamma^{yy}_{11}(f))]} \quad A_2 = SUP[|\Gamma^{yy}_{11}(f)|]e^{jINF[arg(\Gamma^{yy}_{11}(f))]} \tag{4.40}$$

$$A_Q = INF[|\Gamma^{yy}_{11}(f)|]e^{jSUP[arg(\Gamma^{yy}_{11}(f))]} \quad A_{Q-1} = SUP[|\Gamma^{yy}_{11}(f)|]e^{jSUP[arg(\Gamma^{yy}_{11}(f))]} \tag{4.41}$$

$$B_1 = INF[|\Gamma^{yy}_{12}(f)|]e^{jINF[arg(\Gamma^{yy}_{12}(f))]} \quad B_2 = SUP[|\Gamma^{yy}_{12}(f)|]e^{jINF[arg(\Gamma^{yy}_{12}(f))]} \tag{4.42}$$

$$B_Q = INF[|\Gamma^{yy}_{12}(f)|]e^{jSUP[arg(\Gamma^{yy}_{12}(f))]} \quad B_{Q-1} = SUP[|\Gamma^{yy}_{12}(f)|]e^{jSUP[arg(\Gamma^{yy}_{12}(f))]} \tag{4.43}$$

This polygon includes the edges A_1A_2 , $A_{Q-1}A_Q$, A_QA_1 and the curve A_2A_{Q-1}. The arc between A_2A_{Q-1} is approximated with number of vertices. In Fig. 4.4 we just show 3 vertices in the curve as an example. Then complex interval $[B]$ has been bounded with the convex polygons of second cell as it is seen in Fig. 4.4. The arc between B_2B_{Q-1} is approximated with the same three vertices.

- Step II, as shown in Fig. 4.4, by considering two convex polygons encircle complex phasors $[A_q]$ and $[B_q]$, Minkowski sum of these two polygons is a convex polygon. Number of vertices of the resulting polygon is at most equal to sum of vertices of polygon encircling phasors $[A]$ and $[B]$. By iteratively following this procedure the convex polygon of interval Fourier transform can be obtained.

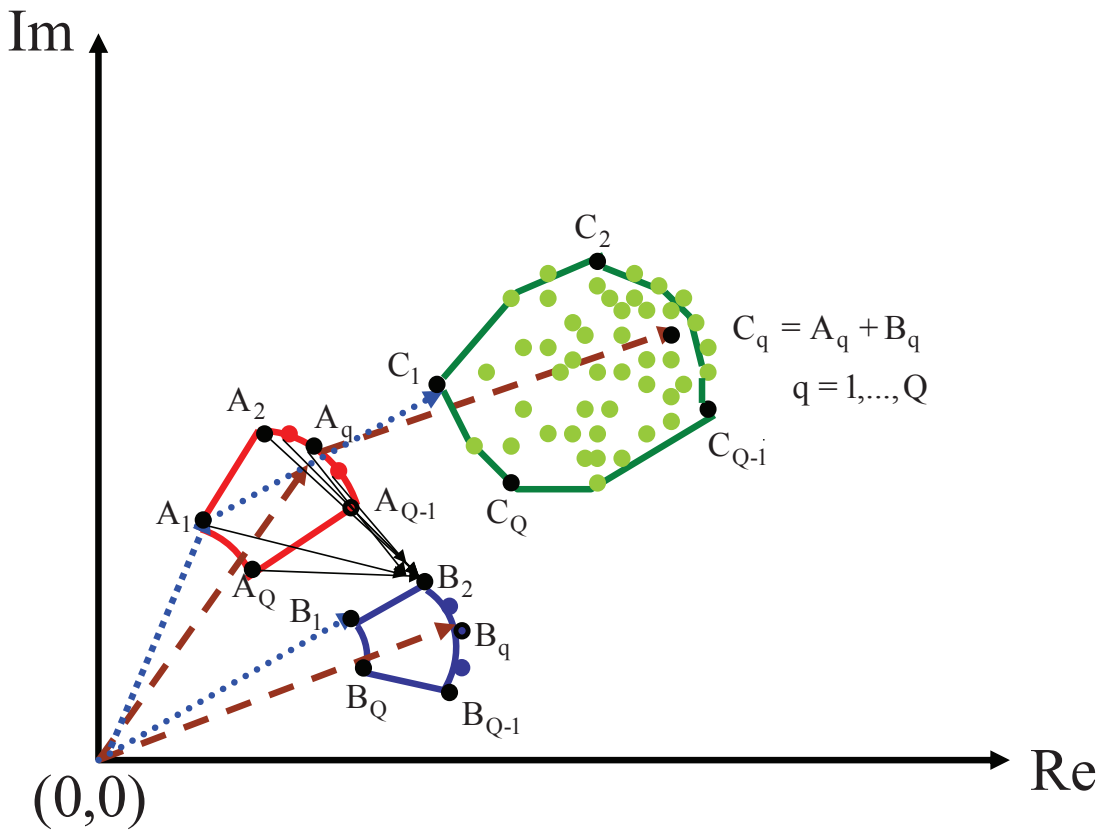

Figure 4.4: IA-Minkowski approach - Minkowski Sum of two interval phasors.

- Step III, Compute the minimum and maximum distances with respect to the center of the complex plane. This can give us the maximum and minimum bounds for $[\widetilde{E}^{ENUM-MS}_{Rx/y}(u,v)]$. Then maximum and minimum of the power pattern are computed with interval arithmetic rules as $inf[P^{ENUM-MS}(\theta,\phi)] = |inf[\widetilde{E}^{ENUM-MS}_{Rx/y}(u,v)]|^2$and $sup[P^{ENUM-MS}(\theta,\phi)] = |sup[\widetilde{E}^{ENUM-MS}_{Rx/y}(u,v)]|^2$.

Chapter 5

Interval Method Validation with Numerical Results

5.1 Introduction

In this chapter manufacturing error in fabrication of the microstrip reflectarray antenna structure is considered. Geometrical parameters of the antenna such as width, length of the patch antenna with the substrate thickness and the dielectric permittivity are deviated from their nominal values due to manufacturing errors. In order to mathematically realize these errors on the analytical computation of the radiation pattern, interval analysis technique is used. Wrapping effect is eliminated by using Minkowski sum approach. Some results are reported for the assessment as well as for comparison purposes. Then a tolerance analysis based on Interval Analysis (IA) together with Minkowski sum approach is implemented to compute the deviation bounds. Interval pattern features for different reflectarray structures with several ratios of the focal-length-to-diameter (F/D) values are computed. The proposed IA-Minkowski ($IA-MS$) based approach provide a reliable tool to predict pattern degradation.

5.1.1 Nominal Pattern Computation

For analytically compute the nominal radiation pattern, Aperture Field method together with the analytical expression of the reflection coefficient from the reference [22] is implemented. In order to be sure about the correct implementation of this analytical method, the nominal radiation pattern is compared with the state of the art for the same reflectarray structure with the following characteristic:

- Frequency- 32 GHz
- Antenna Aperture type- Circular with $15.5\lambda_0$
- Number of element- 749
- Element type- Rectangular Microstrip patch
- periodicity- $p_x = p_y = \lambda_0/2$
- substrate thickness- $d = 5$mil
- dielectric permittivity- $\varepsilon_r = 10.2$
- patch width- $w_{mn} = 2mm$
- feed antenna position- $(0, 0, 36.328mm)$
- $q = 1.5$

The phase distribution in the aperture surface is shown in Fig 5.1. H-plane radiation pattern of my implemented code is compared with the the state-of-the art as shown in Fig 5.2. E-plane radiation pattern of my software with comparison to the the state-of-the art is shown in Fig 5.3 :

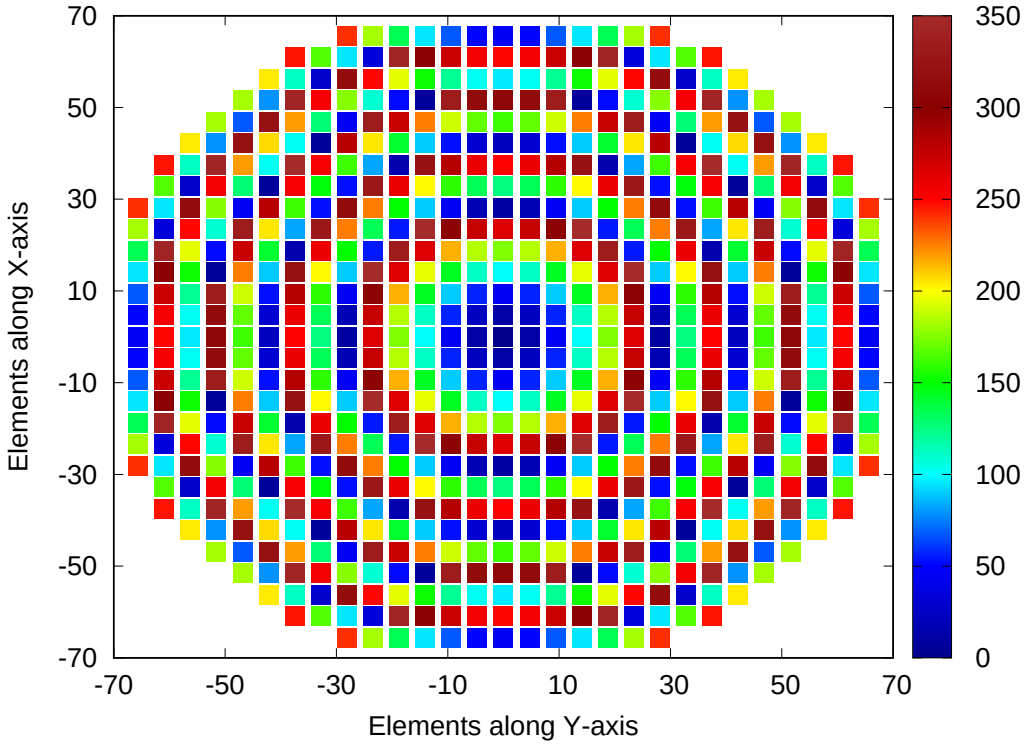

Figure 5.1: Phase distribution on the aperture surface for reflectarray with 749 elements

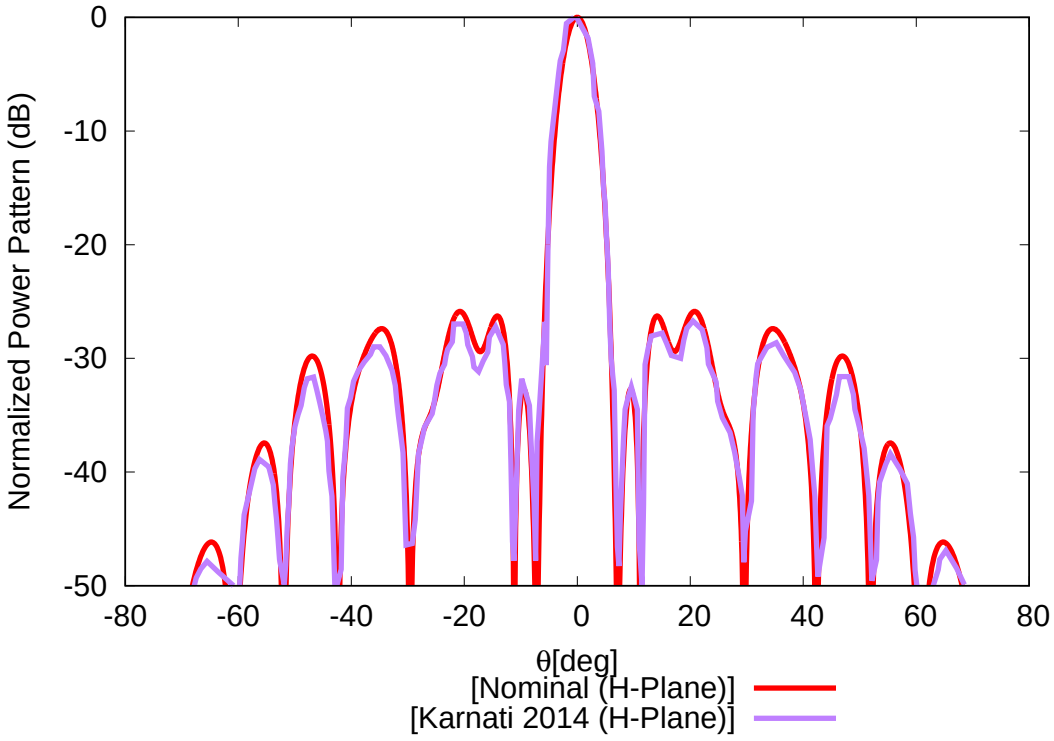

Figure 5.2: H-Plane radiation pattern with comparison with Karnati 2014

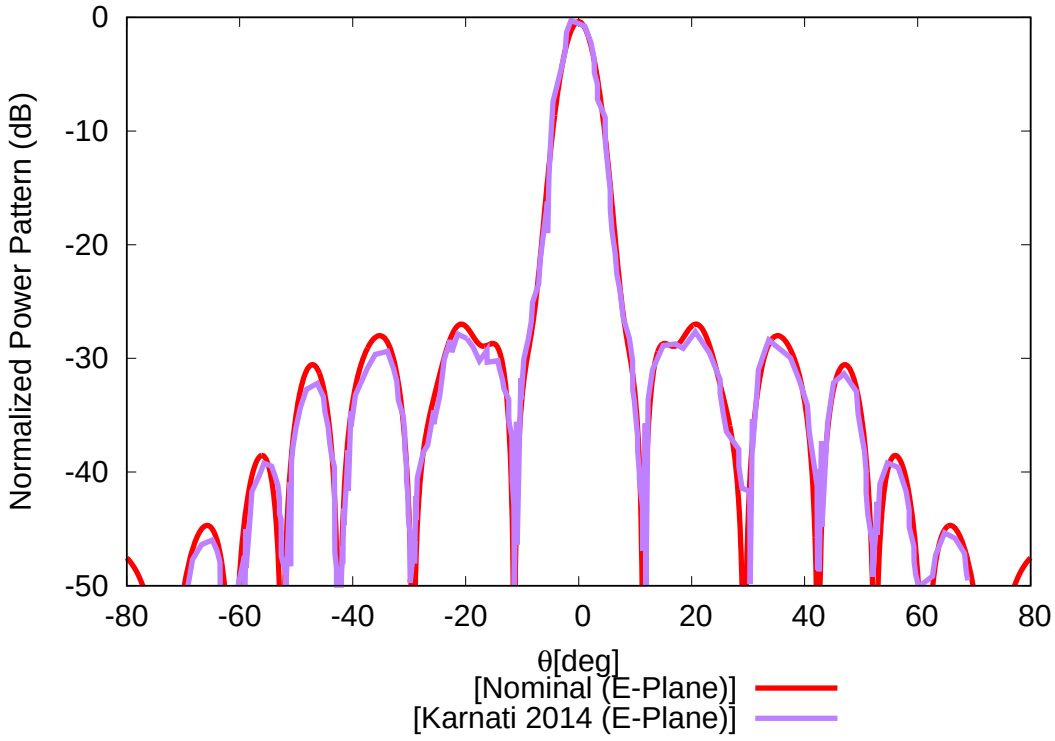

Figure 5.3: E-Plane radiation pattern with comparison with Karnati 2014

In the following part, radiation pattern is computed with the previous mentioned analytical method for the proposed reflectarray structure. Then the Interval bounds for different errors are extracted.

5.2 Interval Computation

5.2.1 Reflector Error

We want to compute the interval power bounds for the reflectarray antenna with the the following structures. Let us consider a center-fed reflectarray made of 529 isotropic rectangular microstrip patches equally-spaced along the x and y axis of $p_x = p_y = \frac{\lambda}{2}$. Reflectarray antenna has a square aperture with diameter of $11.5\lambda_0$ in 30 working frequency. Substrate is a Rogers RT580 with $d = 0.5\ mm$, $\varepsilon_r = 2.2$, $tan\delta = 0.0009$. Feed antenna is a y-polarized horn antenna in 30 GHz modeled as $cos\theta^q$ with $q = 8.5$. It is located in $z = 114.3mm$. Variable patch lengths approach in normal incident angle is used to design the array elements over the aperture surface to obtain the required phased. Nominal width value of each cell is $w_{mn} = 3.95\ mm$. The antenna power pattern antenna is computed by 4.1. Phase distribution on the aperture surface is computed by the expression of (2.25) and it is shown in Fig 5.4.

Then variable patch length approach is applied to realize the desired phase of each cell. The phase behaviour versus changing the patch length is provided in Fig 5.5

5.2.1.1 Tolerance Analysis Against Patch Error

First the impact of patch width error on the power pattern is computed.We consider maximum tolerance $\Delta_w = 50\mu m$ in the width of the patch of each cell while other parameters are fixed in their nominal values. To mathematically model this error, patch width is represented by an interval value. Therefore, real width value of the patch after manufacturing process can be one of the random values among this interval $[3.95 - 0.05, 3.95 + 0.05]$. The interval power pattern for this tolerance is computed with $IA - CS$ method. To avoid dependency problem, the interval power pattern bounds are computed by the $IA - CS^*$. This methodology is valid for simple formulas. To fully remove the dependency problem, we compute the $IA - ENUM$ power pattern bounds. Then Minkowski sum is implemented in the $IA - ENUM - MS$ computation to mitigate the Wrapping problem. The comparative interval result in $v = 0$ plane is presented in Fig.5.6. As can be seen, the $IA - ENUM - MS$ can provide the tightest bounds which avoids the meaningless result of using the other Interval methods. Following principle of

$$\begin{matrix} INF[P_{co}^{ENUM-MS}(\theta,\phi)] > \{INF[P_{co}^{CS}(\theta,\phi)]], INF[P_{co}^{CS^*}(\theta,\phi)], INF[P_{co}^{ENUM}(\theta,\phi)]\} \\ SUP[P_{co}^{ENUM-MS}(\theta,\phi)] < \{SUP[P_{co}^{CS}(\theta,\phi)]], SUP[P_{co}^{CS^*}(\theta,\phi)], SUP[P_{co}^{ENUM}(\theta,\phi)]\} \end{matrix} ,$$

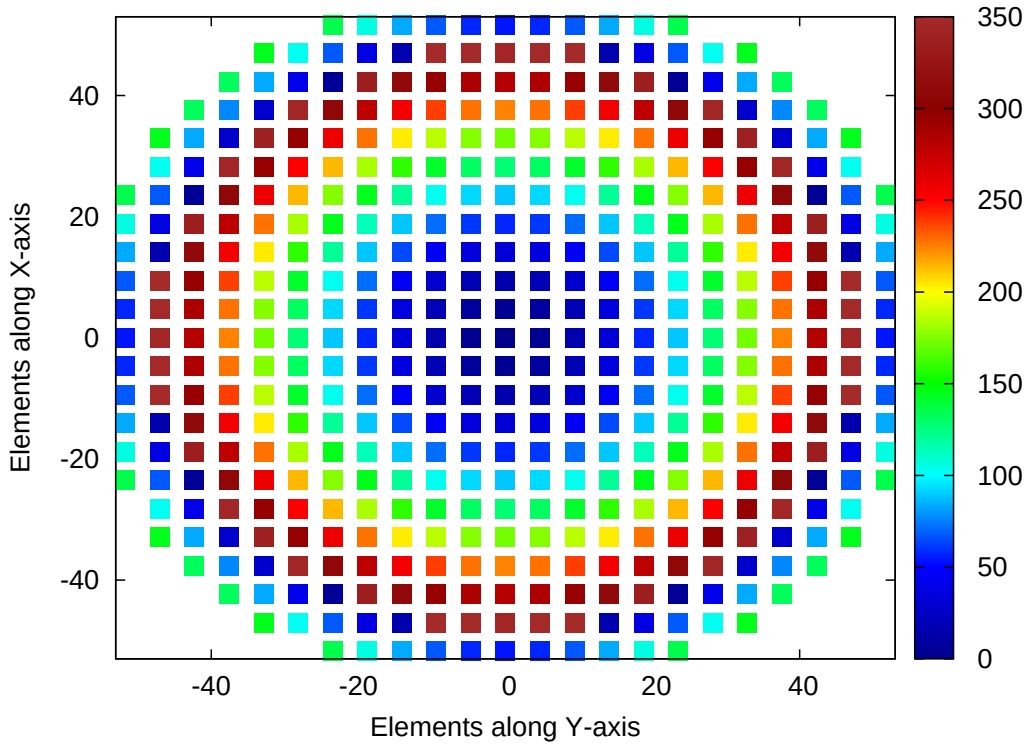

Figure 5.4: Phase distribution on the aperture surface

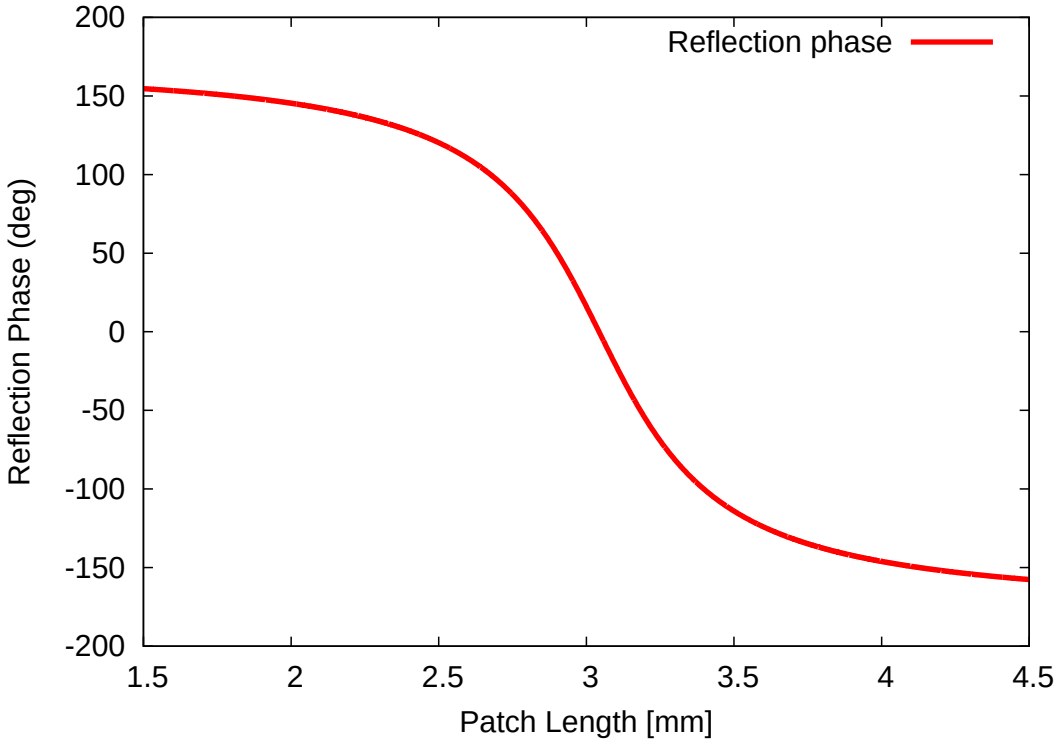

Figure 5.5: Phase behaviour versus patch length in rectangular microstrip patch

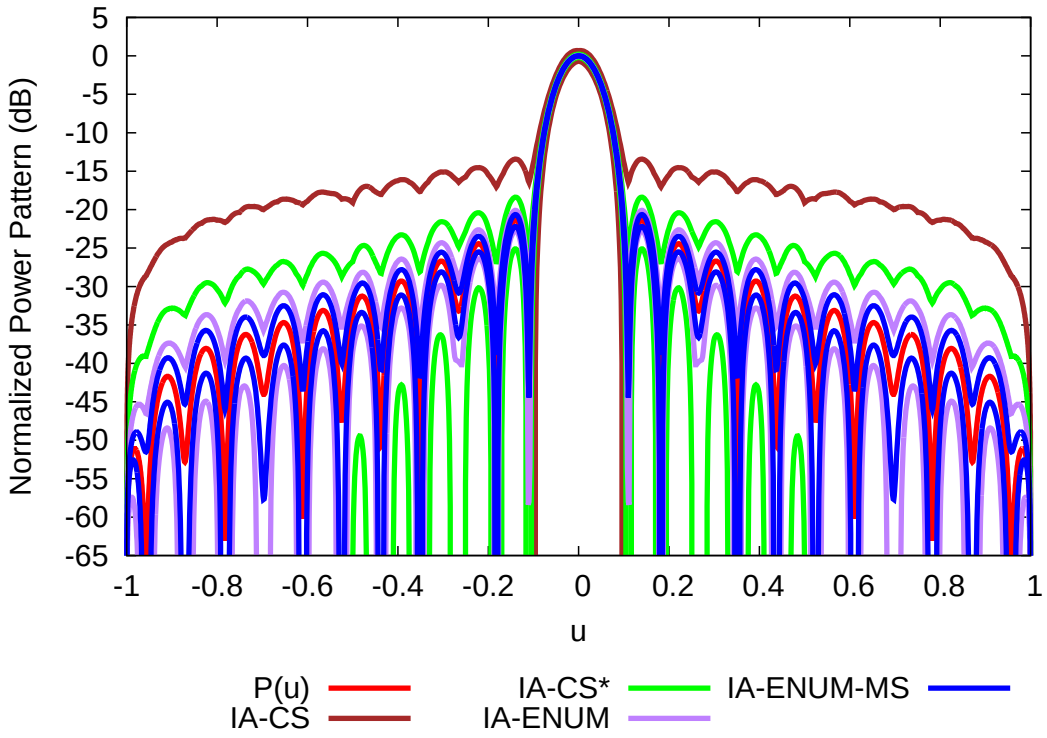

Figure 5.6: *Comparative Assessment* $\triangle w = 50\mu m$*; Plot of the interval power pattern predicted with the* $IA-CS$*, the* $IA-CS^*$*,* $IA-ENUM$*,* $IA-ENUM-MS$ *together with the nominal power patter in H-Plane* ($\phi = 0°$).

hold true. It proved that the $IA-ENUM-MS$ method can provide the tight, reliable, accurate and inclusive bounds.

In order to check the reliability of the $IA-ENUM-MS$, a Monte Carlo test with a set of $T = 5 * 10^5$ trial power patterns has been performed to cover the $IA-MS-ENUM$ bounds. In Fig.5.7, this Monte Carlo pattern is shown to cover $IA-ENUM-MS$ bounds of $\Delta_w = 50[\mu m]$ in $v = 0$ plane. It proves that the whole set of trial nominal power patterns are inside the $IA-ENUM-MS$ bounds. Closeness of the $IA-ENUM-MS$ to the upper and lower part of the Monte Carlo patterns demonstrates the reliability and effectiveness of this method.

5.2.1.2 Method Validation

To validate inclusion properties, interval power pattern for different tolerances in patch width $\triangle_w = 5, 10, 20, 50\mu m$ for two different cuts are shown in Fig. 5.8$(a)v = 0$ plane and Fig. 5.8 $(b)u = 0$ plane . Antenna pattern features such as SLL, BW, P, Δ are shown in table 5.1. In Fig. 5.9$(a)v = 0$ plane and$(b)u = 0$ plane, interval power bounds for different tolerances of $\triangle_l = 5, 10, 20, 50\mu m$ in

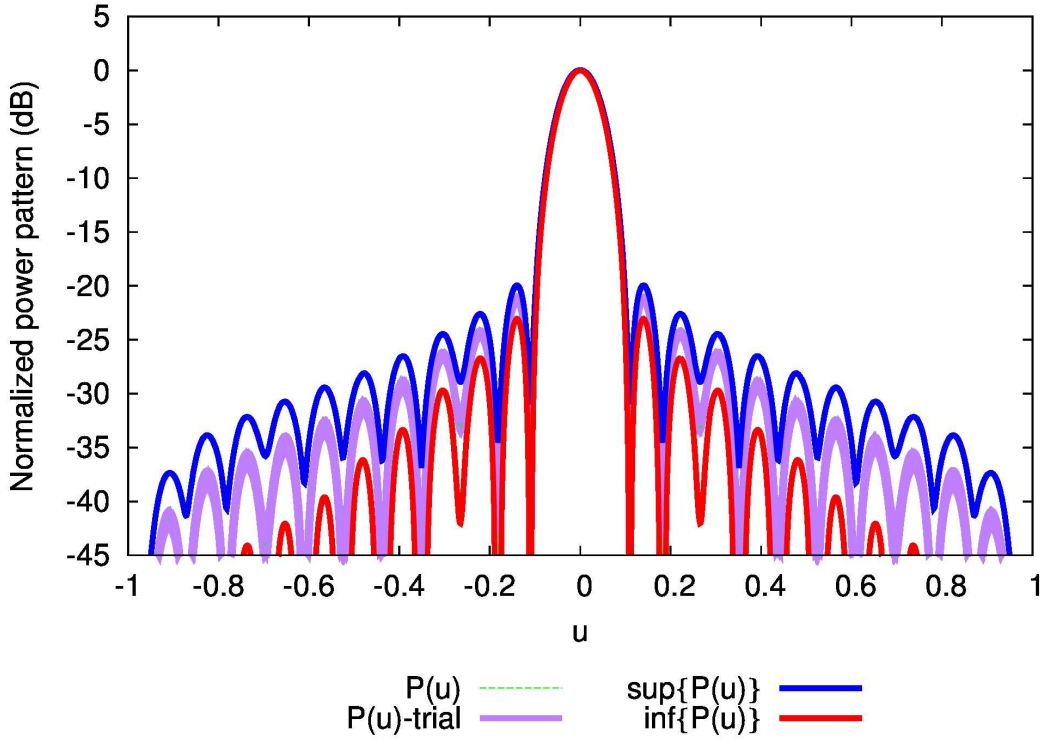

Figure 5.7: *Method Validation* - Comparison of $IA - CS$, $IA - ENUM$, $IA - ENUM - MS$ $IA - CS^*$, together with the Monte Carlo patterns $\triangle w = 50\mu m$.

$\Delta W, \mu m$	$[P(u,v)]$	$[SLL], dB$	$[BW], u$	$\Delta \times 10$
u=0				
0	0	-21.380	0.092	
5	[-0.0008,0.0006]	[-21.457,-21.304]	[0.091,0.092]	0.02
10	[-0.001,0.013]	[-21.536,-21.227]	[0.091,0.092]	0.03
20	[-0.003,0.002]	[-21.659,-21.077]	[0.091,0.092]	0.05
50	[-0.001,0.001]	[-21.659,-21.077]	[0.091,0.092]	0.07
v=0				
0	0	-22.561	0.092	
5	[-0.0008,0.0006]	[-22.657,-22.481]	[0.091,0.092]	0.02
10	[-0.001,0.001]	[-22.740,-22.385]	[0.091,0.092]	0.04
20	[-0.003,0.002]	[-22.925,-22.212]	[0.091,0.092]	0.08
50	[-0.008,0.07]	[-23.504,-21.707]	[0.09,0.09]	0.2

Table 5.1: Analysis of the IA-based pattern prediction vs. patch width errors in $u = 0$ and $v = 0$ planes, $\triangle w = \{5, 10, 20, 50\}\{\mu m\}$- Interval pattern features $[p(u,v), SLL, BW]$ and pattern tolerance index Δ

patch length are depicted. In table 5.2, interval pattern features of the length tolerances are depicted. Inclusion property for interval of length $([l]|_{\Delta_l=5\mu m} \subset [l]|_{\Delta_l=10\mu m} \subset [l]|_{\Delta_l=20\mu m} \subset [l]|_{\Delta_l=50\mu m})$

and $([w]|_{\Delta_w=5\mu m} \subset [w]|_{\Delta_w=10\mu m} \subset [w]|_{\Delta_w=20\mu m} \subset [w]|_{\Delta_w=50\mu m})$ leads to the inclusion of the interval power pattern

$([P_{co}^{ENUM-MS}]|_{\Delta_w=5\mu m} \subset [P_{co}^{ENUM-MS}]|_{\Delta_w=10\mu m} \subset [P_{co}^{ENUM-MS}]|_{\Delta_w=20\mu m} \subset [P_{co}^{ENUM-MS}]|_{\Delta_w=50\mu m})$

and $([P_{co}^{ENUM-MS}]|_{\Delta_l=5\mu m} \subset [P_{co}^{ENUM-MS}]|_{\Delta_l=10\mu m} \subset [P_{co}^{ENUM-MS}]|_{\Delta_l=20\mu m} \subset [P_{co}^{ENUM-MS}]|_{\Delta_l=50\mu m})$.

It is worth to show the dependency of the degradation of the pattern features on patch tolerances against steering angle . Four different nominal reflectarray arrangements have been synthesized to steer the main beam along directions: $(\theta_0, \phi_0) = (10, 0)[deg]$, $(\theta_0, \phi_0) = (20, 0)[deg]$, $(\theta_0, \phi_0) = (30, 0)[deg]$, $(\theta_0, \phi_0) = (40, 0)[deg]$. The plot of interval power pattern features only along the cut $v = 0$ for tolerance values $\Delta_l = \{5, 10, 20, 50\}\{\mu m\}$ are shown in Fig.5.10. These interval features are also represented in table 5.3 . The dependency of the power pattern degradation on patch tolerances against antenna bandwidth is also studied. Four different working frequencies $f = 28.5$, $f = 29.25$, $f = 30.75$, $f = 31.5$ have been investigated. In Fig.5.11 interval pattern features for tolerance values $\Delta_l = \{5, 10, 20, 50\}\{\mu m\}$ for cut $v = 0$ are shown. In table 5.4 these pattern features are presented.

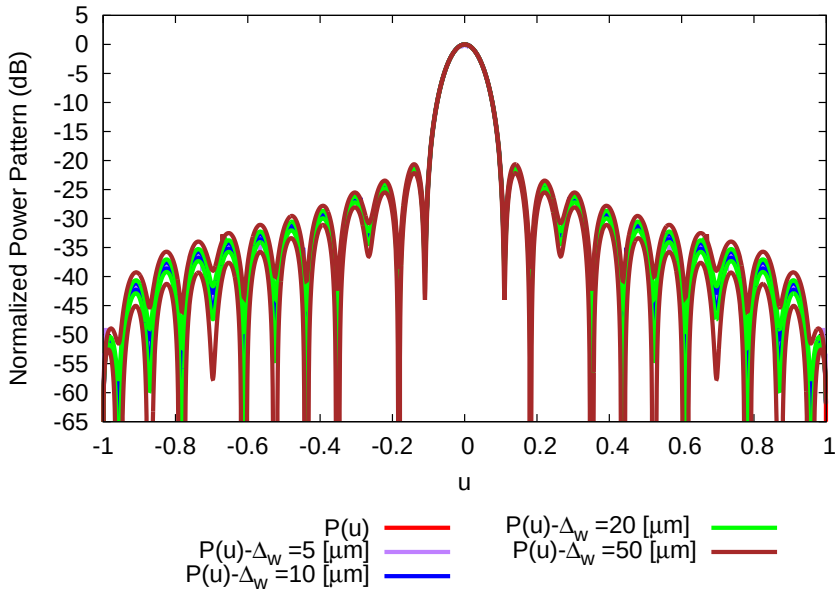

(a)

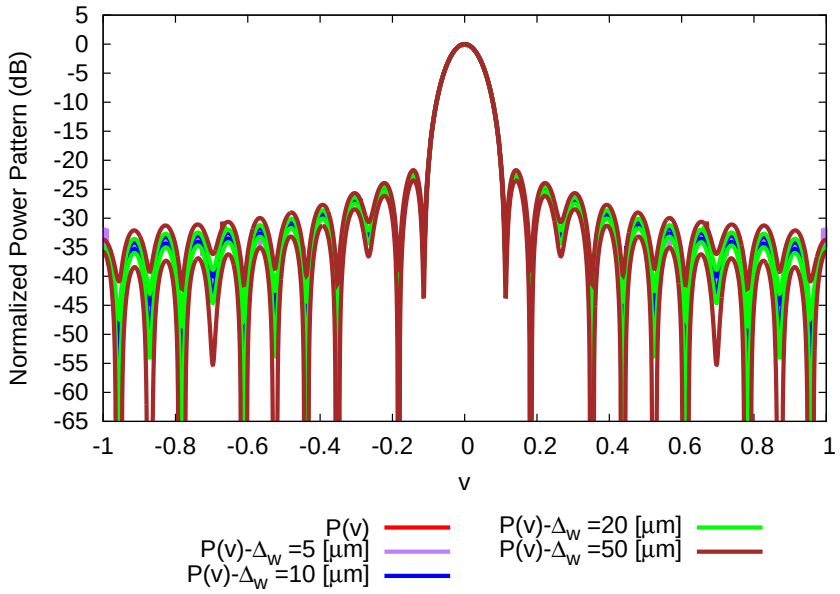

(b)

Figure 5.8: *Inclusion property validation* against patch width error - Nominal power pattern and $IA - ENUM - MS$ interval power pattern for $\triangle w = \{5, 10, 20, 50\}(a)$ in $v = 0$ plane (b) in $u = 0$ plane.

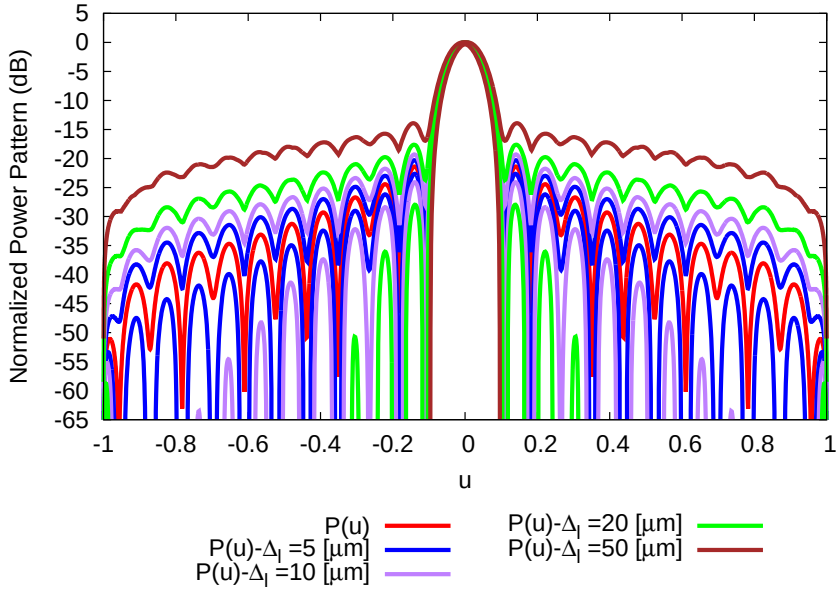

(a)

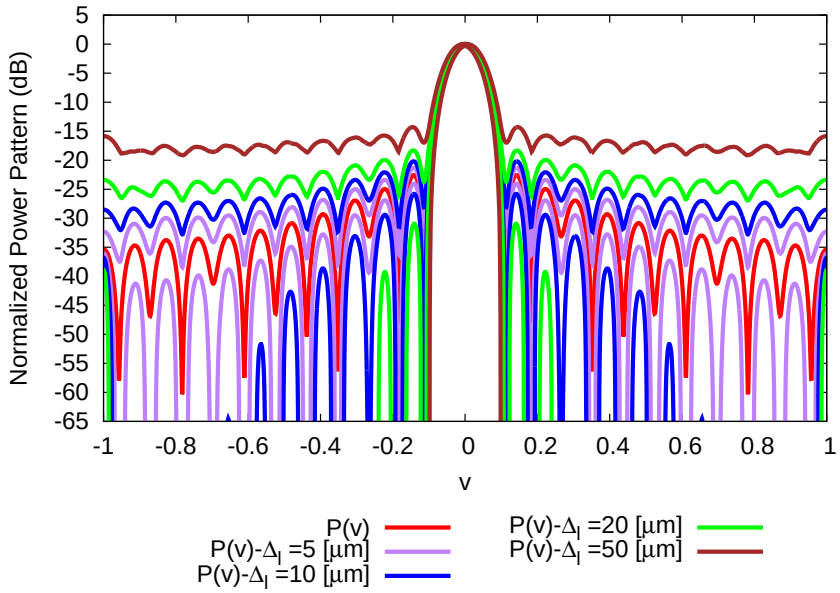

(b)

Figure 5.9: *Inclusion property validation* against patch length error - Nominal power pattern and $IA - ENUM - MS$ interval power pattern for $\triangle l = \{5, 10, 20, 50\}(a)$ in $v = 0$ plane (b) in $u = 0$ plane.

$\Delta l, \mu m$	$[P(u,v)]$	$[SLL], dB$	$[BW], u$	$\Delta \times 10$
u=0				
0	0	-21.380	0.092	
5	[-0.014,0.009]	[-22.641,-20.271]	[0.088,0.090]	0.3
10	[-0.032,0.017]	[-24.101,-19.275]	[0.086,0.094]	0.6
20	[-0.081,0.027]	[-27.997,-17.542]	[0.082,0.098]	1.2
50	[-0.340,0.040]	[-inf,-13.582]	[0.072,0.011]	3.6
v=0				
0	0	-22.561	0.092	
5	[-0.014,0.009]	[-24.046,-21.284]	[0.090,0.094]	0.3
10	[-0.032,0.017]	[-25.821,-20.155]	[0.088,0.096]	0.6
20	[-0.081,0.027]	[-30.969,-18.230]	[0.084,0.100]	1.3
50	[-0.340,0.040]	[-inf,-13.658]	[0.072,0.112]	4.1

Table 5.2: Analysis of the IA-based pattern prediction vs. patch length errors in $u = 0$ and $v = 0$ planes, $\triangle l = \{5, 10, 20, 50\}\{\mu m\}$- Interval pattern features $[p(u,v), SLL, BW]$ and pattern tolerance index Δ

$\Delta l, \mu m$	$[P(u,v)]$	$[SLL], dB$	$[BW], u$	$\Delta \times 10$
$f = 28.5$				
0	0	-17.526	0.096	
10	[-0.113,0.104]	[-18.983,-16.261]	[0.0920,0.102]	0.66
$f = 29.25$				
0	0	-21.110	0.092	
10	[-0.071,0.059]	[-23.479,-19.246]	[0.088,0.098]	0.63
$f = 30.75$				
0	0	-21.085		
10	[-0.069,0.057]	[-23.964,-18.868]	[0.084,0.092]	0.7
$f = 31.5$				
0	0	-18.888	0.086	
10	[-0.112,0.110]	[-21.204,-17.034]	[0.082,0.092]	0.8

Table 5.3: Analysis vs. bandwidth $f = \{28.5, 29.25, 30.75, 31.5\}$ for patch length errors in $v = 0$ plane, $\triangle l = \{10\}\{\mu m\}$- Interval pattern features $[p(u,v), SLL, BW]$ and pattern tolerance index Δ

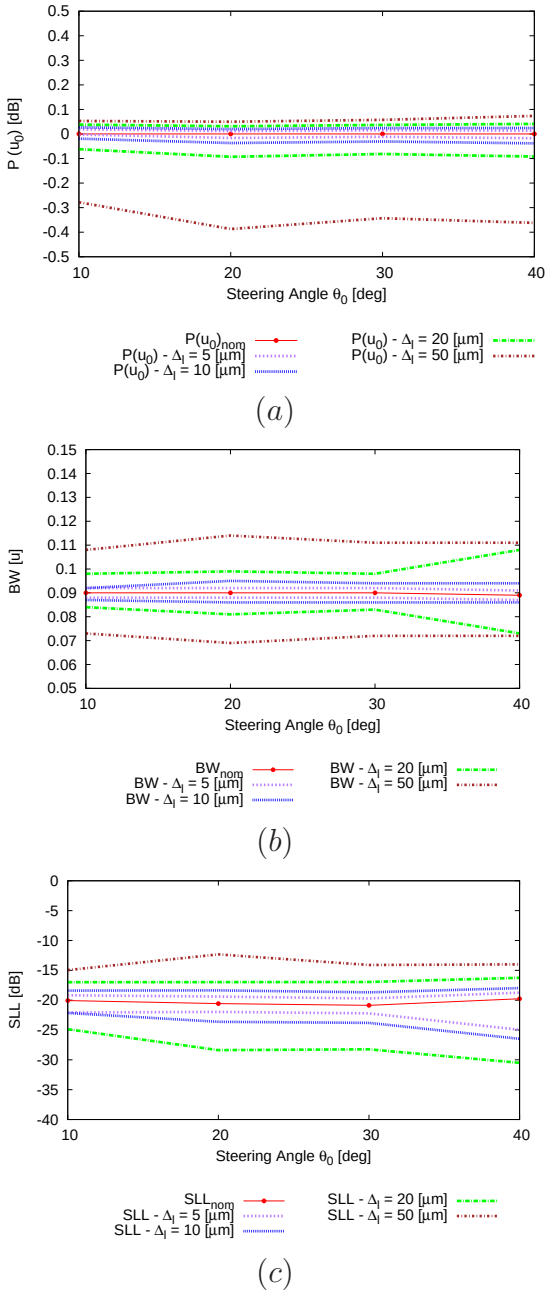

Figure 5.10: *Analysis versus steering angle, IA-pattern features* $(a)P(u_0)$ (b) *SLL* (c) *BW against mainlobe steering angle.*

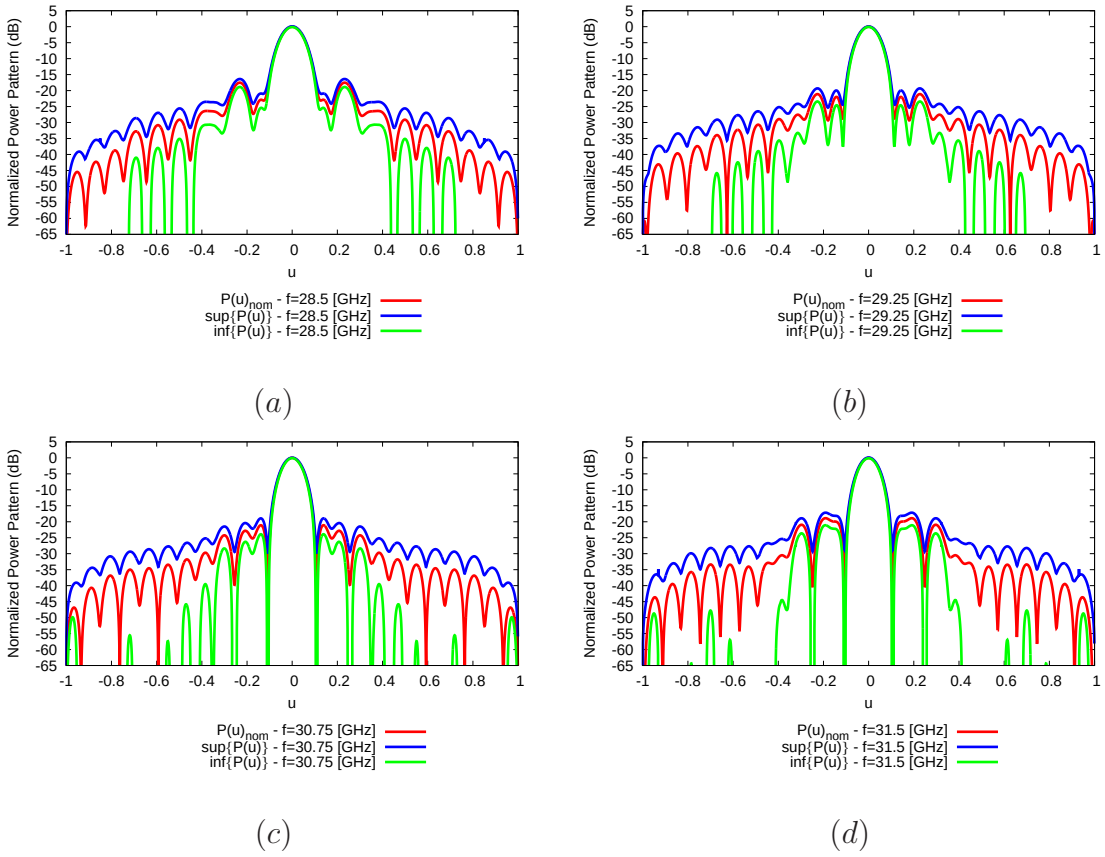

Figure 5.11: *Analysis versus frequency, IA-pattern features* $(a)P(u_0)(b)$ *SLL* (c) *BW against frequency* $(a)f = 28.5$ $(b)f = 29.25$ $(c)f = 30.75(d)f = 31.5$.

$\Delta l, \mu m$	$[P(u,v)]$	$[SLL], dB$	$[BW], u$	$\Delta \times 10$
u=0				
0	0	-21.380	0.092	
5	[-0.014,0.009]	[-22.641,-20.271]	[0.088,0.090]	0.3
10	[-0.032,0.017]	[-24.101,-19.275]	[0.086,0.094]	0.6
20	[-0.081,0.027]	[-27.997,-17.542]	[0.082,0.098]	1.2
50	[-0.340,0.040]	[-inf,-13.582]	[0.072,0.011]	3.6
v=0				
0	0	-22.561	0.092	
5	[-0.014,0.009]	[-24.046,-21.284]	[0.090,0.094]	0.3
10	[-0.032,0.017]	[-25.821,-20.155]	[0.088,0.096]	0.6
20	[-0.081,0.027]	[-30.969,-18.230]	[0.084,0.100]	1.3
50	[-0.340,0.040]	[-inf,-13.658]	[0.072,0.112]	4.1

Table 5.4: Analysis vs. bandwidth $f = \{28,5, 29.25, 30.75, 31.5\}$ for patch length errors in $v = 0$ plane, $\triangle l = \{10\}\{\mu m\}$- Interval pattern features $[p(u,v), SLL, BW]$ and pattern tolerance index Δ

5.2.1.3 Tolerance Analysis Against Substrate Error

Interval power pattern as a result of tolerance error on the substrate thickness is computed by the previous methods. It can be shown that sensitivity of the radiated power pattern toward the substrate thickness error is more than patch width error. Since the nominal value of the substrate thickness is much less than the nominal width of the patch, the effect of the $50\mu m$ substrate thickness deviation on the radiation pattern is more than the same tolerance on the width of the patch. There should be some constraints on the maximum tolerable tolerance error based on the working frequency, nominal value of the parameter and the sensitivity of the resonance frequency, reflection phase toward the specific tolerances. Due to this issues, the same tolerance on each parameter can not make the same effect on the radiation performance of the antenna. In Fig.5.12(a)-(b), the interval power pattern is extracted for tolerances of $\triangle\varepsilon = 0.003, 0.005, 0.007$ in the dielectric permittivity in cut $v = 0$ and $u = 0$,respectively. The errors on the substrate thickness have been fixed in $\Delta_d = \{5, 10, 20, 50\}[\mu m]$. The plot of the nominal power pattern and the interval bounds through the Minkowski-based Interval Analysis is shown in Fig.5.13. The pattern features for interval dielectric permittivity and the interval substrate are shown in table 5.5 and 5.6.

5.3 Feed Error

Reflectarray antennas includes several radiating elements which are illuminated by the feed antenna. Feed antenna can have the displacement from the on-axis

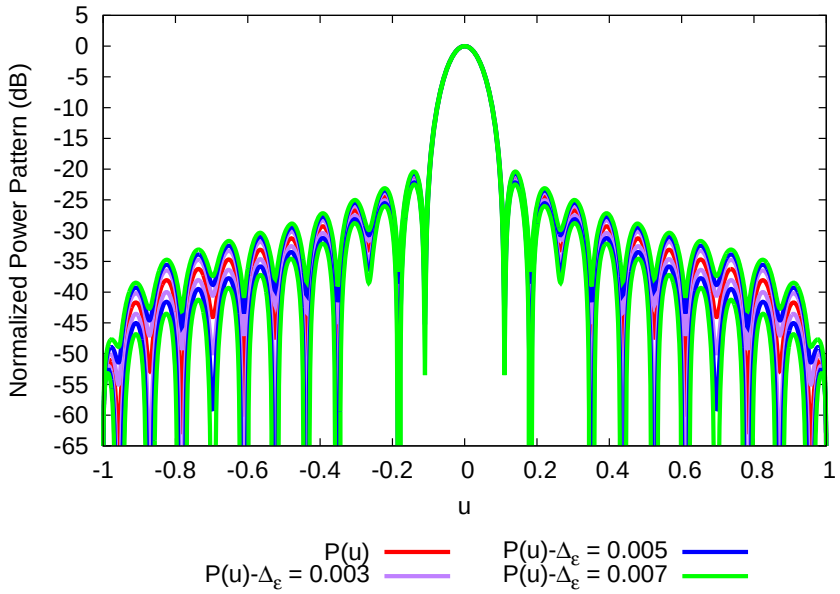

(a)

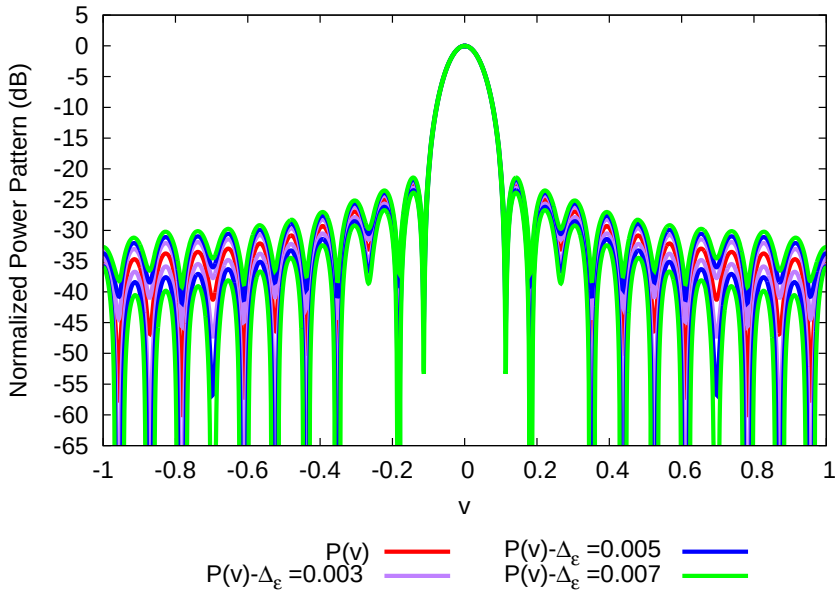

(b)

Figure 5.12: *Inclusion property validation* against patch dielectric permittivity error - Nominal power pattern and $IA - ENUM - MS$ interval power pattern for $\triangle\varepsilon = \{0.003, 0.005, 0.007\}(a)$ in $v = 0$ plane (b) in $u = 0$ plane.

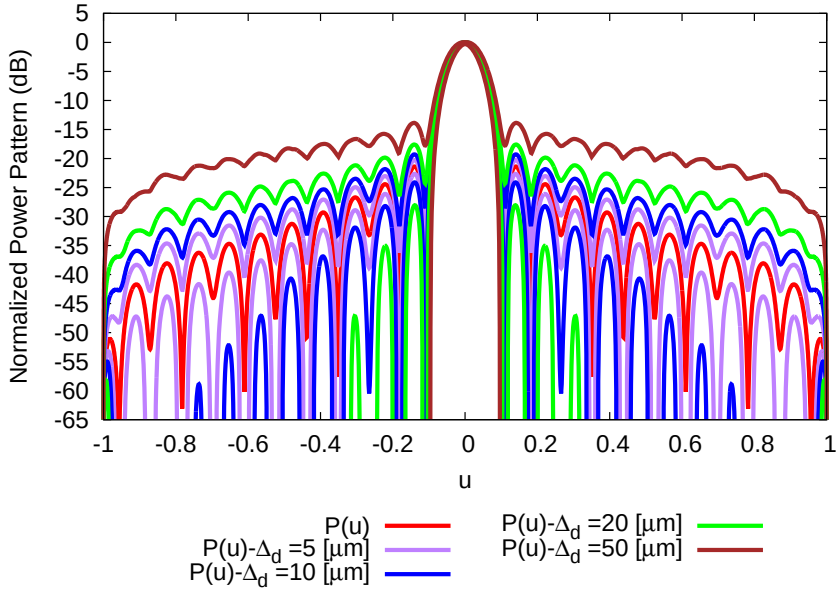

(a)

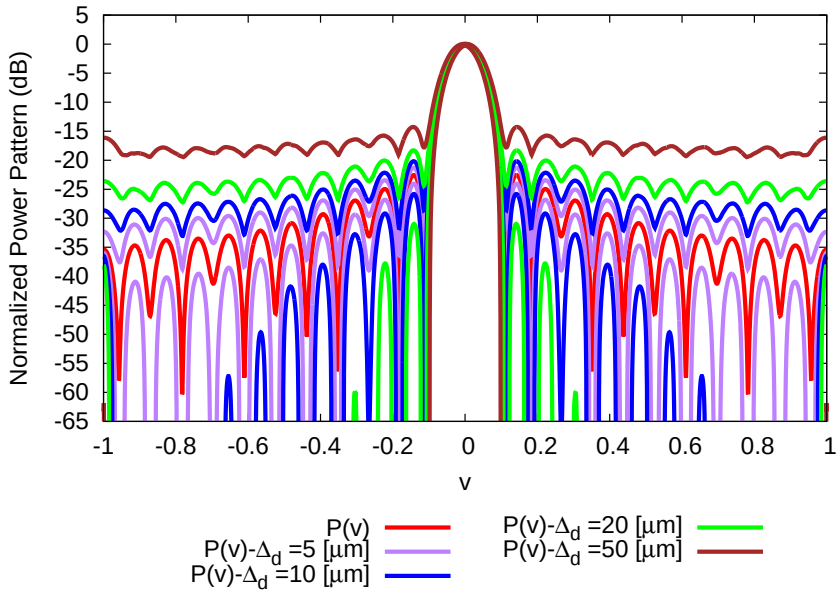

(b)

Figure 5.13: *Inclusion property validation* against patch substrate thickness error - Nominal power pattern and $IA - ENUM - MS$ interval power pattern for $\triangle d = \{5, 10, 20, 50\}(a)$in $v = 0$ plane (b)in $u = 0$ plane.

$\Delta d, \mu m$	$[P(u,v)]$	$[SLL], dB$	$[BW], u$	$\Delta \times 10$
u=0				
0	0	-22.561	0.092	
5	[-0.012,0.009]	[-22.653,-20.261]	[0.088,0.092]	0.2
10	[-0.028,0.017]	[-24.130,-19.259]	[0.086,0.094]	0.5
20	[-0.071,0.029]	[-28.078,-17.519]	[0.084,0.098]	1.2
50	[-0.292,0.044]	[-inf,-13.575]	[0.072,0.108]	3.4
v=0				
0	0	-22.561	0.092	
5	[-0.012,0.009]	[-26.822,-21.296]	[0.09,0.094]	0.3
10	[-0.028,0.017]	[-25.836,-20.150]	[0.088,0.096]	0.6
20	[-0.071,0.029]	[-31.003,-18.224]	[0.084,0.098]	1.3
50	[-0.292,0.044]	[-60.044,-13.821]	[0.074,0.11]	3.9

Table 5.5: Analysis of the IA-based pattern prediction vs. substrate thickness errors in $u = 0$ and $v = 0$ planes, $\triangle d = \{5, 10, 20, 50\}\{\mu m\}$- Interval pattern features $[p(u,v), SLL, BW]$ and pattern tolerance index Δ

$\Delta\varepsilon$	$[P(u,v)]$	$[SLL], dB$	$[BW], u$	$\Delta \times 10$
u=0				
0	0	-21.380	0.092	
0.003	[-0.0052,0.0006]	[-21.457,-21.304]	[0.091,0.092]	0.02
0.005	[-0.001,0.013]	[-21.536,-21.227]	[0.091,0.092]	0.03
0.007	[-0.003,0.002]	[-21.659,-21.077]	[0.091,0.092]	0.05
v=0				
0	0	-22.561	0.092	
0.003	[-0.005,0.004]	[-21.884,-20.975]	[0.091,0.092]	0.1
0.005	[-0.009,0.006]	[-22.511,-20.915]	[0.091,0.092]	0.2
0.007	[-0.013,0.009]	[-22.515,-20.395]	[0.088,0.092]	0.28

Table 5.6: Analysis of the IA-based pattern prediction vs. dielectric permittivity errors in $u = 0$ and $v = 0$ planes, $\triangle\varepsilon = \{0.003, 0.005, 0.007\}\{\mu m\}$- Interval pattern features $[p(u,v), SLL, BW]$ and pattern tolerance index Δ

focus due to some unpredictable uncertainties. This displacement make a phase-error over the aperture surface and consequently distortion on the radiation pattern. Beam distortion due to a lateral feed displacement in a paraboloid antenna is investigated in [43]. The combined effect of lateral and axial displacement of the feed phase center on the secondary performance of a parabolic reflector is described in [44]. The impact of feed location on the operating band of broadband reflectarray antenna is addressed in [45]. Since the nature of these errors is random, we need deterministic approaches to compute the effect of these random errors on the radiation performance. As it is proved in the previous section, Minkowski Enumerative Interval Analysis ($IA-MS-ENUM$) provide more reliable and effective results rather than Cartesian Interval Analysis ($IA-CS$). This novel Minkowski-based Interval analysis is proposed to considered the effect of feed displacement errors on the radiation pattern of reflectarray antenna. The result of the Minkowski-Interval analysis include upper and lower bounds of the power pattern as a result of feed position errors.

5.3.1 Mathematical Representation of Feed Location Distortion

Assume reflectarray antenna in Fig. 5.14 in which the feed position has a displacement error $\triangle \underline{r}_f$ from on-axis focus. Feed position errors can affect the antenna performance. Based on the interval analysis approach and the vertical displacement error [52], feed on-axis focus location can be presented by following errors and intervals as follows :

$$\Delta \underline{r}_f = (\Delta x_f, \Delta y_f, \Delta z_f) \tag{5.1}$$

$$[\underline{r}_f] = [x_f]\hat{x} + [y_f]\hat{y} + [z_f]\hat{z} \tag{5.2}$$

$$[x_f] = [x_f - \triangle x_f; x_f + \triangle x_f] \tag{5.3}$$

$$[y_f] = [y_f - \triangle y_f; y_f + \triangle y_f] \tag{5.4}$$

$$[z_f] = [z_f - \triangle z_f; z_f + \triangle z_f] \tag{5.5}$$

where feed location along x and y and z are x_f , y_f and z_f, respectively. As it is clear in Fig. 5.14, due to the feed displacement errors, distance from feed to element R_{mn} will change to R'_{mn} . Since this displacement can be random so they can be presented by interval values $[R_{mn}]$ to include all of these random

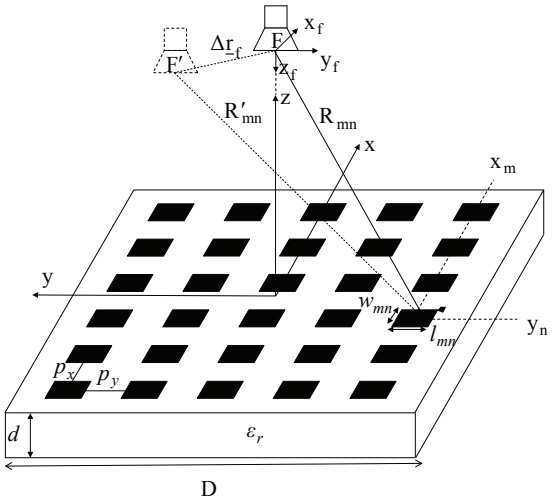

Figure 5.14: Antenna structure with the feed displacement .

distance values R'_{mn}. Since the incident angles are computed by the knowing the feed position and the distance from feed to element so the spherical phases (θ_{mn}, ϕ_{mn}) are also represented by interval values to assess the effect of random errors on feed nominal position.

Incident feed can express by Floquet harmonics. Amplitude and phase of the Floquet harmonics which illuminate each patch are computed from the far field of the feed horn antenna. This amplitude and phase now are the interval values due to interval of the feed position. Interval of the far field of the horn antenna with respect to mn-th patch/element in the reflectarray are:

$$[E^{Fy}([\theta_{mn}],[\phi_{mn}],[\underline{r}_f])] = [E^{Fy}_{\theta}([\theta_{mn}],[\phi_{mn}],[\underline{r}_f])]\hat{\theta} + [E^{Fy}_{\phi}([\theta_{mn}],[\phi_{mn}],[\underline{r}_f])]\hat{\phi} \tag{5.6}$$

$$[E^{Fy}_{\theta}([\theta_{mn}],[\phi_{mn}],[\underline{r}_f])] = \frac{jke^{-jk[R_{mn}]}}{[R_{mn}]}(C_E([\theta_{mn}])sin([\phi_{mn}]) \tag{5.7}$$

$$[E^{Fy}_{\phi}([\theta_{mn}],[\phi_{mn}],[\underline{r}_f])] = \frac{jke^{-jk[R_{mn}]}}{[R_{mn}]}(C_H([\theta_{mn}])cos([\phi_{mn}]) \tag{5.8}$$

Where $[\theta_{mn}]$, $[\phi_{mn}]$ are the interval of the incident angles which illuminate mn-th element in the aperture surface. $C_E(\theta) = cos^{qE}(\theta)$ and $C_H(\theta) = cos^{qH}(\theta)$ are the E- and H- plane patterns of the feed-horn. We need to select a proper value for $qE = qH$ in order to control the aperture efficiency. Interval of the incident angle relates to interval of the feed positions by the following expressions:

$$[\theta_{mn}] = atan\frac{\sqrt{(x_{mn} - [x_f])^2 + (y_{mn} - [y_f])^2}}{z_f} \tag{5.9}$$

$$[\phi_{mn}] = atan\frac{y_{mn} - [y_f]}{x_{mn} - [x_f]} \tag{5.10}$$

Interval of the $[R_{mn}]$, $[r_{mn}]$ depends on the feed locations interval values by the following expression:

$$[R_{mn}] = \sqrt{([r_{mn}])^2 + [z_f^2]} \tag{5.11}$$

$$[r_{mn}] = \sqrt{(x_{mn} - [x_f])^2 + (y_{mn} - [y_f])^2}$$

Incident Floquet harmonics computed from the Cartesian components of the far field of the incident field. Interval of the Cartesian components of the incident field related to the interval of the far field of the feed horn (5.6) antenna by:

$$\begin{bmatrix} [d_x^F([\theta_{mn}],[\phi_{mn}],[\underline{r}_f])] \\ [d_y^F([\theta_{mn}],[\phi_{mn}],[\underline{r}_f])] \\ [d_z^F([\theta_{mn}],[\phi_{mn}],[\underline{r}_f])] \end{bmatrix} = \begin{bmatrix} sin([\theta_{mn}]cos[\phi_{mn}]) & cos([\theta_{mn}]cos[\phi_{mn}]) & -sin([\phi_{mn}]) \\ sin([\theta_{mn}]sin[\phi_{mn}]) & cos([\theta_{mn}]sin[\phi_{mn}]) & cos([\phi_{mn}]) \\ cos([\theta_{mn}]) & -sin([\theta_{mn}]) & 0 \end{bmatrix} \begin{bmatrix} 0 \\ [E_\theta^{Fy}([\theta_{mn}],[\phi_{mn}],[\underline{r}_f])] \\ [E_\phi^{Fy}([\theta_{mn}],[\phi_{mn}],[\underline{r}_f])] \end{bmatrix} \tag{5.12}$$

Then the interval of the Floquet harmonics illuminated each mn-th element related to the interval of the Cartesian components of the far electric field of each element by the following expression:

$$\begin{bmatrix} [d^{TE}([\theta_{mn}],[\phi_{mn}],[\underline{r}_f])] \\ [d^{TM}([\theta_{mn}],[\phi_{mn}],[\underline{r}_f])] \end{bmatrix} = \frac{1}{[k_{cl}([\theta_{mn}],[\phi_{mn}],[\underline{r}_f])]} \begin{bmatrix} -[ky_0([\theta_{mn}],[\phi_{mn}],[\underline{r}_f])] & [kx_0([\theta_{mn}],[\phi_{mn}],[\underline{r}_f])] \\ [kx_0([\theta_{mn}],[\phi_{mn}],[\underline{r}_f])] & [ky_0([\theta_{mn}],[\phi_{mn}];[\underline{r}_f])] \end{bmatrix} \begin{bmatrix} [d_x^F([\theta_{mn}],[\phi_{mn}],[\underline{r}_f])] \\ [d_y^F([\theta_{mn}],[\phi_{mn}],[\underline{r}_f])] \end{bmatrix} \tag{5.13}$$

$$[k_{x0}([\theta_{mn}],[\phi_{mn}];([\underline{r}_f]))] = k_0 sin([\theta_{mn}])cos([\phi_{mn}]) \tag{5.14}$$

$$[k_{y0}([\theta_{mn}],[\phi_{mn}];([\underline{r}_f]))] = k_0 sin([\theta_{mn}])sin([\phi_{mn}]) \tag{5.15}$$

$$[k_{cl}([\theta_{mn}],[\phi_{mn}],[\underline{r}_f])] = \sqrt{[k_{x0}^2([\theta_{mn}],[\phi_{mn}],[\underline{r}_f])] + [k_{y0}^2([\theta_{mn}],[\phi_{mn}],[\underline{r}_f])]} \tag{5.16}$$

After computing the interval of the incident Floquet harmonics illuminating mn-th element. Now we need to compute the interval of the Fourier transform of the reflected electric field on the reflectarray aperture. This Interval Fourier transform is the summation of the interval of reflected Floquet harmonics of each element as follows [10]:

$$[\widetilde{E}^{Rx/y}(u,v;[\theta_{mn}],[\phi_{mn}],[\underline{r}_f])] = K\sum_{m=0}^{M-1}\sum_{n=0}^{N-1}[a_{mn}^{x/y}([\theta_{mn}],[\phi_{mn}],[\underline{r}_f])]e^{jk_0(ump_x+vnp_y)} \tag{5.17}$$

Where $[a^{x/y}]$ is the interval of the Cartesian components of the reflected field illuminating each element. We want to compute the interval of the reflected Floquet harmonics of each cell. This reflected Floquet harmonics related to incident

Floquet harmonics with the reflection coefficient of each cell. The expression for the reflection coefficient includes the interval of the incident angle. Therefore the effect of the feed displacements is seen in both incident angle and the reflection coefficient. The relation between the interval of the reflected Floquet harmonics $([a^{TE}([\theta_{mn}],[\phi_{mn}],[\underline{r}_f])],[a^{TM}([\theta_{mn}],[\phi_{mn}],[\underline{r}_f])])$ and the Cartesian components of the reflected electric field $([a^{x}([\theta_{mn}],[\phi_{mn}],[\underline{r}_f])],[a^{y}([\theta_{mn}],[\phi_{mn}],[\underline{r}_f])])$ of each element are as follows:

$$\begin{bmatrix} [a^x([\theta_{mn}],[\phi_{mn}],[\underline{r}_f])] \\ [a^y([\theta_{mn}],[\phi_{mn}],[\underline{r}_f])] \end{bmatrix} = \frac{1}{[k_{cl}([\theta_{mn}],[\phi_{mn}],[\underline{r}_f])]} \begin{bmatrix} -[ky_0([\theta_{mn}],[\phi_{mn}],[\underline{r}_f])] & [kx_0([\theta_{mn}],[\phi_{mn}],[\underline{r}_f])] \\ [kx_0([\theta_{mn}],[\phi_{mn}],[\underline{r}_f])] & [ky_0([\theta_{mn}],[\phi_{mn}],[\underline{r}_f])] \end{bmatrix} \begin{bmatrix} [a^{TE}([\theta_{mn}],[\phi_{mn}],[\underline{r}_f])] \\ [a^{TM}([\theta_{mn}],[\phi_{mn}],[\underline{r}_f])] \end{bmatrix} \tag{5.18}$$

interval of the reflected electric field related to the interval of the incident Floquet harmonics by:

$$\begin{bmatrix} [a^{TE}([\theta_{mn}],[\phi_{mn}],[\underline{r}_f])] \\ [a^{TM}([\theta_{mn}],[\phi_{mn}],[\underline{r}_f])] \end{bmatrix} = \begin{bmatrix} [\Gamma^{TE}([\theta_{mn}],[\phi_{mn}],[\underline{r}_f])] & [\Gamma^{cross}([\theta_{mn}],[\phi_{mn}],[\underline{r}_f])] \\ [\Gamma^{cross}([\theta_{mn}],[\phi_{mn}],[\underline{r}_f])] & [\Gamma^{TM}([\theta_{mn}],[\phi_{mn}],[\underline{r}_f])] \end{bmatrix} \begin{bmatrix} [d^{TE}([\theta_{mn}],[\phi_{mn}],[\underline{r}_f])] \\ [d^{TM}([\theta_{mn}],[\phi_{mn}],[\underline{r}_f])] \end{bmatrix} \tag{5.19}$$

Then the interval of the TE and TM and *cross* reflection coefficient are as follows:

$$[\Gamma^{TE}([\theta_{mn}],[\phi_{mn}],[\underline{r}_f])] = \frac{\frac{1}{[QradTE([\theta_{mn}],[\phi_{mn}],[\underline{r}_f])]} - (\frac{1}{[QradTM([\theta_{mn}],[\phi_{mn}],[\underline{r}_f])]} + \frac{1}{Q_0}) - 2j\frac{(f-f_0)}{f_0}}{\frac{1}{[QradTE([\theta_{mn}],[\phi_{mn}],[\underline{r}_f])]} + \frac{1}{[QradTM([\theta_{mn}],[\phi_{mn}],[\underline{r}_f])]} + \frac{1}{Q_0} + 2j\frac{(f-f_0)}{f_0}} \tag{5.20}$$

$$[\Gamma^{TM}([\theta_{mn}],[\phi_{mn}],[\underline{r}_f])] = \frac{\frac{1}{[QradTM([\theta_{mn}],[\phi_{mn}],[\underline{r}_f])]} - (\frac{1}{[QradTE([\theta_{mn}],[\phi_{mn}],[\underline{r}_f])]} + \frac{1}{Q_0}) - 2j\frac{(f-f_0)}{f_0}}{\frac{1}{[QradTM([\theta_{mn}],[\phi_{mn}],[\underline{r}_f])]} + \frac{1}{[QradTE([\theta_{mn}],[\phi_{mn}],[\underline{r}_f])]} + \frac{1}{Q_0} + 2j\frac{(f-f_0)}{f_0}} \tag{5.21}$$

$$[\Gamma^{cross}([\theta_{mn}],[\phi_{mn}],[\underline{r}_f])] = \frac{\frac{2}{\sqrt{[QradTE([\theta_{mn}],[\phi_{mn}],[\underline{r}_f])][QradTM([\theta_{mn}],[\phi_{mn}],[\underline{r}_f])]}}}{\frac{1}{[QradTM([\theta_{mn}],[\phi_{mn}],[\underline{r}_f])]} + \frac{1}{[QradTE([\theta_{mn}],[\phi_{mn}],[\underline{r}_f])]} + \frac{1}{Q_0} + 2j\frac{(f-f_0)}{f_0}} \tag{5.22}$$

Here we have the expression for quality factors which depends on the incident angles and the geometrical parameters of the element. Since the incident angle are interval, the quality factors can be represented by interval values as follows:

$$[QradTE([\theta_{mn}],[\phi_{mn}],[\underline{r}_f])] = \frac{f_0\pi\varepsilon}{4d}\frac{l_{mn}}{w_{mn}}\frac{p_x p_y}{cos[\theta_i]} \tag{5.23}$$

$$[QradTM([\theta_{mn}],[\phi_{mn}],[\underline{r}_f])] = \frac{f_0\pi\varepsilon}{4d}\frac{l_{mn}}{w_{mn}}p_x p_y cos[\theta_i] \tag{5.24}$$

periodicity of array along x and y are p_x and p_y, respectively. Length and with of the patch are l_{mn} and w_{mn}. d is the substrate thickness. f_0 is the resonance

frequency of each element. Q_0 is the combined quality factors as expressed in [22]. After computing the interval of the Fourier transform of the reflected electric field in reflectarray aperture surface . Interval function of the power pattern of the electric field is as:

$$[E(\theta,\phi;[\theta_{mn}],[\phi_{mn}],[\underline{r}_f])] = [E_\theta(\theta,\phi;[\theta_{mn}],[\phi_{mn}],[\underline{r}_f])]\hat{\theta} + [E_\phi(\theta,\phi;[\theta_{mn}],[\phi_{mn}],[\underline{r}_f])]\hat{\phi} \tag{5.25}$$

$$[E^{co}(\theta,\phi;[\theta_{mn}],[\phi_{mn}],[\underline{r}_f])] = sin\phi[E_\theta(\theta,\phi;[\theta_{mn}],[\phi_{mn}],[\underline{r}_f])]\hat{\theta} + cos\phi[E_\phi(\theta,\phi;[\theta_{mn}],[\phi_{mn}],[\underline{r}_f])]\hat{\phi} \tag{5.26}$$

$$[E^{cross}(\theta,\phi;[\theta_{mn}],[\phi_{mn}],[\underline{r}_f])] = cos\phi[E_\theta(\theta,\phi;[\theta_{mn}],[\phi_{mn}],[\underline{r}_f])]\hat{\theta} - sin\phi[E_\phi(\theta,\phi;[\theta_{mn}],[\phi_{mn}],[\underline{r}_f])]\hat{\phi} \tag{5.27}$$

$$[E_\theta(\theta,\phi;[\theta_{mn}],[\phi_{mn}],[\underline{r}_f])] = \frac{e^{-jkr}}{r}(cos\phi[\widetilde{E}^{Rx}(u,v;[\theta_{mn}],[\phi_{mn}],[\underline{r}_f])] + sin\phi[\widetilde{E}^{Ry}(u,v;[\theta_{mn}],[\phi_{mn}],[\underline{r}_f])]) \tag{5.28}$$

$$[E_\phi(\theta,\phi;[\theta_{mn}],[\phi_{mn}],[\underline{r}_f])] = \frac{e^{-jkr}}{r}(sin\phi cos\theta[\widetilde{E}^{Rx}(u,v;[\theta_{mn}],[\phi_{mn}],[\underline{r}_f])] + cos\phi cos\theta[\widetilde{E}^{Ry}(u,v;[\theta_{mn}],[\phi_{mn}],[\underline{r}_f])]) \tag{5.29}$$

where $j=\sqrt{-1}$, $k=\frac{2\pi}{\lambda}$ is the wavenumber, λ being the wavelength, and $u = \sin\theta\cos\phi$ and $v = \sin\theta\sin\phi$ are the direction cosine coordinates with $\theta \in \left[0;\frac{\pi}{2}\right]$ and $\phi \in [0;\pi]$.

5.3.2 IA-based Approach

In the following the $IA-ENUM-MS$ approach is explained for feed errors:

- Divide the interval of feed displacement to efficient number of sampling points $i = i,...,I_i$. construct each point ψ_i by infimum and supremun of $[x_f]$, $[y_f]$ and $[z_f]$ as

  $\psi_i = inf([x_f]/[y_f]/[z_f]) + \frac{i}{I_i}(sup([x_f]/[y_f]/[z_f]) - inf([x_f]/[y_f]/[z_f]))$

- Compute the amplitude and phase of the reflected Floquet harmonics $a_{mn}^{x/y}(\psi_i)$ for each sampling point, then compute the maximum and minimum among the amplitude and phase of the reflected Floquet harmonics.

- Encircle a small convex polygon including the combination of the maximum and minimum of the amplitude and phase of the reflected Floquet harmonics.

- Perform Minkowski sum among the convex polygons.

5.3.3 Numerical Results

In this section, some numerical results are proposed to validate the effectiveness of $IA-ENUM-MS$ in computing feed displacement errors. *co*−polar component of the nominal pattern are computed by Aperture Field method together with the *co* and *cross* reflection coefficient of the element. Bounds of the deviation of power pattern for different tolerance errors on the feed position are investigated. Then we check the inclusion properties of the power bounds by comparing the bounds with Monte Carlo results. Then feed antenna is relocated in different values of the focal points (F), then the sensitivity of the Minkowski power bounds versus these changing is evaluated.

5.3.3.1 Comparative Assessment

Let us consider a center-fed reflectarray made of 529 isotropic rectangular microstrip patches equally-spaced along the x and y axis of $p_x = p_y = \frac{\lambda}{2}$. Reflectarray antenna has a square aperture with diameter of $11.5\lambda_0$ in 30GHz working frequency. Substrate is a Rogers RT580 with $d = 0.5\ mm$, $\varepsilon_r = 2.2$, $tan\delta = 0.0009$. Feed antenna is a y-polarized horn antenna in 30 GHz modeled as $cos\theta^{qH}$ with $qH = 8.5$. It is located in $(x_f, y_f, z_f) = (0, 0, 114.3)mm$. Variable patch lengths approach in normal incident angle is used to design the array elements over the aperture surface to obtain the required phased. Nominal width value of each cell is $w_{mn} = 3.95\ mm$.

5.3.3.2 Tolerance Analysis Feed Error

First the impact of error on feed location along z axis on the lower and upper bounds of *co*-polar components of the electric field $[E^{co}(\theta, \phi; [\theta_{mn}], [\phi_{mn}], [\underline{r}_f])]$ is analyzed. The nominal location is fixed in $(x_f, y_f, z_f) = (0, 0, 114.3mm)$. We assume the feed antenna has displacement error within the interval of $z_f \in [z_f - \Delta z_f, z_f + \Delta z_f]$ and $\Delta z_f = \lambda/200, \lambda/100, \lambda/50, \lambda/20, \lambda/10$. $IA - ENUM - MS$ power bounds related to different errors on z axis in cut $v = 0.0$ and $u = 0.0$ are presented in Fig.5.15 (a) and (b). The value for the pattern features are presented in table 5.7. In order to check the reliability and inclusion feature of $IA - ENUM - MS$ power bounds, a set of $T = 10^5$ Monte Carlo trial values within the interval of $z_f^t \in [z_f - \lambda/20; z_f + \lambda/20]$ have been chosen and their patterns computed. As can be observed in Fig.5.16, all Monte Carlo patterns are within the $IA-ENUM-MS$ bounds which validate the inclusion property.

The effect of feed deviation errors along x and y axis can also be evaluated. In order to calculate the error effects on these two axis, different tolerance errors along x and y are considered. Interval of the power bounds versus tolerances errors $\Delta x_f = \lambda/200, \lambda/100, \lambda/50, \lambda/20, \lambda/10$ along x directions for *co*-polar pattern is presented in Fig. 5.17 (a) and (b) for cut $v = 0$ and $u = 0$, respectively.

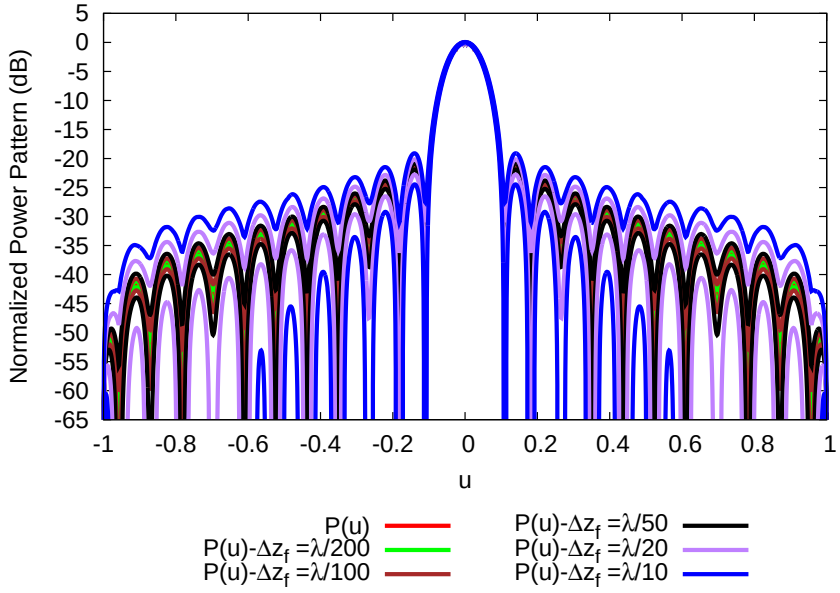

(a)

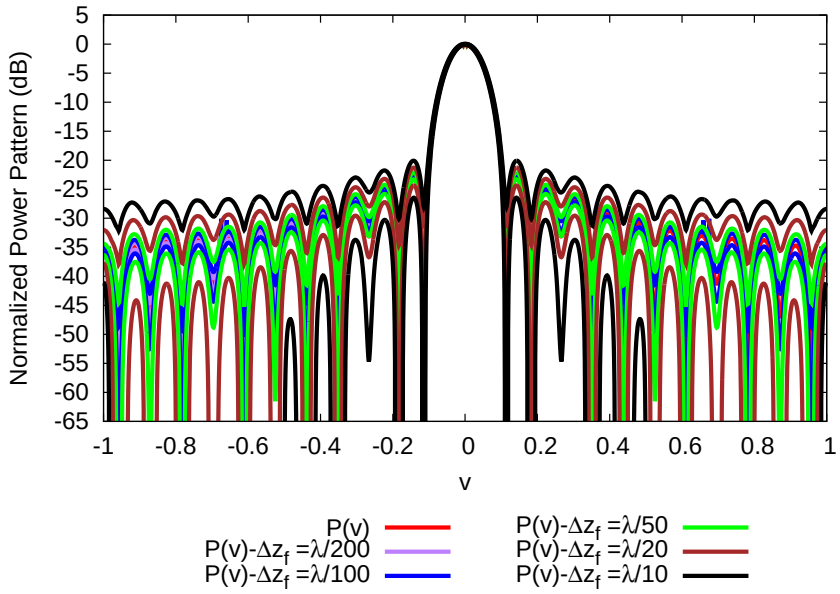

(b)

Figure 5.15: *Inclusion property validation* against feed location error - Nominal power pattern and $IA - MS$ *co*-polar interval power pattern for $\triangle z_f = \{\lambda/200, 100, 50, 20, 10\}(a)$in $v = 0$ plane (b)in $u = 0$ plane.

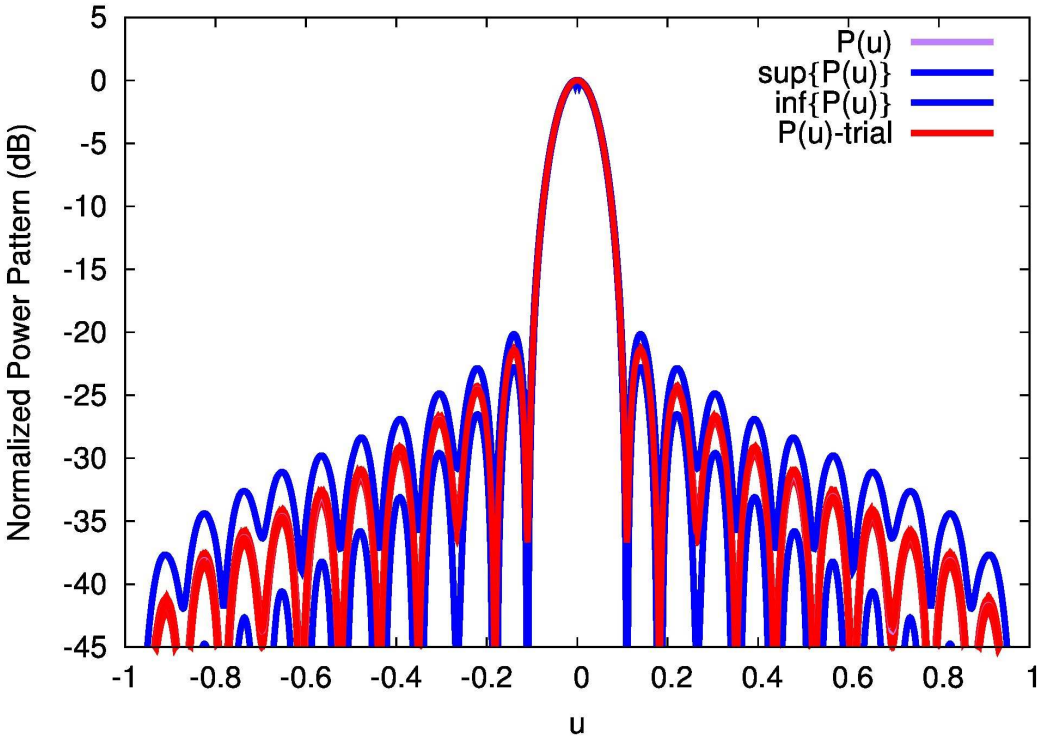

Figure 5.16: *Monte Carlo power pattern cover $IA-MS$ bounds with $\triangle z_f = \lambda/20$.*

Δz_f	$[P(u,v)]$	$[SLL], dB$	$[BW], u$	$\Delta \times 10$
u=0				
0	0	-21.349	0.090	
$\lambda/200$	[-0.015,0.007]	[-21.551,-21.293]	[0.09,0.09]	0.04
$\lambda/100$	[-0.0191,0.003]	[-21.711,-21.184]	[0.09,0.09]	0.09
$\lambda/50$	[-0.026,0.003]	[-22.051,-20.987]	[0.09,0.09]	0.17
$\lambda/20$	[-0.051,0.024]	[-23.970,-20.830]	[0.088,0.094]	0.44
$\lambda/10$	[-0.095,0.057]	[-24.528,-19.018]	[0.084,0.096]	0.88
v=0				
0	0	-22.561	0.092	
$\lambda/200$	[-0.015,0.002]	[-23.032,-22.530]	[0.092,0.092]	0.02
$\lambda/100$	[-0.019,0.003]	[-23.033,-22.425]	[0.092,0.092]	0.08
$\lambda/50$	[-0.026,0.004]	[-23.310,-22.090]	[0.090,0.094]	0.18
$\lambda/20$	[-0.051,0.024]	[-24.386,-21.295]	[0.09,0.096]	0.45
$\lambda/10$	[-0.095,0.057]	[-26.514,-19.994]	[0.086,0.098]	0.09

Table 5.7: Analysis of the IA-based *co*-polar pattern prediction vs. feed displacement errors errors in $u = 0$ and $v = 0$ planes, $\triangle z_f = \{\lambda/200, 100, 50, 20, 10\}$-Interval pattern features $[p(u,v), SLL, BW]$ and pattern tolerance index Δ

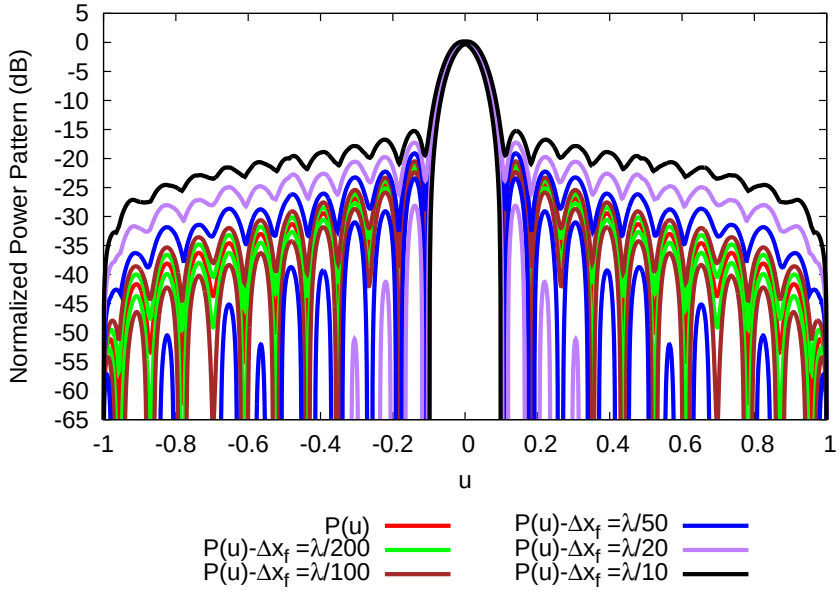

(a)

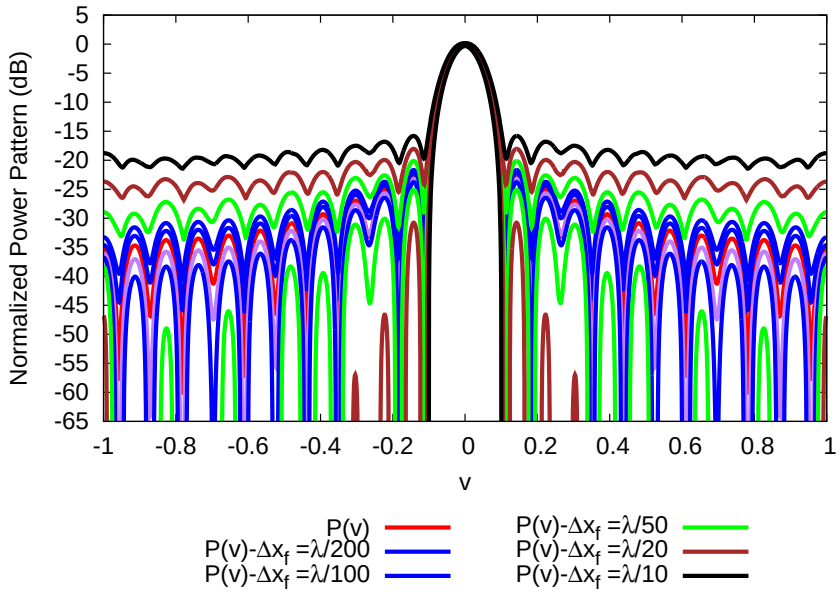

(b)

Figure 5.17: *Inclusion property validation* against feed location error - Nominal power pattern and $IA - MS$ *co*-polar interval power pattern for $\triangle x_f = \{\lambda/200, 100, 50, 20, 10\}(a)$in $v = 0$ plane (b)in $u = 0$ plane.

Δx_f	$[P(u,v)]$	$[SLL], dB$	$[BW], u$	$\Delta \times 10$
u=0				
0	0	-21.349	0.090	
$\lambda/200$	[-0.022,0.003]	[-21.831,-20.891]	[0.09,0.092]	0.15
$\lambda/100$	[-0.0353,0.010]	[-22.347,-20.453]	[0.088,0.092]	0.3
$\lambda/50$	[-0.124,0.0314]	[-23.486,-18.994]	[0.084,0.096]	0.7
$\lambda/20$	[-0.214,0.086]	[-28.217,-17.044]	[0.074,0.102]	1.74
$\lambda/10$	[-0.335,0.164]	[-inf,-14.923]	[0.07,0.112]	3.37
v=0				
0	0	-22.561	0.092	
$\lambda/200$	[-0.022,0.0003]	[-23.213,-22.145]	[0.092,0.092]	0.138
$\lambda/100$	[-0.035,0.010]	[-23.805,-21.649]	[0.090,0.094]	0.27
$\lambda/50$	[-0.124,0.031]	[-25.120,-20.009]	[0.088,0.095]	0.7
$\lambda/20$	[-0.214,0.086]	[-30.854,-17.844]	[0.082,0.102]	1.62
$\lambda/10$	[-0.335,0.164]	[-inf,-14.933]	[0.074,0.11]	3.26

Table 5.8: Analysis of the IA-based *co*−polar pattern prediction vs. feed displacement errors in $u = 0$ and $v = 0$ planes, $\triangle x_f = \{\lambda/200, 100, 50, 20, 10\}$-Interval pattern features $[p(u,v)]$

The value of the pattern features and the peak power for *co*-polar pattern is shown in Table 5.8 and 5.9 respectively. Inclusion properties for the interval of feed ($[x_f]|_{\triangle x_f=\lambda/200} \subset [x_f]|_{\triangle x_f=\lambda/100} \subset [x_f]|_{\triangle x_f=\lambda/50} \subset [x_f]|_{\triangle x_f=\lambda/20} \subset [x_f]|_{\triangle x_f=\lambda/10}$) leads to the inclusion properties of the *co*-polar power pattern ($[P^{co}]|_{\triangle x_f=\lambda/200} \subset [P^{co}]|_{\triangle x_f=\lambda/100} \subset [P^{co}]|_{\triangle x_f=\lambda/50} \subset [P^{co}]|_{\triangle x_f=\lambda/20} \subset [P^{co}]|_{\triangle x_f=\lambda/10}$).

Interval of the *co*-polar power bounds for tolerances of $\Delta y_f = \lambda/200,100, 50, 20, 10$ in Fig. 5.18. We can see the values of the pattern features in table 5.9.

We consider errors on the feed locations based on the error range for reflector antenna. Reflectarray antenna are more sensitive to the feed error. We will consider the more practical feed errors in the z axis, then we will show that this method is consistent to any error. The interval pattern with the tolerance of $\{\lambda/5, \lambda/2, \lambda\}$ is as shown in 5.19. As it is clear the bounds are larger than the previous errors but it is still inclusive.

5.3.3.3 Performance Analysis Versus Different Focal-length-to-diameter Ratio (F/D)

After evaluating the reliability of the Interval Minkowski with respect to feed position errors, we want to check the dependency of tolerance analysis to different focal-length-to-diameter values (F/D). With this analysis, robustness and stability of the method will be assessed. The analysis versus focal-length-to-diameter values has been carried out by considering $F/D = \{0.3; 0.5; 0.7; 0.9\}$. A suitable

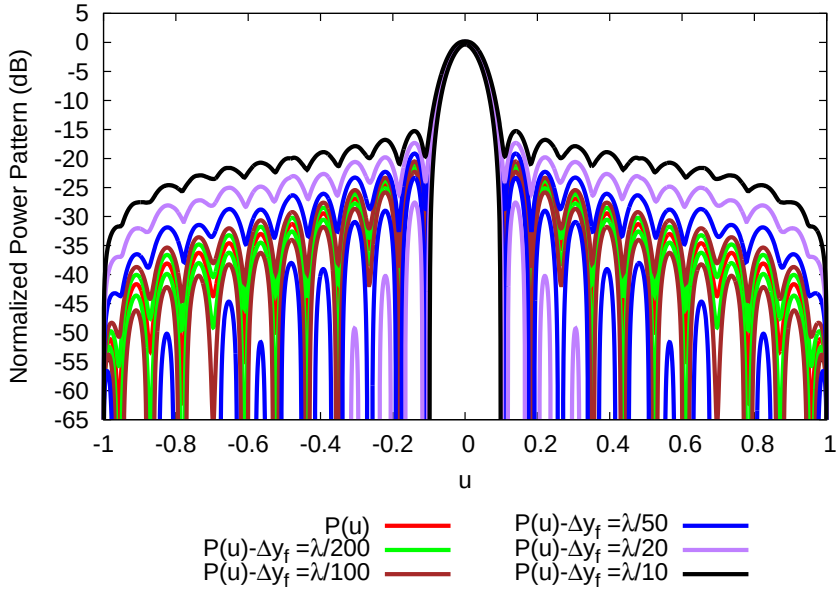

(a)

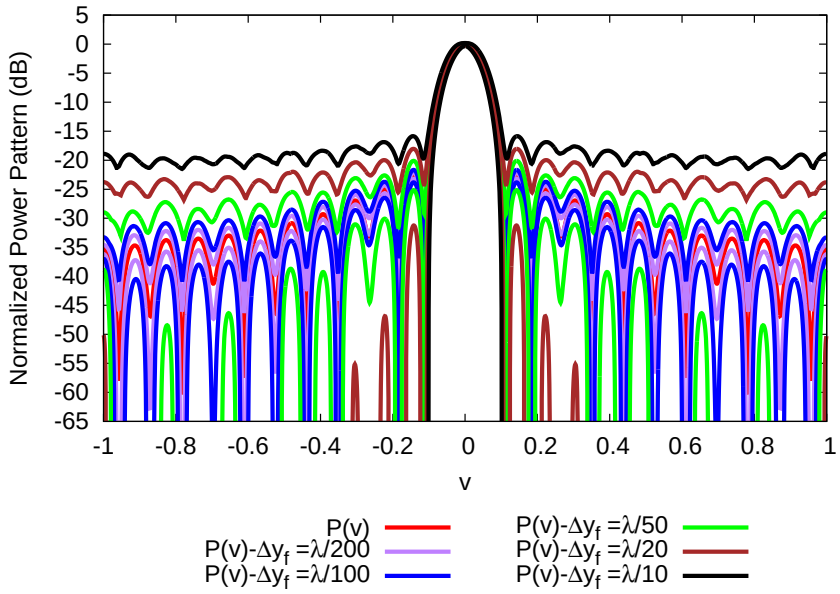

(b)

Figure 5.18: *Inclusion property validation* against feed location error - Nominal power pattern and $IA - MS$ *co*-polar interval power pattern for $\triangle y_f = \{\lambda/200, 100, 50, 20, 10\}(a)$in $v = 0$ plane (b)in $u = 0$ plane.

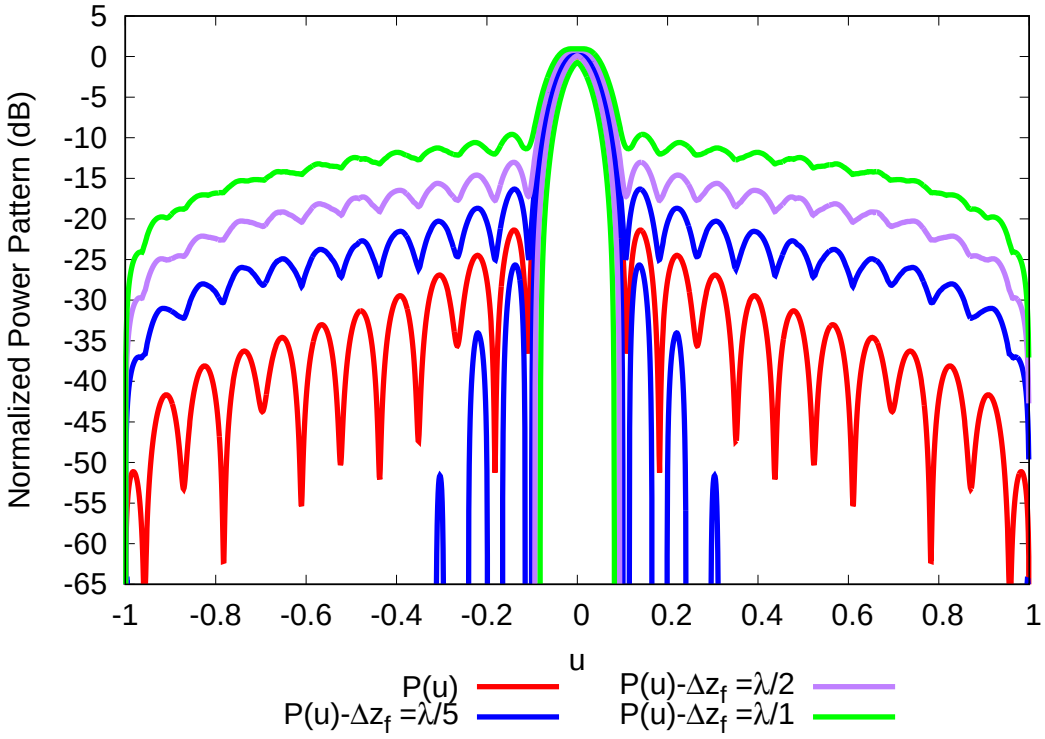

Figure 5.19: Analysis of the IA-based *co*−polar pattern prediction vs. feed displacement errors in $u = 0$ and $v = 0$ planes, $\triangle z_f = \{\lambda/5, 2, 1\}$- Interval pattern features $[p(u, v)]$.

Δy_f	$[P(u,v)]$	$[SLL], dB$	$[BW], u$	$\Delta \times 10$
u=0				
0	0	-21.349	0.090	
$\lambda/200$	[-0.024,0.001]	[-21.817,-20.903]	[0.09,0.092]	0.13
$\lambda/100$	[-0.038,0.0137]	[-22.309,-20.477]	[0.088,0.092]	0.27
$\lambda/50$	[-0.13,0.0372]	[-23.388,-19.029]	[0.086,0.094]	0.68
$\lambda/20$	[-0.229,0.098]	[-27.695,-17.084]	[0.080,0.100]	1.53
$\lambda/10$	[-0.359,0.179]	[-inf,-14.915]	[0.072,0.100]	2.95
v=0				
0	0	-22.561	0.092	
$\lambda/200$	[-0.024,0.0001]	[-23.228,-22.134]	[0.092,0.094]	0.159
$\lambda/100$	[-0.0383,0.013]	[-23.832,-21.633]	[0.090,0.094]	0.31
$\lambda/50$	[-0.130,0.037]	[-25.194,-19.984]	[0.086,0.098]	0.78
$\lambda/20$	[-0.229,0.098]	[-31.342,-17.817]	[0.080,0.104]	1.82
$\lambda/10$	[-0.359,0.179]	[-inf,-15.068]	[0.072,0.114]	3.65

Table 5.9: Analysis of the IA-based $co-$polar pattern prediction vs. feed displacement errors errors in $u = 0$ and $v = 0$ planes, $\triangle y_f = \{\lambda/200, 100, 50, 20, 10\}$.Interval pattern features $[p(u,v), SLL, BW]$ and pattern tolerance index Δ

design for nominal lengths of reflectarray patches is needed to realize required phase for the proposed F/D values. Four different reflectarray arrangements have been synthesized for different ratios of F/D.

The behaviour of the peak power pattern versus $F/D = \{0.3; 0.5; 0.7; 0.9\}$ in tolerances of $\Delta x_f = \{\lambda/200, \lambda/100, \lambda/50, \lambda/20, \lambda/10\}$ is shown in Fig. 5.20(a). Beam width and sidelobe level for these ratios are presented in Fig. 5.20 (b) and Fig. 5.20(c) , respectively. It is clear from these figures, as the (F/D) is increasing, the sensitivity of the power pattern to the tolerance errors are decreasing. The value of the pattern features such as peak power, beam width and sidelobe level are shown in table 5.10.
Since F/D ratio is changing, we need to apply the appropriate values for $qH = qE$ in (5.7), (5.8) to achieve the same aperture efficiency of the structure in each value of F/D . This value is computed in each F/D . The following values of $qH = \{1; 1.2; 3.2; 6\}$ are chosen for $F/D = \{0.3; 0.5; 0.7; 0.9\}$[10].

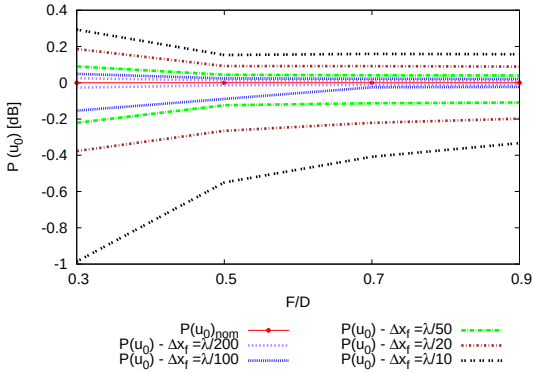

(a)

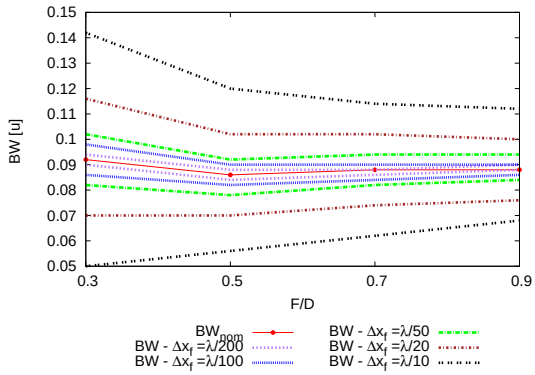

(b)

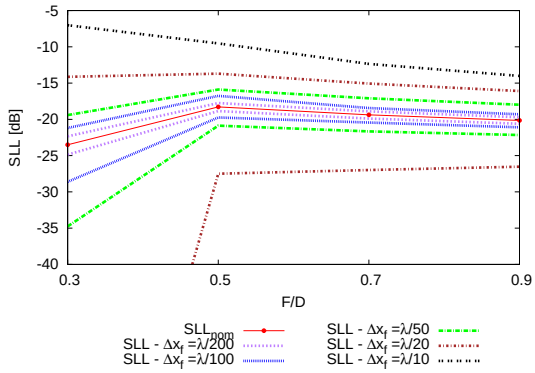

(c)

Figure 5.20: *Analysis versus F/D, IA-pattern features* $(a)P(u_0)(b)$ *SLL* (c) *BW*.

Δx_f	$[P(u,v)]$	$[SLL], dB$	$[BW], u$
$F/D = 0.3$			
0	0	-23.510	0.092
$\lambda/200$	[-0.027,0.025]	[-24.856,-22.340]	[0.09,0.094]
$\lambda/100$	[-0.154,0.049]	[-28.615,-21.197]	[0.086,0.098]
$\lambda/50$	[-0.221,0.090]	[-34.763,-19.414]	[0.082,0.102]
$\lambda/20$	[-0.377,0.186]	[-inf,-14.143]	[0.070,0.116]
$\lambda/10$	[-0.986,0.293]	[-inf,-7.017]	[0.05,0.142]
$F/D = 0.5$			
0	0	-18.286	0.086
$\lambda/200$	[-0.014,0.012]	[-18.858,-17.752]	[0.084,0.088]
$\lambda/100$	[-0.089,0.024]	[-19.474,-16.769]	[0.082,0.090]
$\lambda/50$	[-0.124,0.044]	[-20.867,-15.888]	[0.078,0.092]
$\lambda/20$	[-0.265,0.092]	[-27.498,-13.699]	[0.076,0.100]
$\lambda/10$	[-0.550,0.153]	[-inf,-12.355]	[0.056,0.120]
$F/D = 0.7$			
0	0	-19.380	0.088
$\lambda/200$	[-0.012,0.011]	[-18.858,-17.752]	[0.086,0.088]
$\lambda/100$	[-0.025,0.021]	[-19.474,-16.769]	[0.082,0.090]
$\lambda/50$	[-0.113,0.041]	[-21.662,-17.098]	[0.082,0.094]
$\lambda/20$	[-0.221,0.091]	[-26.990,-15.066]	[0.076,0.100]
$\lambda/10$	[-0.408,0.159]	[-12.355,-19.380]	[0.062,0.114]
$F/D = 0.9$			
0		-20.153	0.088
$\lambda/200$	[-0.011,0.010]	[-20.611,-19.717]	[0.088,0.090]
$\lambda/100$	[-0.023,0.020]	[-21.097,-19.305]	[0.086,0.090
$\lambda/50$	[-0.109,0.040]	[-22.166,-17.979]	[0.084,0.094]
$\lambda/20$	[-0.198,0.089]	[-26.523,-16.102]	[0.076,0.100]
$\lambda/10$	[-0.333,0.157]	[-inf,-14.012]	[0.068,0.112]

Table 5.10: Analysis vs. F/D ,$F/D = \{0.3, 0.5, 0.7, 0.9\}$ for feed displacement errors in $v = 0$ plane, $\triangle x_f = \{\lambda/200, 100, 50, 20, 10\}$- Interval pattern features $[p(u,v), SLL, BW]$ and pattern tolerance index Δ

Chapter 6

Conclusions and Future Developments

In this last chapter, some conclusions are drawn and further advances are envisaged in order to address the possible developments of the proposed technique.

In this thesis, an approach for the tolerance analysis of reflectarray antennas has been presented and validated. The method is based on the Interval Analysis. Interval Arithmetic rules are exploited to model the effect of uncertainties on the radiation pattern of antenna which is analyzed with Aperture field method. In the interval extension of the reflectarray power pattern functions with Cartesian Interval method ($IA-CS$), the so called Wrapping and Dependency problems are appeared and these problems overestimate the power bounds. In this thesis, the proper way to deal with these redundancy problems is addressed. Reformulating the interval function is the first method to eliminate the dependency effect ($IA-CS^*$). Since the radiation pattern expression has a complex relation with the geometrical parameters, reformulating ($IA-CS^*$) can not remove all dependency problems. To fully remove the dependency, Interval Enumerative ($IA-ENUM$) method is applied. Then the Minkowski Sum approach is implemented to eliminate the Wrapping effect ($IA-ENUM-MS$). The numerical analysis has proved that:

- the $IA-ENUM-MS$ power pattern bounds are narrower, more reliable than those predicted by the $IA-CS$, $IA-CS^*$, $IA-ENUM$
- the $IA-ENUM-MS$ bounds are still inclusive and satisfy the *Inclusion Theorem* of IA;

To validate the dependency of the degradation of the pattern features against varying steering angle, different reflectarray antennas structures are considered and analyzed, in different patch tolerances. Similar to the previous validation, the analysis is considered in several bandwidths. The results proved the effectiveness and robustness of the $IA-ENUM-MS$ analysis in different steering angles and frequencies. After checking the method validity with patch and substrate errors, the tolerance effect on the feed position is considered. Then, the interval bounds of the *co-* polar components of the power pattern are calculated by Interval arithmetic rules together with Minkowski sum approach. Furthermore, different structures of reflectarray antenna for several F/D are considered and their interval bounds are computed. Larger F/D ratio can increase the system robustness to the tolerance of error. Effectiveness of this tolerance analysis toward feed error is obvious from the results.

For the future of this work, probabilistic interval analysis can be considered to predict the power pattern deviations. The statistical behaviour of the geometrical parameters are modeled with probability density function. Then according to this function, probabilistic upper and lower bounds of the power pattern can be defined with Interval Arithmetic rules.

For further examination of the proposed method, we can apply the Interval Analysis method for reflectarray with different shapes, especially aperture coupled and FSS shape scattering elements. Furthermore, multilayered reflectarray structure can be considered to estimate the effect of geometrical tolerances in

different layers and the combination of all errors for the whole structure. Since reflectarray antenna with different structures is one of the most useful antennas for space communication, this complete tolerance analysis in reflectarray antenna could be a very useful tool for an antenna engineer to make a more robust design against manufacturing and other unpredictable tolerances.

References

[1] H. Jasik, *Antenna Engineering Handbook*, MaGraw-Hill, New York, 1961.

[2] R.Mailloux, *Phased Array Antennas Handbook*, USA: Artch House, 2005.

[3] D. G. Berry, R. G. Malech, and W. A. Kennedy, " The reflectarray antenna," *IEEE Trans. Antennas Propag.*, vol. 11, pp. 645-651, Nov. 1963.

[4] H. R. Phelan, "Spiralphase reflectarray for multitarget radar." *Microw Journal.* vol.20, pp. 186-192, Jul. 1977.

[5] C. S. Malagisi, " Microstrip disc element reflect array," *Electronics and Aerospace System Convention*, pp. 186-192, Sept. 1978.

[6] D. M. Pozar, S. D. Targonski, and R. Pokuls, " A shaped-beam microstrip patch reflectarray," *IEEE Trans. Antennas Propag.*, vol. 47, pp. 1167-1173, Jul. 1999.

[7] J. A. Encinar and J. A. Zornoza, "Three-layer printed reflectarrays for contour beam space applications," *IEEE Trans. Antennas Propag.*, pp. 1138-1148, vol. 52, May 2004.

[8] D. M. Pozar and S. D. Targonski, "A microstrip reflectarray using crossed dipoles," *IEEE Antennas Propag Symp*, pp. 1008-1011. Jun. 1998.

[9] M. R. Chaharmir, J. Shaker, M. Cuhaci, and A. Sebak, "Reflectarray with variable slots on ground plane," *IEE Proc, Microw. Antennas Propag.*, vol. 150, no.6, pp. 436-439, Dec. 2003.

[10] J. Huang, J.A.Encinar, *Reflectarray Antennas,* New York, NJ, USA: Artech House, 2008.

[11] D. C. Chang and M. C. Huang, "Multiple polarization microstrip reflectarray antenna with high efficiency and low cross-polarization," *IEEE Trans, Antennas Prpag.*, vol.43, pp. 829-834, Aug. 1995.

[12] D. M. Pozar and T. A. Metzler, "Analysis of a reflectarray antenna using microstrip patches of variable size," *Electron, Lett.*, vol.45, pp. 287-296, Feb. 1997.

[13] J. Huang and R. J. Pogorzelski, " A Ka-band microstrip reflectarray with elements having variable rotation angles," *IEEE Trans. Antennas Propag.*, vol. 46, pp. 650-656, May 1998.

[14] D. M. Pozar, " Bandwidth of reflectarrays," *Electron Lett.*, vol.39, pp. 1490-1491, Oct. 2003.

[15] J. A. Encinar, " Design of two-layer printed reflectarray using patches of variable size," *IEEE Trans. Antennas Propag.*, vol. 49, pp. 1403-1410, Oct. 2001.

[16] J. A. Encinar and J. A. Zornoza, "Broadband design of three-layer printed reflectarrays," *IEEE Trans. Antennas Propag.*, vol. 51, pp. 1662-1664, Jul. 2003.

[17] J. Huang, V. A. Feria, and H. Fang, "Improvement of the three-meter Ka-band inflatable reflectarray antenna," *IEEE AP-S/URSI Symp*, Boston, Massachusett, Jul. 2001, pp. 122-125.

[18] M. Bialkowski, A. W. Robinson, and H. J. Song, "Design, development, and testing of X-band amplifying reflectarrays," *IEEE Trans. Antennas Propag.*, vol. 50, pp. 1065-1976, Aug. 2002.

[19] M. Karimipour, A. Pirhadi and N. Ebrahimi, "Accurate method for synthesis of shaped-beam non-uniform reflectarray antenna," *IET Microw, Antennas Propag*, vol. 7, no. 15, pp. 1247-1253, Dec. 2013.

[20] D. G. Kurup, M. Himdi and A. Rydberg, "Design of an unequally spaced reflectarray," *IEEE Antennas and Wireless Propag Lett*, vol. 2, no. 1, pp. 33-35, 2003.

[21] M. A. Moharram and A. A. Kishk, "Optically Transparent Reflectarray Antenna Design Integrated With Solar Cells," *IEEE Trans Antennas and Propag*, vol. 64, no. 5, pp. 1700-1712, May 2016.

[22] K. K. Karnati, Y. Yusuf, S. Ebadi and X. Gong, "Q factor analysis of reflectarray elements investigating the effects from angle of incidence using floquet modes," *IEEE Trans. Antennas Propag.*, vol. 62, no. 10, pp. 5017-5028, Oct. 2014.

[23] H. T. Chou, H. K. Ho and Y. J. Chen, "Radiation Discrepancy Analysis for Metallic Reflectarray Antennas With Random Manufacture Distortion at mmW Frequencies," *IEEE Antennas and Wireless Propag Lett*, vol. 15, pp. 1885-1888, 2016.

[24] D.M. Pozar, D.S. Targonski, "Design of millimeter wave microstrip reflectarrays", *IEEE Trans. Antennas Propag.*, vol. 45, no. 2, pp. 287-296, Feb. 1997.

[25] R.Elliott, “Mechanical and electrical tolerances for two-dimensional scanning antenna arrays”, *IRE Trans. Antennas Propag*, vol. 6, pp.114-120, Jan. 1958.

[26] W.F.Richards, Y.T. Lo, “Antenna Pattern Synthesis based on optimization probabilistic sense”, *IEEE Trans. Antennas Propag.*, vol. 23, no. 2, pp. 165-172, Mar. 1975.

[27] J. K. Hsiao, "Design of error tolerance of a phased array," *Electron Lett.*, vol. 21, no. 19, pp. 834-836, Sept.1985.

[28] J. Lee, Y Lee and H. Kim, "Decision of error tolerance in array element by the Monte Carlo method," *IEEE Trans. Antennas Propag.*, vol. 53, no. 4, pp. 1325-1331, Apr 2005.

[29] A. Neumaier, “Interval iteration for zeros of system of equations,”*BIT*, vol.25, pp. 256-273, Mar. 1985.

[30] E. Hansen, Global Optimization Using Interval Analysis, New York, M.Dekker, 1992.

[31] G. Saxena and D. A. Lowther, "The use of interval mathematics in electromagnetic design," *IEEE Trans. Mag.*, vol. 37, no. 5, pp. 3588-3591, Sept. 2001.

[32] L. Egiziano, P. Lamberti, G. Spagnuolo and V. Tucci, "Robust Design of Electromagnetic Systems Based on Interval Taylor Extension Applied to a Multiquadric Performance Function," *IEEE Trans.* Mag., vol. 44, no. 6, pp. 1134-1137, Jun. 2008.

[33] N. Anselmi, L. Manica, P. Rocca and A. Massa, "Tolerance Analysis of Antenna Arrays Through Interval Arithmetic," *IEEE Trans. Antennas Propag*, vol. 61, no. 11, pp. 5496-5507, Nov. 2013.

[34] P. Rocca, L. Manica and A. Massa, "Interval-based analysis of pattern distortions in reflector antennas with bump-like surface deformations," *IET Microw. Antennas Propag.*, vol. 8, no. 15, pp. 1277-1285, 2014.

[35] P.Nayeri, A. Elsherbeni, F.Yang, "Radiation Analysis Approaches for Reflectarray Antennas [An-tenna Designer’s Notebook", *IEEE Antennas Propag Mag.*, vol.55, no.1, pp. 127-134, Feb. 2013.

[36] R. E. Moore, Interval Analysis Prentice, Hall, Englewood Cliffs, New Jersey 1966.

[37] G.W. Walster, Interval arithmetic: The new floating point arithmetic paradigm.

[38] R. Boche, “Complex Interval Arithmetic with some Applications”, Lockheed Missile and Space Company, technical report, Feb. 1966.

[39] L. Jualin, M. Kieffer, O. Didrit, and E. Walter, *Applied Interval Analysis*. London, UK: Springer, 2001.

[40] L. Tenuti, N. Anselmi, P. Rocca, M. Salucci and A. Massa, "Minkowski Sum Method for Planar Arrays Sensitivity Analysis With Uncertain-But-Bounded Excitation Tolerances," *IEEE Trans. Antennas Propag*, vol. 65, no. 1, pp. 167-177, Jan. 2017.

[41] P. Rocca, L. Poli, N. Anselmi, M. Salucci and A. Massa, "Predicting antenna pattern degradations in microstrip reflectarrays through interval arithmetic," *IET Microw. Antennas Propag.*, vol. 10, no. 8, pp. 817-826, 2016.

[42] M. de Berg, O. Cheong, M. van Kreveld, and M. Overmars, *Computational Geometry - Algorithms and Applications* (3rd ed.). Berlin Heidelberg, Germany: Springer-Verlag, 2008.

[43] J. Ruze, "Lateral feed displacement in a paraboloid," *IEEE Antennas Propag. Society International Symp. (APSURSI)*, Long Island, NY, USA, 1964, pp. 186-189.

[44] P. A. McInnes, E. W. Munro and A. J. T. Whitaker, “Lateral displacement of log-periodic paraboloid feed,” *Electron. Lett.*, vol. 8, pp. 249-250, 1972.

[45] M. Mohammadirad, N. Komjani, M. R. Chaharmir, J. Shaker and A. R. Sebak, "Impact of feed position on the operating band of broadband reflectarray antenna," *IEEE Antennas Wireless Propag. Lett.*, vol. 11 , pp. 1104-1107, 2012.

[46] J. Ruze, “The effect of aperture errors on the antenna radiation pattern”, *Nuovo Cimento Suppl.* vol. 9, no. 3, pp. 364-380, 1952.

[47] J. Lee, Y. Lee, H. Kim, "Decision of error tolerance in array element by the Monte Carlo method," *IEEE Trans. Antennas Propag.*, vol. 53, no. 4, pp. 1325-1331, Apr. 2005.

[48] P. Rocca, L. Manica, N. Anselmi, and A. Massa, “Analysis of the pattern tolerance in linear arrays with arbitrary amplitude errors,” *IEEE Antennas Wireless Propag. Lett.*, vol. 12, pp. 639-642, 2013.

[49] P. Rocca, N. Anselmi, and A. Massa, “Optimal synthesis of robust beamformer weights exploiting interval analysis and convex optimization,” *IEEE Trans. Antennas Propag.*, vol. 62, no. 7, pp. 3603-3612, Jul. 2014.

[50] P. Rocca, N. Anselmi and A. Massa, "Interval arithmetic for pattern tolerance analysis of parabolic reflectors," *IEEE Trans. Antennas Propag.*, vol. 62, no. 10, pp. 4952-4960, Oct. 2014.

[51] P. Li, W. Xu and S. Li-Wei, "Power pattern tolerance analysis of radome with the material property error based on Interval Arithmetic," *IEEE Antennas Wireless Propag. Lett.*, vol. 16, pp. 1321-1324, 2017.

[52] P. Rocca, L. Poli, N. Anselmi, M. Salucci and A. Massa, "Predicting antenna pattern degradations in microstrip reflectarrays through interval arithmetic," *IET Microw. Antennas Propag.*, vol. 10, no. 8, pp. 817-826, 2016.

[53] N. Ebrahimi, N. Anselmi, P. Rocca and A. Massa, "Tolerance analysis of the reflectarray antenna through Minkowski-based interval analysis," *Proc. Eur. Conf. Antennas Propag. (EuCAP)*, Paris, France, Mar. 19-24, 2017, pp. 2392-2395.

[54] N. Ebrahimi, P. Rocca and A. Massa, "Power pattern sensitivity analysis of reflectarray antennas to substrate uncertainties through the minkowski interval analysis," *Proc. Conf. Applied Computational Electromagnetics Society Symp. (ACES)* , Florence, Italy, Mar. 26-30, 2017, pp. 1-2.